1-1-1973

Rheo-optical property studies of cis-1,4-polybutadiene.

Christine Shih-May Ong
University of Massachusetts Amherst

RHEO-OPTICAL PROPERTY STUDIES

OF

CIS-1,4-POLYBUTADIENE

A Dissertation Presented

By

CHRISTINE SHIH-MAY ONG

Submitted to the Graduate School of the
University of Massachusetts in
partial fulfillment of the requirements for the degree of

DOCTOR OF PHILOSOPHY

December 1973

Major Subject: Polymer Science and Engineering

RHEO-OPTICAL PROPERTY STUDIES

OF

CIS-1,4-POLYBUTADIENE

A Dissertation

By

CHRISTINE SHIH-MAY ONG

Approved as to style and content by:

Richard S. Stein
Chairman of Committee

R S Porter
Head of Department

Member

Member

December 1973

DEDICATED

TO

MY PARENTS

ACKNOWLEDGMENTS

The author wishes to express her sincere appreciation to Professor Richard S. Stein, thesis director, for his guidance and his constant encouragement throughout the course of this work. The helpful suggestions of Professors Fraser P. Price and Otto Vogl, the other members of the thesis committee, are also gratefully acknowledged.

The author wishes to express her sincere appreciation to Professor S. S. Sternstein of Rennsselaer Polytechnic Institute for many helpful discussions.

Sincere thanks are also extended to Dr. C. Picot and Mr. M. Fukuda for their assistance in the achievement of the first chapter of this thesis, and to Dr. D. Yoon for his discussions.

Thanks are also extended to Mrs. Gay Flannelly for typing the thesis.

Computer calculations were carried out at the University of Massachusetts Research Computing Center.

RHEO-OPTICAL PROPERTY STUDIES OF

CIS-1,4-POLYBUTADIENE

(December 1973)

Christine Shih-May Ong

Directed by: Professor Richard S. Stein

ABSTRACT

The H_v small angle light scattering patterns from crosslinked swollen rubbers containing glass bead filler were measured. The theoretical patterns were calculated using the stress field calculated by Sternstein. Good agreement was found between experiments and theory.

When rubbers containing small glass spheres are stretched, the strain is inhomogeneous in the vicinity of the spheres. For small strains, the stress field may be calculated by using the theory of Goodier. From the experimental stress-optical coefficient, the optic axis orientation and magnitude of the birefringence may then be calculated. From this, the retardation of a ray passing through the sample may be obtained. Theoretical values are found to agree favorably with experimentally measured retardation patterns found for stretched samples of crosslinked cis-1,4-polybutadiene containing silane bonded glass spheres. From the theoretical birefringence distribution, we have calculated the H_v (crossed polaroid) low angle light scattering pattern arising from this refractive index heterogeneity. The

theoretical light scattering pattern agrees well with that which is experimentally obtained from the stretched rubber described above. It is postulated that similar light scattering arises from inhomogeneous strains in stretched unfilled rubbers because of heterogeneity in the degree of crosslinking.

Both the stress-strain and the birefringence-strain curves deviate from their ideal values, predicted by the kinetic theory of rubber elasticity, in a manner described by a Mooney-Rivlin type equation with non-ideality coefficients C_2 and B_2. Both C_2 and B_2 are significantly reduced by measuring in the swollen state. C. Price has shown that if rubbers are crosslinked in the swollen state and then dried before measurement, the stress coefficient C_2 is reduced. We have carried out corresponding measurements of the birefringence-strain variation for cis-1,4-polybutadiene samples which were crosslinked in the swollen state and then dried, and have found that the B_2 coefficient is appreciably smaller than for conventionally crosslinked rubbers. A further reduction in B_2 (and C_2) is found upon measuring in the swollen state. These results confirm the conclusion of Price, et al., that deviations from ideal rubber elasticity are largely related to chain topology and not to chain packing or internal energy effects.

The correct measurement of birefringence in a non-uniform medium was discussed. The birefringence of an object is usually obtained from its retardation. For an object of variable refractive index and optic axis orientation, a matrix procedure should be used for relating the

retardation to the birefringence. The correct procedure is illustrated for the case of a polymer spherulite.

TABLE OF CONTENTS

INTRODUCTION

New engineering composites have been developed which are creating a material revolution. Modification of rubbers and plastics by other polymers becomes more and more important; the results are new materials having combinations of properties hitherto unachievable.

Reinforcement of elastomers by particulate filler such as carbon black or silica is very important and widely used in the rubber industry. The incorporation of a colloidal material into a high polymer with subsequent conversion to a filler network by vulcanization is a relatively simple art but a complex science.

These reinforcement effects are generally measured by the resistance to abrasion, tearing, cut growth, flex cracking and tensile failure. In unfilled vulcanizates of homopolymers and random copolymers, the equilibrium stress predicted by kinetic theory is proportional to the number of elastically effective network chains supporting the load.[1] This number will depend on the primary molecular weight of the rubber, the number of crosslinks forming the rubber, and the number of chain entanglements isolated between these crosslinks.

Equilibrium swelling measurement is a common technique to measure the crosslinking density for unfilled elastomers. In filled systems, the swelling is anomalous in that simple correction for the volume fraction of elastomer is insufficient to account for the observed swelling diminution. While the mechanism by which reinforcement occurs is not

completely understood, it is believed[2,3] that the heterogeneous stress field in the elastomeric matrix must be a significant factor.

In Chapter 1, the effects of inhomogeneous swelling about spherical filler particles upon the scattering patterns were studied.

In Chapter 2, the effects of stretching upon the scattering and birefringence patterns from the filled rubber in the dry state were studied.

This research work serves as models for filled systems and the results may be extrapolated to apply to filled rubbers having shapes, particle sizes and concentrations of fillers of commercial interest, and it can be extended to any two-phase composite system of which the moduli of two phases are different.

CHAPTER I

DEPOLARIZED LIGHT SCATTERING FROM SWOLLEN-FILLED RUBBER

Synopsis

The H_v small angle light scattering patterns from crosslinked swollen rubbers containing glass bead filler particles are shown to arise from the birefringence patterns associated with the inhomogeneous swelling in the vicinity of the particles. Theoretically calculated patterns are obtained by using the stress field calculated by Sternstein and are found to agree with the experimental results.

Introduction

In recent publications,[1,2] Stein and Wilkes have pointed out that light scattering can originate from deformed regions surrounding voids and inclusions in solid high polymers. As it arises from birefringence gradients in such strained regions, the light scattering will be depolarized.

Rubbers containing fillers such as glass spheres are inhomogeneous and scatter light. However, if the glass and rubber are isotropic, the scattering will be principally of the V_v type (vertically polarized scattered light from vertically polarized incident light) and the depolarized H_v component (horizontally polarized scattered light) will be weak.

When such a filled rubber is swollen, however, stresses result

because of inhomogeneity of swelling. Assuming that the rubber remains firmly bound to the sphere during swelling, a tangential strain is not possible at the rubber-glass interface; but a radial strain can occur as a result of swelling. Thus, the rubber will be subjected to a biaxial strain in the vicinity of the glass sphere with a resulting biaxial stress. This will result in a uniaxial birefringence having its principal axis along the radial direction and asymptotically approaching zero with increasing distance from the center of the sphere. This birefringence gradient fulfills the requirements of the Stein-Wilkes theory and will lead to an enhanced H_v scattering component.

Sternstein Theory

In recent calculations Sternstein[3] has worked out the problem of swelling of rubber containing spherical filler particles subject to the boundary condition that the tangential strain is zero at the surface of the particle. He has obtained expressions for the radial and tangential stress and strain as a function of distance r away from the center of the particle. Figure 1 gives an example of his results of the variation of the anisotropic stress, $(\sigma_r - \sigma_t) = \sigma(R_o)$, as a function of the reduced variable $R_o = r/r_o$, where r_o is the size of the particle. This variation corresponds to a volume fraction of the rubber in the swollen state $v_2 = 0.25$. It is then possible to relate the stress to the resulting optical birefringence.

Strain-Birefringence Relationship

According to Kuhn and Grün theory,[4] indeed, the birefringence of an unswollen rubber network submitted to a homogeneous strain can be expressed by the relationship:

$$\Delta n = \frac{2}{45} \pi \frac{(\bar{n}^2 + 2)^2}{\bar{n}} N_c (b_1 - b_2) (\alpha_1^2 - \alpha_2^2) \qquad (1)$$

where Δn is the difference of the refractive indices along and perpendicular to the elongation directions, $\bar{n}$ is the average refractive index, N_c is the number of network chains per cm^3, b_1 and b_2 are the polarizabilities parallel and perpendicular to the direction of a link, and α_1 and α_2 are the principal extension ratios.

In the case of a swollen network, this relationship becomes:

$$\Delta n' = \frac{2}{45} \pi \frac{(\bar{n}^2 + 2)^2}{\bar{n}} N_c (b_1 - b_2) v_2^{1/3} (\alpha_1^2 - \alpha_2^2) \qquad (2)$$

where v_2 is the volume fraction of rubber in the swollen state.

Now, the anisotropic stress $(\sigma_1 - \sigma_2)$ is related to the extension ratios by

$$\sigma_1 - \sigma_2 = kT N_c v_2^{1/3} (\alpha_1^2 - \alpha_2^2) \qquad (3)$$

where k is Boltzmann's constant and T is the absolute temperature.

In our particular case, as we are dealing with a spherically

symmetrical distribution of the stresses, we can identify $\sigma_1 - \sigma_2$ with $\sigma_r - \sigma_t$ and in the same way $\Delta n'$ with $n_r - n_t$, n_r and n_t being the radial and tangential refractive indices. Thus from (2) and (3),

$$\frac{n_r - n_t}{\sigma_r - \sigma_t} = \frac{(\bar{n}^2 + 2)^2}{\bar{n}} \frac{2\pi}{45kT} (b_1 - b_2) \qquad (4)$$

which is nothing else than the stress optical coefficient, C. In the case of natural rubber, $C = 2.38 \cdot 10^{-10}$ cm^2/dyne. It is possible that this value may be affected by solvent as indicated by studies of Gent[5] and Nagai[6] on polyisoprene and polybutadiene. Since such an effect depends upon v_2, which varies with radius, it may be that the stress-optical coefficient varies to some extent with radius. This possibility was neglected in the studies reported here.

A direct test of this birefringence variation has been carried out by Kotani and Sternstein[7] by observation of the polarization pattern between crossed polaroids using a microscope. They have found a distribution of birefringence which quantitatively agrees with the prediction of their theory.

Light Scattering Calculations

The amplitude of light scattered at small angles can be calculated by using the expression derived by Stein and Wilkes[1] for symmetrical regions where the optic axis is directed along the radius. For crossed polarizer and analyzer (H_v), it can be written:

$$(E_S)_{H_v} = C' \cos\rho_2 \sin\mu \cos\mu \frac{r_o^3}{U^3} \int_{R_o=0}^{\infty} [n_r(R_o) - n_t(R_o)]$$

$$\left[3 \cos(UR_o) + UR_o \sin(UR_o) - 3 \frac{\sin(UR_o)}{UR_o}\right] dR_o \qquad (5)$$

where C' is a numerical coefficient, $\cos\rho_2 = \cos\theta/[\cos^2\theta + \sin^2\theta \sin^2\mu]^{1/2}$, θ and μ are the scattering and azimuthal angles defining the scattering direction, $U = (4\pi r_o/\lambda) \sin(\theta/2)$, and λ is the light wavelength in the medium.

By substituting into (5) the value of $(n_r - n_t)$ as a function of $(\sigma_r - \sigma_t)$ for $r > 1$ and taking $(n_r - n_t) = 0$ for r less than one and using Sternstein's values, we calculated the scattered intensity distribution by numerical integration $\left(I_{H_v} = (E_S)_{H_v} \cdot (E_S)^*_{H_v}\right)$ using the CDC 3600 computer at the University of Massachusetts Research Computing Center.

Figure 2(a) gives the theoretical patterns observed in the polar coordinates (U, μ). The patterns possess four-fold symmetry where the intensity along the 45° azimuthal direction [see Figure 2(b)] passes through several maxima whose position characterizes the size of the filler particles.

It is noted that the scattered intensity is zero at $\mu = 0°$ and 90° as a result of the $\sin\mu \cos\mu$ term in Eqn. (5). With increasing size of the glass sphere, the scattering occurs at smaller angles.

Film Preparation

Experiments were carried out on samples of synthetic cis-polyisoprene (kindly supplied by Dr. K. W. Scott of the Goodyear Tire and Rubber Co., Akron, Ohio). This rubber is called Natsyn-400.

Samples containing one to five parts of dicumyl peroxide (dicup) crosslinking agent per hundred parts of rubber were used to prepare two types of film: one containing a large number of small glass spheres and a second containing a smaller number of larger spheres.

For the first type, glass spheres having a size range of 5 - 10μ were used (Microbeads Div., Cataphote Corp., Jackson, Miss.). These were added to an approximately 3% solution of the rubber in benzene, mixed, and cast into films of about 0.5 mm thickness on a Teflon pan. After evaporating the benzene at room temperature, these were dried for about 16 hrs. in an oven at 45°C, then transferred to a press where they were cured by heating at 90°C for 20 min. and then heated to 140°C for 40 min. under 3000 psi pressure.

A second type film was prepared which contained larger beads of about 29μ diameter, identical to those used by Kotani and Sternstein[7] (3M Company Superbrite glass beads). These scattered sufficiently to permit observation of the scattering patterns arising from deformed regions about single beads. Some difficulty was experienced in binding these beads to the rubber sufficiently well so that they did not separate under the swelling stresses. Kotani and Sternstein used an epoxy adhesive for this purpose; we found a silane treatment more convenient.

The beads were first washed with acetone and then treated with a 10% aqueous NaOH solution at 50°C for 1 hr. After washing, the beads were treated with a freshly prepared 10% aqueous solution of Dow Corning Z-6020 silane coupling agent at room temperature for 30 min. (Dow Corning Corp., Midland, Mich.). This agent is N-β-aminoethyl-γ-aminopropyl trimethoxy silane. The beads were then removed from the silane and dried in an oven at 110°C for 3 hrs.

Two procedures were used for dispersing these beads with the rubber. The first was a solution blending procedure similar to that previously described. The second, which was somewhat more satisfactory, involved dusting the glass spheres on the surface of the rubber film, folding the film, pressing at 60°C, releasing the pressure, refolding and repressing about one hundred times to achieve uniformity of dispersion. In all cases the concentration of glass was less than 0.01 g/cm^3.

Films were swollen by immersing in xylene for 24 hrs. at room temperature to approach equilibrium swelling in the range of v_2 of about 0.35. They were then placed while wet between glass microscope slides for optical investigations.

Light Scattering

Light scattering photographic patterns were obtained using a laser scattering apparatus as described by Rhodes and Stein.[9]

The set of pictures (Figure 3) shows some characteristic H_v patterns which have been obtained. Figure 3(a) corresponds to unswollen

filled rubber and is characterized by weak diffuse scattering, probably due to important dipolarizing reflections at the particle (n = 1.486) and rubber (n = 1.519) interface. Figure 3(b) shows that unfilled swollen rubber produces only a very weak anisotropic pattern which can be attributed to network inhomogeneities giving rise to some local orientation fluctuation.[9] This contribution seems to be much smaller than the scattering arising from the anisotropic regions of a filled swollen rubber. This can be seen in Figure 3(c) which, for the same experimental conditions, exhibits a strong H_v scattering intensity.

Figure 3(d) shows that by decreasing the crosslinking degree, the scattering intensity is lowered as a result of the decrease of the stress at the particle-rubber boundary. The comparison of experimental pictures to the theoretical patterns in Figure 2(a) leads one to conclude that only the central part of the pattern can be observed experimentally. This hypothesis seems justified by the fact that in this condition the dimension of the pattern [Figure 3(c)] corresponds to particle sizes of about 8μ, which is in the range of sizes of the particles introduced into the rubber. On the other hand, the secondary maximum intensity is about one hundred times weaker than the first maximum intensity, and as the distribution in size of the particles washes out the modulation of intensity, it appears difficult to record a complete scattering pattern.

Thus, it is seen that the presence of a filler within a swollen rubber leads to heterogeneity in anisotropy, which gives rise to H_v scattering which is not seen with either the unfilled swollen rubber

or the filled unswollen rubber and characterizes the stress field in the vicinity of the heterogeneity.

The higher order part of the scattering pattern may be seen in Figure 3(e), which corresponds to a particular location of the sample where the glass balls aggregated, leading to an effective filler particle of about 25μ size which dominates the scattering. Such a sample effectively represents the scattering from this single large particle so that the higher order maxima are not averaged out because of heterogeneity of particle size.

This hypothesis may be tested by examining samples of the second type, which are intentionally prepared with a low concentration of large glass spheres. In this case, the spheres are sufficiently far apart so that regions containing single or just a few spheres are localized in the area of the sample illuminated by the laser beam; and, because of the r_o^3 term in Eqn. (5), the intensity of light scattered is sufficient so that such single-particle scattering patterns may be conveniently observed.

In Figure 4, a photomicrograph is shown for a xylene swollen sample between crossed polaroids of a crosslinked rubber containing 29μ average diameter silane coated glass beads. The four-leaf clover pattern which extends into the rubber over distances greatly exceeding the diameter of the beads is evident and is similar to the patterns first experimentally obtained and theoretically predicted by Kotani and Sternstein.[7]

Scattering patterns are shown in Figure 5, in which the higher order scattering maxima are clearly seen. It is noted that fine

structure is seen within the pattern of a type previously seen for scattering from starch particles and polystyrene spherulites,[10] which is believed to arise from interference between the scattered rays from a small number of scattering regions. The patterns are qualitatively similar to those predicted in Figure 2.

Scattering patterns similar to those observed here for model systems are observed for filled rubbers of commercial interest. For example, Figure 6 shows a scattering pattern obtained for a swollen natural rubber sample obtained from Dr. P. Thirion of the Institut Francais du Caoutchouc, Paris, France, consisting of a natural rubber sample containing 20 parts/100 of Hi-Sil 233 (PPG Industries, Barberton, Ohio) hydrated silica filler. Similar patterns were obtained from crosslinked swollen films of Natsyn-400 containing 5 parts/100 of Hi-Sil 233, furnished through the courtesy of Dr. K. W. Scott of Goodyear Tire and Rubber Co. The patterns are characteristic of stress patterns surrounding heterogeneities several microns in size. The ultimate particle size of these filler particles is of the order of 200Å, but histograms and electron micrographs furnished by Dr. M. P. Wagner of PPG Industries show the existence of aggregates ranging up to several microns in size. It is believed that the intense scattering arising from these larger aggregates completely dominates the scattering pattern.

An obvious extension of the present work (now in progress) is to observe the patterns arising from inhomogeneous deformation of the rubber in the vicinity of the filler particle. So long as no phase separation occurs at the particle-rubber interface, the resultant strains

should predominately contribute to the H_v pattern. However, when phase separation does occur, the very pronounced density discontinuities resulting should give rise to an intense V_v scattering pattern, the angular distribution of which should be characteristic of the size and shape of the phase-separated region.

It is noted that the light scattering method complements the photoelastic investigation of strains in filled systems. Its advantages are that it permits extension of measurements to cases where the size of the heterogeneity is too small to be readily resolved in the microscope and also permits the ready determination of the average properties for systems containing a very large number of heterogeneities in the field of view. Furthermore, the light scattering technique may be readily adopted to the determination of the time-dependent changes of a system.

References

1. R. S. Stein and G. L. Wilkes, J. Polymer Sci., A2, 7, 1696 (1969).
2. G. L. Wilkes and R. S. Stein, ONR Technical Report No. 122, Project NR 056-378, Contract: NONR 3357(01), University of Massachusetts, 1969.
3. S. S. Sternstein, J. Macromol. Sci.(Phys.), B6(1), 243 (1972).
4. L. R. G. Treloar, "The Physics of Rubber Elasticity," Oxford Press, 1967.
5. A. N. Gent, Macromolecules, 2, 262 (1969).
6. K. Nagai, J. Polymer Sci., A2, 7, 1123 (1969); Polymer Journal (Japan), 1, 116 (1970).
7. T. Kotani and S. Sternstein in "Polymer Networks--Structural and Mechanical Properties," edited by A. J. Chompff and S. Newman, Plenum Press, New York, New York.
8. M. B. Rhodes and R. S. Stein, Symposium on Resinographic Methods, Special Tech. Publ. No. 348, ASTM (1963); M. B. Rhodes, D. A. Keedy, and R. S. Stein, J. Polymer Sci., 62, S73 (1962).
9. R. S. Stein, J. Polymer Sci., B, 7, 657 (1969).
10. J. Borch, R. H. Marchessault, C. Picot, and R. S. Stein, Macromolecules, 4, 467 (1971).

Captions for Figures

1. Variation of $(\sigma_r - \sigma_t)\, V_1/RT$ vs. R_o, where V_1 is the molar volume of solvent in the swollen state.
2. (a) Theoretical H_v small angle light scattering pattern resulting from the anisotropic surrounding of particles embedded in a swollen crosslinked polymer network ($v_2 = 0.25$).
   (b) Variation of I_{H_v} along the 45° azimuthal direction.
3. Experimental H_v small angle light scattering patterns. The line segment indicates 10° of scattering angle.
   (a) Filled crosslinked rubber unswollen (Sample 1).
   (b) Unfilled swollen crosslinked rubber (Sample 1 without glass balls).
   (c) Filled swollen crosslinked rubber (Sample 1).
   (d) Filled swollen crosslinked rubber (Sample 2).
   (e) Filled swollen crosslinked rubber (Sample 1, large aggregates).
4. A photomicrograph between crossed polaroids of a xylene swollen crosslinked rubber containing silane coated glass beads with an average particle size of 29μ.
5. An H_v small angle light scattering pattern from the sample of Figure 4. The line segment represents 5° of scattering angle.
6. An H_v small angle light scattering pattern from a crosslinked swollen natural rubber sample containing 20 parts/100 of Hi-Sil 233 silica filler.

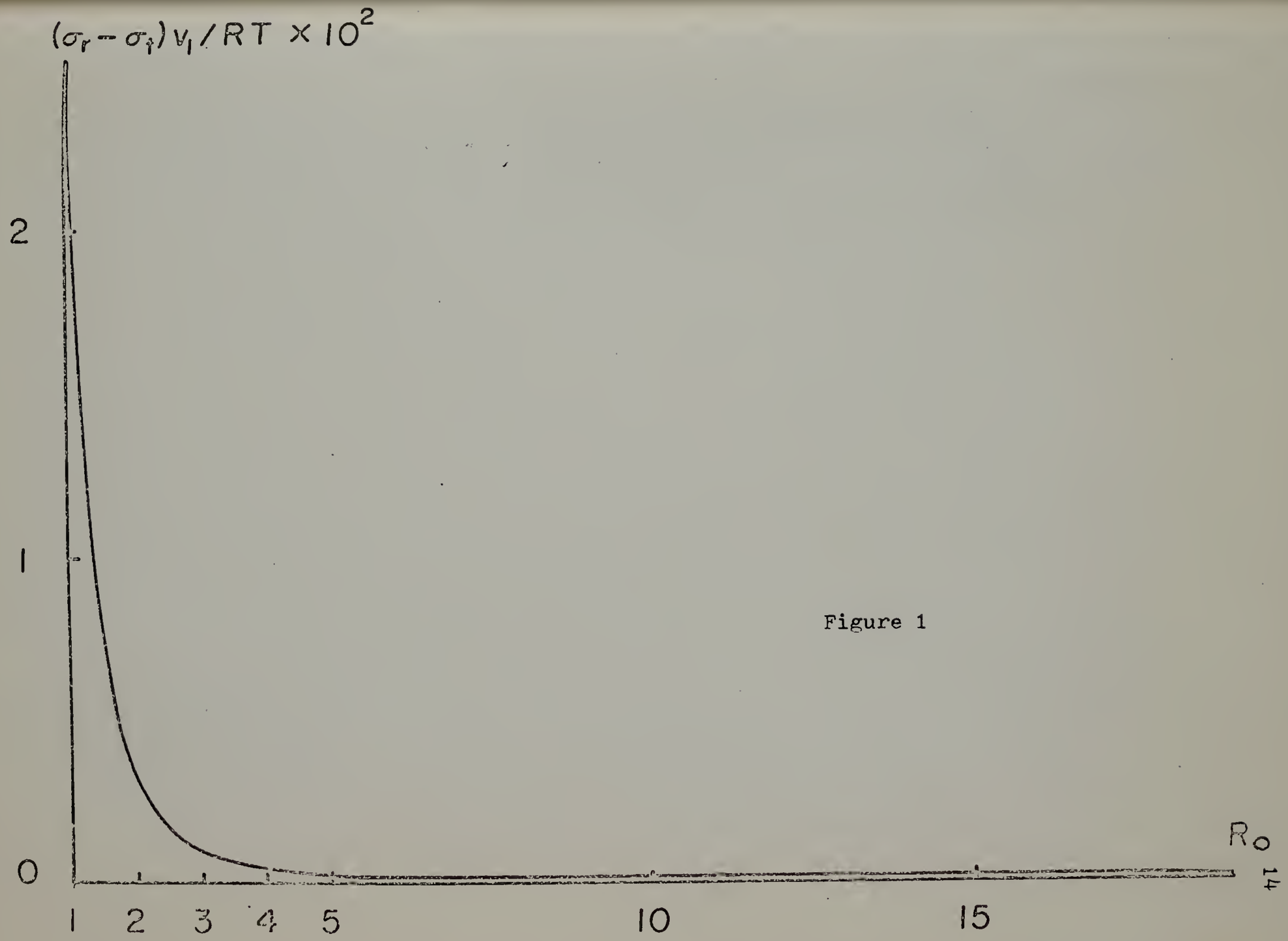

Figure 1

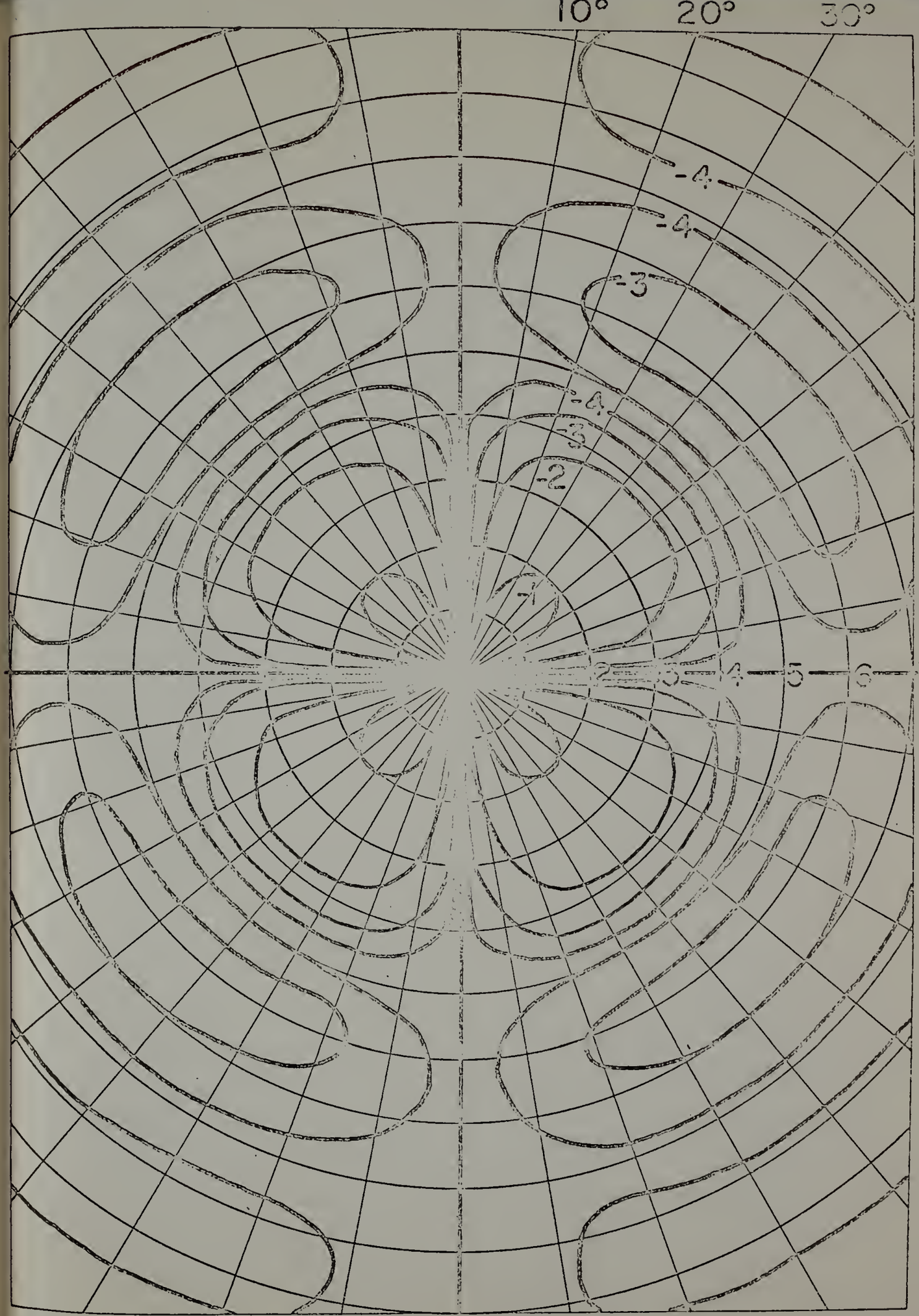

Figure 2(a)

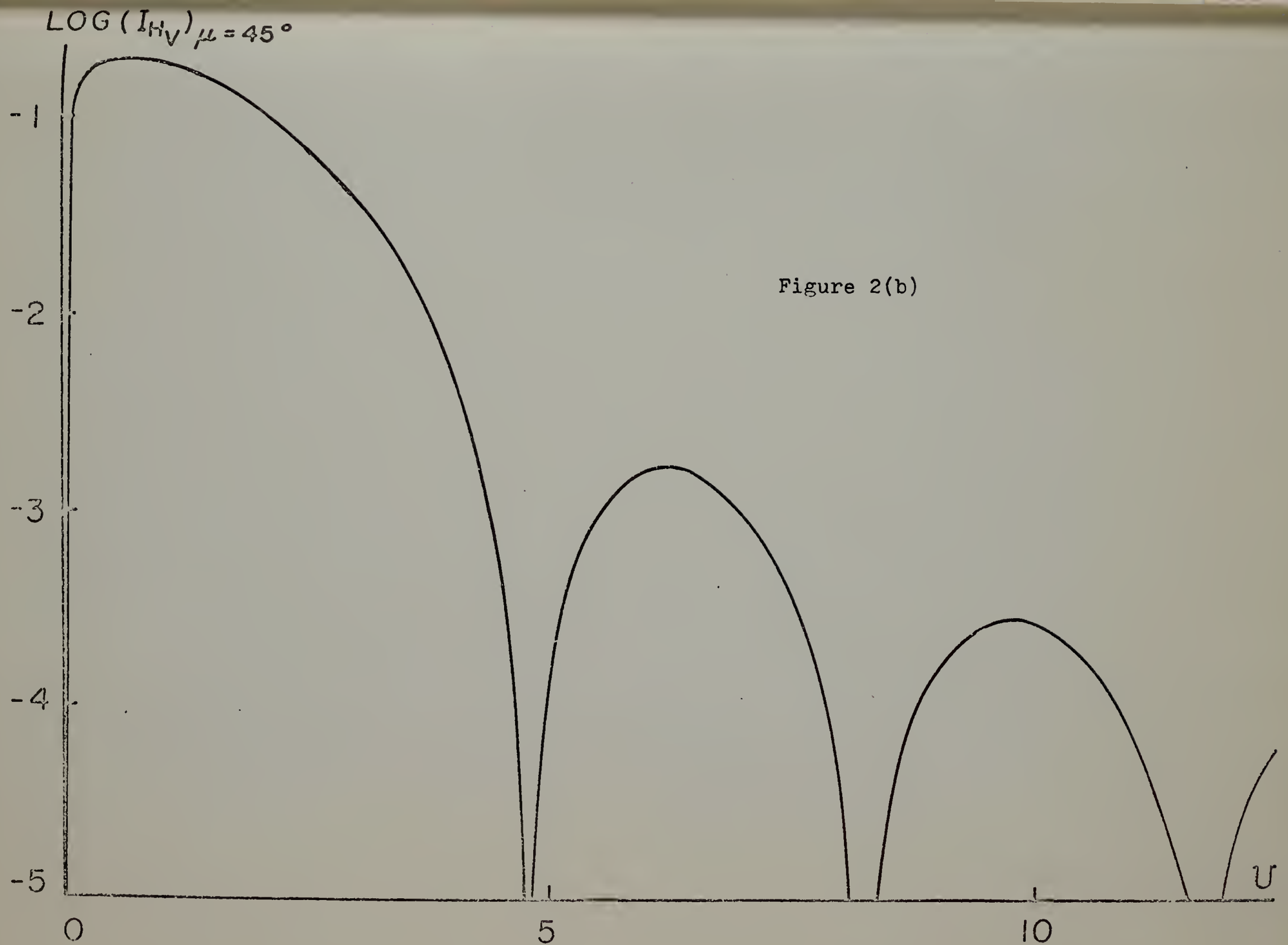

Figure 2(b)

Figure 3

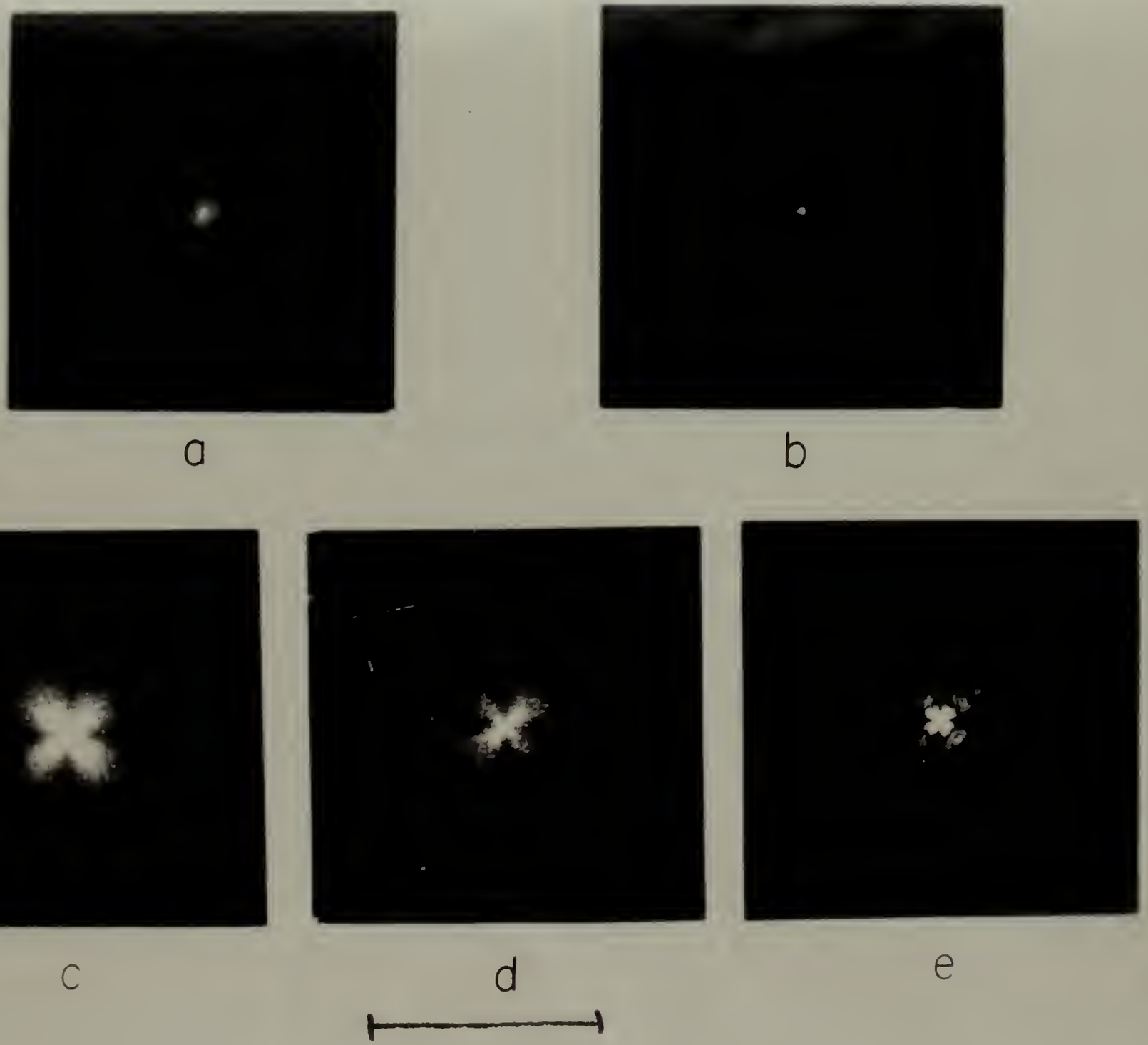
a
b
c
d
e

Figure 4

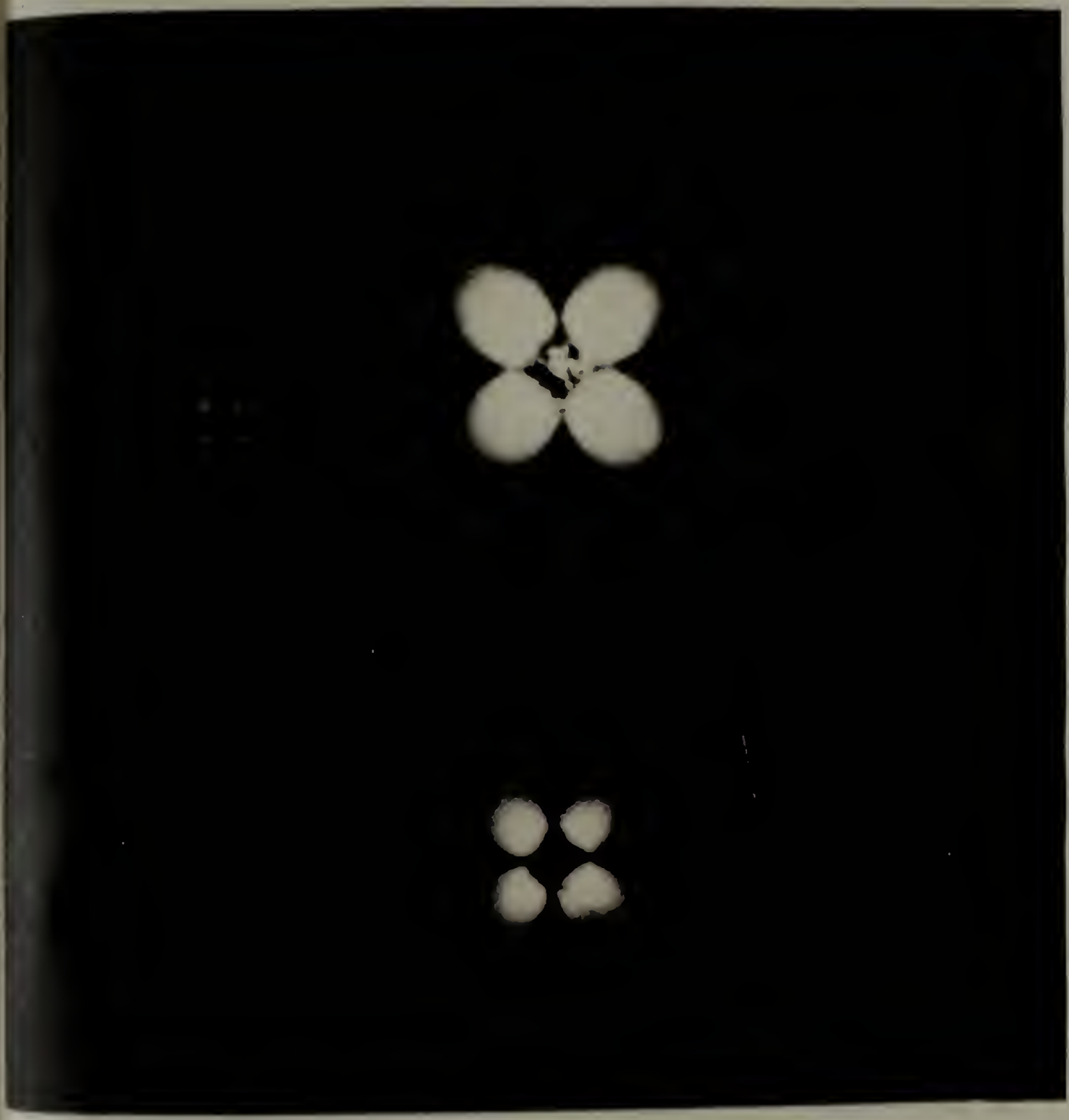

100μ

Figure 5

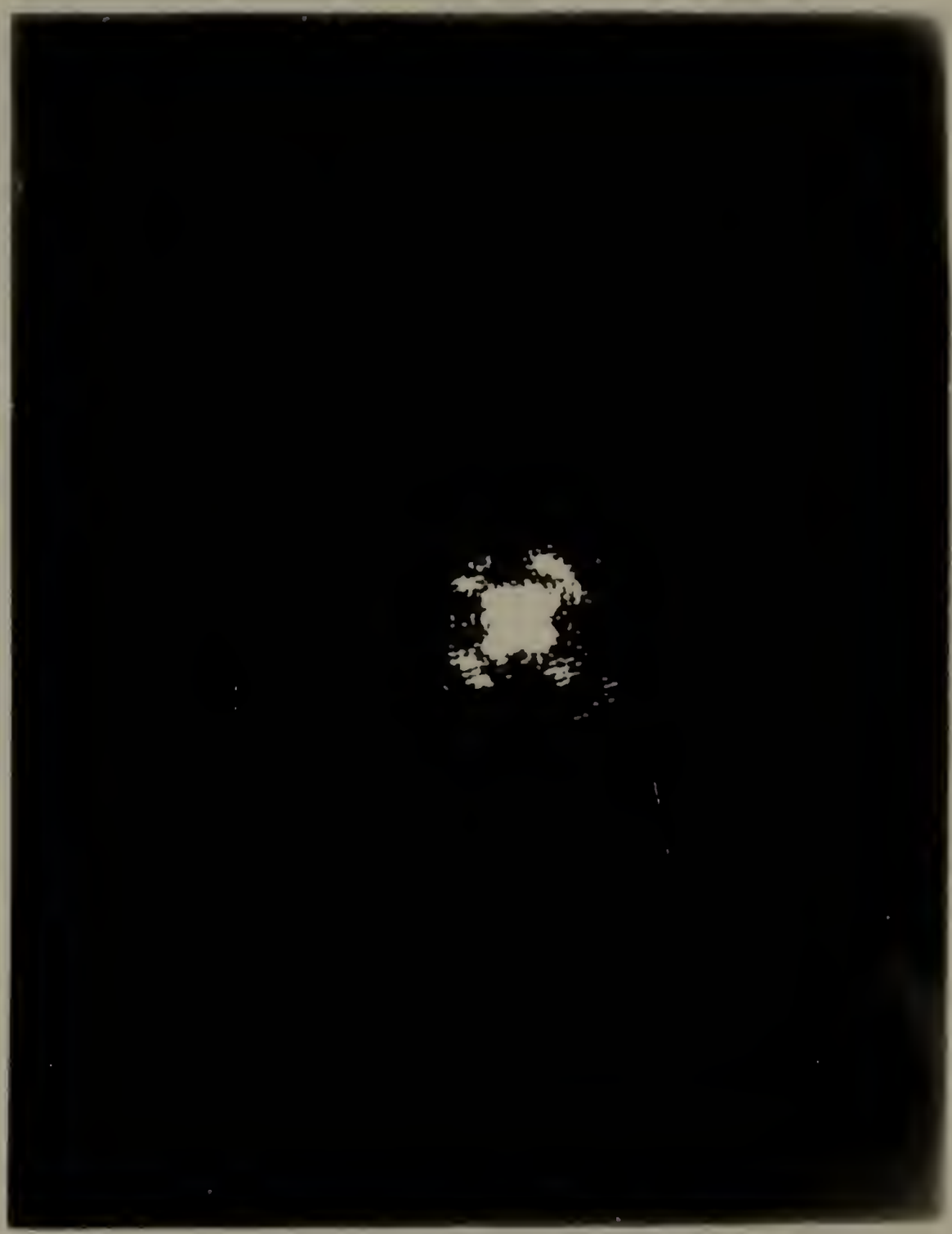

Figure 6

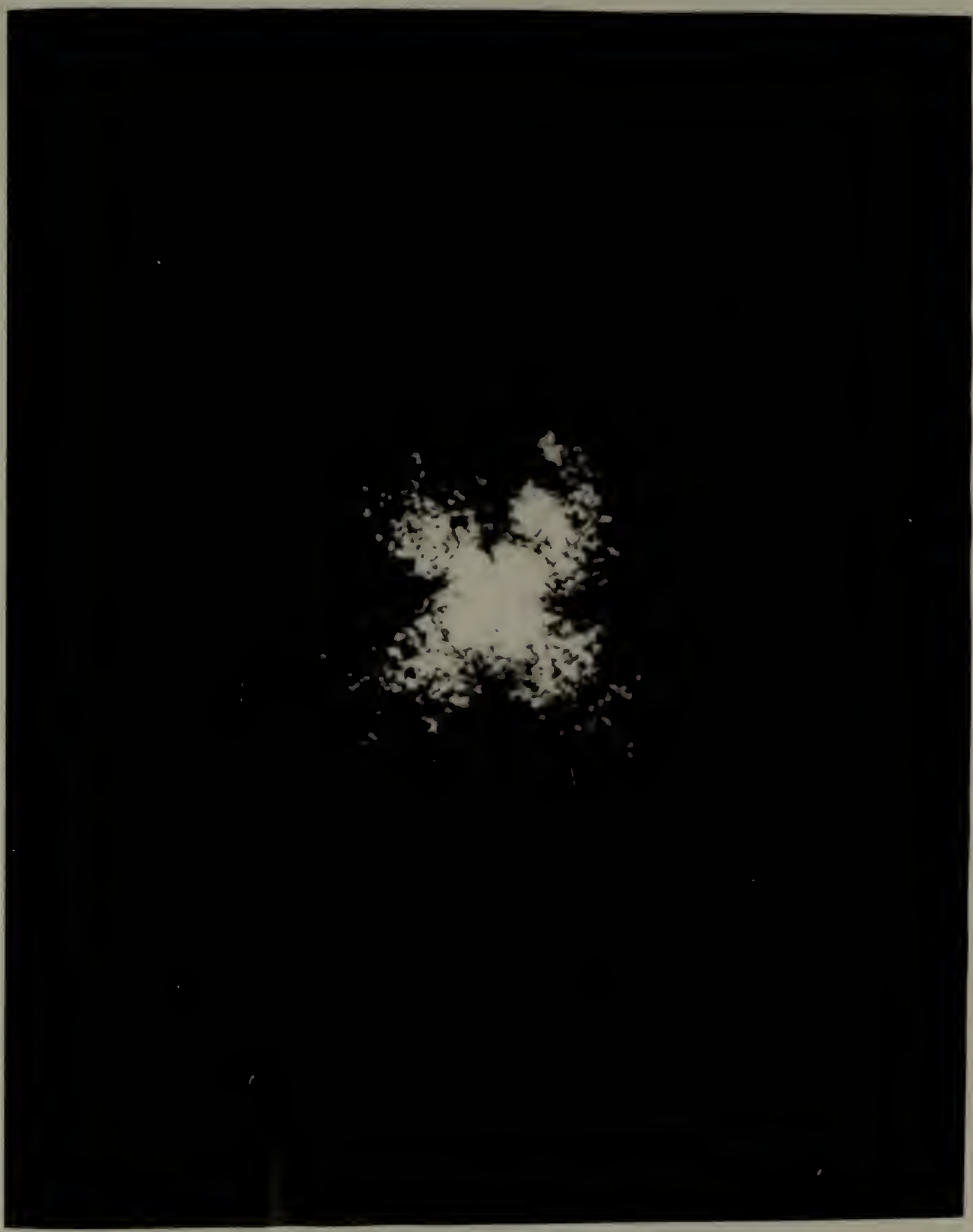

CHAPTER II

LIGHT SCATTERING AND BIREFRINGENCE STUDIES OF STRETCHED FILLED CIS-1,4-POLYBUTADIENE

Summary

The unusual eight-leaf H_v small angle light scattering patterns and birefringence patterns are shown to arise from the deformed region around the beads of a filled crosslinked rubber upon stretching. Goodier's theory and Jones Calculus were used to obtain the theoretical patterns; a good agreement was found between theoretical and experimental results.

Introduction

In the publications of Stein and Wilkes,[4] it was pointed out that light scattering patterns can originate from the deformed region surrounding voids and inclusions in high polymers. In a recent publication,[5] Fukuda, Picot, Ong (Chou) and Stein have reported that the four-leaf clover type H_v small angle light scattering pattern arises from the birefringence patterns associated with the inhomogeneous swelling in the vicinity of the particles.

When the filled crosslinked rubber is stretched in the dry state, assuming there is no separation of matrix from filler, classical elasticity analyses for single cavity and inclusion have been carried out by Goodier.[6] One finds that, for rigid spherical inclusion, at the

interface the rubber is subjected to a tensile stress along the stretching direction and to a compressive stress along the perpendicular direction. Shear stresses play an important role in the intermediate directions. This heterogeneous stress field will result in a complex biaxial birefringence pattern surrounding the inclusion and will contribute to the H_v small angle light scattering pattern. When the phase separation does occur at the polymer-filler interface, Goodier's classical theory no longer applies; the very pronounced density discontinuity becomes the dominant effect and will give rise to an intense V_v scattering pattern. In this work, the effects of sizes, concentrations and chemical bonding on the birefringence and light scattering patterns were also studied.

Experimental

Sample Preparation

High cis-1,4-(93%)polybutadiene samples were obtained from Phillips Petroleum Co. (Bartlesville, Okla.).

The starting polymer, which was purified by precipitation from benzene solution by methanol, was dissolved in benzene to give a 5 volume percent solution; after which 4% dicumyl peroxide, 1% antioxidant, 2-2'-methylene-bis(4 methyl-6 tertbutyl) phenol and glass beads were added, and the sample was cast into films of about 0.5 mm thickness on a Teflon pan. These were crosslinked by heating at 90°C for 20 min. and then heated to 140°C for 40 min. at 3000 psi pressure in a small laboratory press holding the films between sheets of cellophane.

The samples used contained different treatments of glass beads: beads uncoated and coated with organic silane of different concentrations (0.002 g/g and 0.0002 g/g), and beads of different sizes (0-5μm, 29μm and 290μm).

The procedures used to treat glass beads with organic silane were as follows. The beads were first washed with acetone, $CHCl_3$, and then treated with a 10% aqueous NaOH solution at 50°C for 1 hr. After washing, the beads were dipped in a 10% aqueous solution of Dow Corning Z-6020 silane coupling agent (N-β-aminoethyl-γ-aminopropyl trimethoxy silane) at room temperature for 30 min. These beads were then removed from the silane and dried in an oven below 110°C for 3 hrs.

In order to avoid aggregation of the beads, a high-speed electric blender was used to mix these treated glass beads with rubber benzene solution.

Birefringence Measurement

A Carl Zeiss polarizing microscope, movable mechanical stage and Ehringhaus rotary compensator were used to measure the retardations and slow directions of the birefringence pattern around the beads. In this case, the crosslinked rubber containing 290μm beads was used. Retardations and slow directions at different strain ratios were measured as a function of distance away from the center of the beads and as a function of azimuthal angle from 0° to 90°. For radial readings, 10 measurements were made; for angular readings, 5 measurements were made. Therefore, the retardations and slow directions of the whole birefringence pattern

were determined. The detailed measurement procedures are shown in Appendix I.

The photomicrographs of the transmittance intensity patterns at different strain ratios were obtained using a Carl Zeiss polarizing microscope with an attached camera. The photomicrographs were taken when the polarizer and analyzer were crossed.

Light Scattering Measurement

For light scattering measurements, 0-5μm and 29μm beads were used. Light scattering patterns at different strain ratios were recorded at room temperature by a low angle light scattering photographic setup developed in this laboratory.[7] The schematic arrangement for this setup is shown in Figure 1. A parallel monochromatic polarized light beam was provided from a laser source. The beam was passed normally through the sample, through an analyzer and finally onto a photographic film. Specimens with dimensions of 2 in. x 0.7 cm x (10-15) mils were used. The sample was stretched by a stretcher and was put on the stage of the equipment.

To avoid surface scattering by the film, both sides of the film were covered with microscope cover glasses using a silicon oil immersion fluid. The refractive index of the silicon oil was chosen to match that of the polymer film.

Negative films were used to record the light scattering patterns at 25% elongation. From these negative films, the relative scattering intensities along 25° and 70° azimuthal angles were measured with a

microdensitometer.

The "photographic calibration curve," the relationship between light intensity and film blackening, was determined as follows. In plotting the calibration curve, the ordinate is usually expressed by density D or % transmission Tr. If we set the unabsorbed beam as 100 units of intensity and the center of the pattern, the incident beam, as 0, then

$$D = \log_{10} (I_0/I) = \log_{10} (100/Tr) \qquad (1)$$

where I_0 = the intensity of the unabsorbed beam of light from the microdensitometer;

I = the intensity of the partly absorbed beam, after passing through an area of the photographic negative which has been exposed to light;

Tr = the transmission in percentage of intensity unit for an area of the negative being measured.

Figure 2 gives the photographic calibration curve, with log Tr% as ordinate and with log t (exposure time) as abscissa. Exposure is defined as

$$E = I \times t \qquad (2)$$

where I is the intensity of the source and t is exposure time.

For constant I, the exposure E is proportional to exposure time t. From this curve, the relative scattering intensities were determined

from the transmittance intensity obtained from the microdensitometer.

Light Scattering Results

When filled crosslinked rubber was stretched, an eight-leaf H_v small angle light scattering pattern was obtained, rather than the four-leaf clover type H_v pattern in the case of filled swollen crosslinked rubber.

The set of pictures in Figure 3 shows the changes in H_v small angle light scattering patterns during stretching. At 0% elongation, there was only a diffuse scattering pattern due to the imperfect extinction of polarizer and analyzer. The eight-leaf pattern first appeared at around 20% elongation, and the intensity of the eight-leaf pattern increased with strain. Besides that, an intensity variation was also found; the intensity increased with increasing strain at the beginning, then decreased and increased again at higher strain.

The unfilled crosslinked rubber was also studied. A series of H_v small angle light scattering patterns at different elongations are shown in Figure 4. In this case, there was only a diffuse H_v pattern which did not have an eight-leaf appearance. Its intensity was found to vary with strain. In comparing this with the filled case, it is reasonable to expect that the intensity variation is due to the sample itself and is not related to the beads, and that it might be due to the effect of heterogeneity of crosslinking.[8] Because of heterogeneous crosslinking, the local strain will not be uniform upon stretching. The more highly crosslinked parts of the network will deform less than the rest; this will lead to the occurrence of orientation fluctuations upon stretching

and will result in enhanced H_v scattering.

A series of V_v small angle light scattering patterns for filled rubber at different elongations are shown in Figure 5. In both filled and unfilled cases, the observation of no change in the shape and intensity of V_v patterns during stretching indicates that the results are primarily a consequence of density fluctuations which remain almost the same during stretching.

The effect of bead size on the H_v small angle light scattering patterns was studied. The H_v patterns for the 29μm bead and 0-5μm bead filled crosslinked rubber are shown in Figures 6(a) and 6(b). We found that the larger the beads, the smaller the eight-leaf H_v patterns and the higher the intensity, suggesting larger deformed regions around the beads. The effect of different concentrations of beads on the H_v pattern was also examined. The higher the concentration, the higher the intensity, as illustrated by the H_v patterns for the 0.0002 g/g and 0.002 g/g bead concentrations in Figures 7(b) and 7(a). We also concluded that the shape of the H_v pattern does not depend upon either size or concentration. (However, in very concentrated systems, where the decrease of localized surface stress at a given particle due to the perturbing effects of neighboring particles will be compensated by the increase in the number of scattering elements in the diameter of the light beam, it becomes more complicated.)

The H_v patterns for the filled sample in which glass beads were treated and that in which the beads were not treated with organic silane are shown in Figures 8(a) and 8(b). The shape and intensity of these

two patterns are almost the same.

In Figure 9, the V_v light scattering patterns of the filled sample in which glass beads were not treated with organic silane are presented for different elongations. There were no abrupt changes in the intensities of the patterns, indicating that there is no failure and void formation at the rubber-bead interface for the strain ratios up to 40%.

Polarizing Microscope Results

A series of photomicrographs of the transmittance light intensity patterns produced by stretching in the vicinity of a rigid spherical inclusion at various strain ratios, when viewed between crossed polaroids, are shown in Figure 10. The 0% elongation picture is shown in Figure 10(a); it possesses a four-fold symmetry and exhibits a four-leaf clover pattern similar to the patterns obtained in the swollen case. Such a pattern must originate from an initial stress, which is caused by the different contractions of rubber matrix and beads in cooling. For the 3% elongated sample, the four lobes shift toward a direction perpendicular to the stretching direction, as shown in Figure 10(b). For the 7% elongated sample, four additional lobes appear with a ±25° orientation, but these have a lower intensity than the original four as shown in Figure 10(c). As the strain increases, the intensity of the additional four lobes continues to increase. As the strain ratio reaches 12% elongation, as shown in Figure 10(d), the intensity of the eight lobes becomes almost the same.

Contour plots of retardations for elongations of 6% and 12% are

given in Figure 11 and Figure 12. The data are presented as a function of reduced distances r/a and azimuthal angle α, where a is the radius of the glass bead. It is clearly seen that retardations at 90° are larger than those at 0° for the 6% elongation sample, but that they become pretty close as the strain goes up to 12% elongation.

The slow direction contour plots for elongations of 6% and 12% are given in Figure 13 and Figure 14. The marked value is the angle between the slow direction and 0° (the stretching direction). The positive sign means counterclockwise and the negative sign means clockwise. We can also see that the size difference between two lobes becomes smaller as the strain increases.

Theoretical Calculation

Goodier's Theory

The problem, that of determining the stresses in the neighborhood of a spherical particle of radius a imbedded in an elastic medium of infinite extent--the latter being subjected to a uniform tension T at infinity--has been considered by Goodier.[9] For a rigid inclusion, the normal stresses and shear stresses as a function of distance r and azimuthal angle θ from the center of the particle, as shown in Figure 15, are given by the following equations:

$$\frac{\sigma rr}{T} = \left[\frac{1-\mu}{1+\mu} + \frac{3+5\mu}{4(4-5\mu)}\right]\left(\frac{a}{r}\right)^3 - \frac{3}{2(4-5\mu)}\left(\frac{a}{r}\right)^5$$

$$+ \left[\frac{-18\left(\frac{a}{r}\right)^5 + 5(5-\mu)\left(\frac{a}{r}\right)^3}{4(4-5\mu)}\right]\cos 2\theta + \frac{1}{2}(1+\cos 2\theta) \qquad (3)$$

$$\frac{\sigma\theta\theta}{T} = -\frac{1}{2}\left[\frac{1-\mu}{1+\mu} + \frac{3-10\mu}{4(4-5\mu)}\right]\left(\frac{a}{r}\right)^3 + \frac{3}{8(4-5\mu)}\left(\frac{a}{r}\right)^5$$

$$+ \left[\frac{21\left(\frac{a}{r}\right)^5 - 5(1-2\mu)\left(\frac{a}{r}\right)^3}{8(4-5\mu)}\right]\cos 2\theta + \frac{1}{2}(1-\cos 2\theta) \qquad (4)$$

$$\frac{\sigma\phi\phi}{T} = -\frac{1}{2}\left[\frac{1-\mu}{1+\mu} - \frac{7-10\mu}{4(4-5\mu)}\right]\left(\frac{a}{r}\right)^3 + \frac{9\left(\frac{a}{r}\right)^5}{8(4-5\mu)}$$

$$+ \frac{15}{8(4-5\mu)}\left[\left(\frac{a}{r}\right)^5 - (1-2\mu)\left(\frac{a}{r}\right)^3\right]\cos 2\theta \qquad (5)$$

$$\frac{\sigma r\theta}{T} = \left[\frac{5(1+\mu)\left(\frac{a}{r}\right)^3}{4(4-5\mu)} - \frac{3}{(4-5\mu)}\left(\frac{a}{r}\right)^5\right] \sin 2\theta - \frac{1}{2}\sin 2\theta \qquad (6)$$

where a is the radius of the inclusion;

μ is Poission's ratio of the rubber matrix;

θ is the azimuthal angle;

ϕ is the angle in the plane $\perp$ to the applied tension; and

T is the applied uniaxial tension.

Figure 16 gives an example of the variations of σrr, $\sigma\theta\theta$, and $\sigma r\theta$ as a function of azimuthal angle θ at reduced distance $r/a = 1.1$.

Figure 17 is a polar plot of radial stress σrr and tangential stress $\sigma\theta\theta$ as a function of azimuthal angle θ at reduced distance $r/a = 1.1$.

Initial Stress Consideration

The stress concentration around the inclusion induced by the applied tensile stress is usually aided by the other effect, local residue stress due to different contractions of surrounding medium and inclusion in cooling. This residual stress can be expressed by the following equations proposed by Goldstein:[10]

$$Pr = -\frac{a^3 P_a}{r^3} \qquad (7)$$

$$Pt = \frac{1}{2} \cdot \frac{a^3 P_a}{r^3} \qquad (8)$$

where Pr is the radial stress;

Pt is the tangential stress;

a is the radius of the inclusion; and

-Pa is the hydrostatic pressure in the center of the inclusion.

Principal Stress Calculation

When such a filled rubber is stretched, an inhomogeneous stress field surrounding the beads is produced. The birefringence at each point (r, θ, ϕ) can be determined completely from a knowledge of the local configuration of optical indicatrix whose principal semi-axes are the principal refractive indices n_1, n_2 and n_3, which can be determined from known values for principal stresses P_1, P_2 and P_3 at each point. From this information, the birefringence and light scattering patterns can be calculated.

Since $\sigma r\theta$ is the only non-zero shear stress, $(\sigma\phi\phi + Pt)$ is one principal stress; the two remaining principal stresses are obtained by a rotation of axes in the plane, as shown in Figure 18.

According to tensor transformation law, the following relation must hold:

$$\begin{pmatrix} P_1 & 0 \\ 0 & P_2 \end{pmatrix} = \begin{pmatrix} \cos\Delta\theta & \sin\Delta\theta \\ -\sin\Delta\theta & \cos\Delta\theta \end{pmatrix} \begin{pmatrix} \sigma rr + Pr & \sigma r\theta \\ \sigma r\theta & \sigma\theta\theta + Pt \end{pmatrix} \begin{pmatrix} \cos\Delta\theta & -\sin\Delta\theta \\ \sin\Delta\theta & \cos\Delta\theta \end{pmatrix} \quad (9)$$

By solving this, the rotation angle $\Delta\theta$ and P_1, P_2 and P_3 can be expressed in the following ways:

$$\tan 2\Delta\theta = \frac{2\,\sigma r\theta}{(\sigma rr + Pr) - (\sigma\theta\theta + P\theta)} \tag{10}$$

$$P_1 = (\sigma rr + Pr)\cos^2\Delta\theta + 2\,\sigma r\theta \sin\Delta\theta \cos\Delta\theta + (\sigma\theta\theta + Pt)\sin^2\Delta\theta \tag{11}$$

$$P_2 = (\,rr + Pr)\sin^2\Delta\theta - 2\,\sigma r\theta \sin\Delta\theta \cos\Delta\theta + (\sigma\theta\theta + Pt)\cos^2\Delta\theta \tag{12}$$

$$P_3 = \sigma\phi\phi + Pt \tag{13}$$

Birefringence-Stress Relationship

The birefringence of uniaxially stretched rubber can be expressed by the relationship[11]

$$n = C \cdot \sigma \tag{14}$$

where C is the stress optical coefficient of the rubber network and σ is applied stress.

For a biaxial indicatrix,[12] three principal refractive indices--n_1, n_2, n_3--can be calculated from Eqn. (14):

$$\begin{aligned} n_1 - n_2 &= C \times (P_1 - P_2) \\ n_2 - n_3 &= C \times (P_2 - P_3) \\ n_1 - n_3 &= C \times (P_1 - P_3) \end{aligned} \tag{15}$$

For our purposes, the actual magnitude of the indicatrix is unimportant, so that we may take one semi-axis to be fixed and reduce the number of independent parameters to two: n_1/n_2, n_3/n_2. In this case, we take $n_2 = 1.5$, and then n_1 and n_3 can be determined accordingly.

Light Scattering Calculation

In the Raleigh-Gans approximation, the light scattering amplitude E of an anisotropic system is given by[13]

$$E = C' \int (\underset{\sim}{M} \cdot \underset{\sim}{O}) \exp [ik (\underset{\sim}{r} \cdot \underset{\sim}{s})] \, d\underset{\sim}{r} \tag{16}$$

where C' = constant;

$\underset{\sim}{M}$ = induced dipole moment in the scattering element located by the vector $\underset{\sim}{r}$;

$\underset{\sim}{O}$ = unit vector perpendicular to the scattered ray and in the plane of polarization of the light transmitted by the analyzer;

k = $2\pi/\lambda$ wave number in the medium;

λ = wavelength of the light in the medium; and

$\underset{\sim}{s}$ = propagation vector $(\underset{\sim}{s}_o - \underset{\sim}{s}')$ where $\underset{\sim}{s}_o$ and $\underset{\sim}{s}'$ are the unit incident and scattered beam vectors.

However, in order to calculate the integral, it is necessary to find expressions for $\underset{\sim}{M}$ and $\underset{\sim}{O}$. The value of $\underset{\sim}{M}$ is given by

$$\underset{\sim}{M} = \alpha_1(\underset{\sim}{E} \cdot \underset{\sim}{a})\underset{\sim}{a} + \alpha_2(\underset{\sim}{E} \cdot \underset{\sim}{b})\underset{\sim}{b} + \alpha_3(\underset{\sim}{E} \cdot \underset{\sim}{c})\underset{\sim}{c} \tag{17}$$

where $\underset{\sim}{E}$ is the vector of the incident beam, and $\underset{\sim}{a}$, $\underset{\sim}{b}$ and $\underset{\sim}{c}$ are the three unit vectors along the three principal directions of a biaxial indicatrix whose three principal polarizabilities are α_1, α_2, and α_3 respectively.

Consider point L (r, θ, ϕ) in a three-dimensional cartesian coordinate system as shown in Figure 19. Assuming the polarizer as being along Z direction and the analyzer as being along Y direction, it can be seen that the vectors $\underset{\sim}{E}$ and $\underset{\sim}{O}$ will be

$$\underset{\sim}{E} = E_o \cdot \underset{\sim}{k} \tag{18}$$

$$\underset{\sim}{O} = E_o \cdot \underset{\sim}{j} \tag{19}$$

The relations between $\underset{\sim}{a}$, $\underset{\sim}{b}$, $\underset{\sim}{c}$ and $\underset{\sim}{x}$, $\underset{\sim}{y}$, $\underset{\sim}{z}$ can be obtained as follows:

$$\begin{aligned}\underset{\sim}{a} = {} & (\cos\Delta\theta \sin\theta \cos\phi + \sin\Delta\theta \cos\theta \cos\phi)\ \underset{\sim}{i} + \\ & (\cos\Delta\theta \sin\theta \sin\phi + \sin\Delta\theta \sin\phi \cos\theta)\ \underset{\sim}{j} + \\ & (\cos\Delta\theta \cos\theta - \sin\Delta\theta \sin\theta)\ \underset{\sim}{k}\end{aligned} \tag{20}$$

$$\begin{aligned}\underset{\sim}{b} = {} & (\cos\Delta\theta \cos\theta \cos\phi - \sin\Delta\theta \sin\theta \cos\phi)\ \underset{\sim}{i} + \\ & (-\sin\Delta\theta \sin\theta \sin\phi + \cos\Delta\theta \sin\phi \cos\theta)\ \underset{\sim}{j} - \\ & (\sin\Delta\theta \cos\theta + \cos\Delta\theta \sin\theta)\ \underset{\sim}{k}\end{aligned} \tag{21}$$

$$\underset{\sim}{c} = -\sin\phi\ \underset{\sim}{i} + \cos\phi\ \underset{\sim}{j} \tag{22}$$

The resulting values for $(\underset{\sim}{M} \cdot \underset{\sim}{0})_{H_v}$ will thus be given by

$$(\underset{\sim}{M} \cdot \underset{\sim}{0})_{H_v} = \alpha_1(\underset{\sim}{E} \cdot \underset{\sim}{a})\ (\underset{\sim}{a} \cdot \underset{\sim}{0}) + \alpha_2(\underset{\sim}{E} \cdot \underset{\sim}{b})\ (\underset{\sim}{b} \cdot \underset{\sim}{0}) + \alpha_3(\underset{\sim}{E} \cdot \underset{\sim}{c})\ (\underset{\sim}{c} \cdot \underset{\sim}{0})$$

$$= (\alpha_1 - \alpha_2)\ (\cos^2\Delta\theta \cos\theta \sin\theta - \sin\Delta\theta \cos\Delta\theta \sin^2\theta + \cos\Delta\theta \sin\Delta\theta \cos^2\theta - \sin^2\Delta\theta \sin\theta \cos\theta) \sin\phi \qquad (23)$$

$(\alpha_1 - \alpha_2)$ is related to the birefringence $(n_1 - n_2)$ by this relation:[14]

$$\alpha_1 - \alpha_2 = \frac{9}{2\pi} \cdot \frac{\bar{n}}{(\bar{n}^2 + 2)^2} (n_1 - n_2)$$

$$= \frac{9}{2\pi} \cdot \frac{\bar{n}}{(\bar{n}^2 + 2)^2} (P_1 - P_2) \cdot C \qquad (24)$$

By combining (16) with (23) and (24), it can be shown that

$$E_{H_v} = C' \times C \times \frac{9}{2\pi} \times \frac{\bar{n}}{(\bar{n}^2 + 2)^2} \int_{\theta=0}^{\pi} \int_{r=a}^{\infty} (P_1 - P_2)$$
$$(\cos^2\Delta\theta \cos\theta \sin\theta - \sin\Delta\theta \cos\Delta\theta \sin^2\theta +$$
$$\cos\Delta\theta \sin\Delta\theta \cos^2\theta - \sin^2\Delta\theta \sin\theta \cos\theta) \times$$
$$I \times \sin\theta\ r^2\ dr\ d\theta \qquad (25)$$

where $I = -2\pi \sin (2kr \sin\frac{\theta'}{2} \cos\frac{\theta'}{2} \cos\theta)\, J_1(2kr \sin\frac{\theta'}{2} \cos\frac{\theta'}{2} \sin\mu \sin\theta)$;

$J_1(x)$ is the first order Bessel function of x;

θ' is the scattering angle; and

μ is the azimuthal angle.

Different values of applied tensile stress T, which were determined from stress-strain measurement for different strain ratios, were used; the hydrostatic pressure P_a which was determined from the retardation measurement at 0% elongation, as shown in Figure 20, was assumed to change affinely with applied tensile stress. From this, the values of P_1, P_2, P_3 and $\Delta\theta$ were calculated easily. By substituting these values into Eqn. (25) we calculated the scattered intensity distribution ($I_{H_v} = E_{H_v} \times E_{H_v}$) by numerical integration with the CDC 3600 computer at the University of Massachusetts Research Computing Center. The computer program for the calculations is given in Appendix II.

The theoretical H_v light scattering patterns for different elongations (0%, 8%, 20%, and 30%) observed in the polar coordinates (θ', μ) are given in Figures 21, 22, 23 and 24, in which the differences in the character of the scattering patterns are clearly seen. In comparing these with Figure 3, we found that the calculated 0% and 8% patterns differed from those observed in the experiment. For 0% elongation we believe that the intensity of the four-lobe pattern is too weak to be recorded; for 8% elongation it is due to both the weak intensity of the pattern and the interference of the intensity variation discussed before. With increasing size of the glass sphere, the scattering

occurs at smaller angles.

The relative small angle H_v scattering intensities, measured with a microdensitometer as a function of scattering angle θ', are given in Figure 25 and Figure 26 for azimuthal angles 25° and 70° at 25% elongation. They were compared with the calculated values. It is noted that the positions and values of maximum intensity agree well with the calculated ones, but the scattering intensity falls off more rapidly with scattering angle for the theoretical value than for the measured value. The deviations may be explained by the fact that the interference effect between strained regions, the multiple scattering effect, and size distribution of glass beads were neglected.

Birefringence Calculations

The inhomogeneous stress field of a stretched elastomer matrix containing a rigid, spherical inclusion has been described above.

The cylindrical symmetry of the stress field produced by stretching is illustrated in Figure 19 and is characterized by three principal stresses P_1, P_2 and P_3, which represent the three principal components of the stress tensor. This anisotropic deformation state results in a birefringence field which can be determined completely from a knowledge of the local configuration of the optical indicatrix whose principal semi-axes are the principal refractive indices n_1, n_2 and n_3 of the optical indicatrix. In general, a birefringence crystal restricts the character of the light which it transmits in a given direction with a given wave normal $\underset{\sim}{1}$ to only two possible rays, plane-polarized in

mutually perpendicular planes and traveling with different phase velocities. The indicatrix serves to determine these planes of polarization and phase velocities in the following way: a diametral section of the indicatrix normal to $\underset{\sim}{1}$ is an ellipse, the ellipse of the section, whose principal semi-axes lie in the allowed polarization planes and denote by their lengths the refractive indices for the rays. The major semi-axis indicates the refractive index for the slow ray whose electric vector vibrates in a direction parallel to it, and the minor semi-axis gives the corresponding information for the fast ray. In the case of a stretched, filled rubber under examination on the horizontal stage of a polarizing microscope, therefore, the observed retardation in any selected small area is an additive value which is determined by the horizontal diametral sections of all the indicatrixes oriented along the light beam path.

Consider a stretched sample on the horizontal stage of a polarizing microscope. Let us take coordinate axes OY and OZ in the directions parallel to the analyzer and polarizer (OZ is also the stretching direction) respectively, and center on O, the center of the glass sphere. The axis OX is parallel to the axis of the microscope (the incident beam direction) as shown in Figure 27. Let the thickness of the sample be $2H_0$; it can be divided into m divisions. Assume each division is a single optical indicatrix in a determinable orientation. In order to calculate the retardation of light at a point Q which is at a distance r from the center of projection of the inclusion onto the polarizer-analyzer plane, at an angle α with respect to the

polarizer axis, it is necessary to determine the orientations of the principal axes of the ellipse of section in the YZ plane at point Q for all divisions which lie on a line parallel to the transmission axis. Holding r, α and H constant, i.e. r, θ, and ϕ constant, the three principal directions $\underset{\sim}{a}$, $\underset{\sim}{b}$ and $\underset{\sim}{c}$ of the three principal stresses P_1, P_2 and P_3 for each division can be calculated by three rotations:

$$\begin{pmatrix} \underset{\sim}{b} \\ \underset{\sim}{c} \\ \underset{\sim}{a} \end{pmatrix} = \begin{pmatrix} \cos\Delta\theta & 0 & -\sin\Delta\theta \\ 0 & 1 & 0 \\ \sin\Delta\theta & 0 & \cos\Delta\theta \end{pmatrix} \begin{pmatrix} \cos\theta & 0 & -\sin\theta \\ 0 & 1 & 0 \\ \sin\theta & 0 & \cos\theta \end{pmatrix} \begin{pmatrix} \cos\phi & \sin\phi & 0 \\ -\sin\phi & \cos\phi & 0 \\ 0 & 0 & 1 \end{pmatrix} \begin{pmatrix} \underset{\sim}{x} \\ \underset{\sim}{y} \\ \underset{\sim}{z} \end{pmatrix} \tag{26}$$

So,

$$\underset{\sim}{a} = (\sin\Delta\theta\ \cos\theta\ \cos\phi + \cos\Delta\theta\ \sin\theta\ \cos\phi)\ \underset{\sim}{i} + (\sin\Delta\theta\ \cos\theta\ \sin\phi + \cos\Delta\theta\ \sin\theta\ \sin\phi)\ \underset{\sim}{j} + (-\sin\theta\ \sin\Delta\theta + \cos\theta\ \cos\Delta\theta)\ \underset{\sim}{k} \tag{27}$$

$$\underset{\sim}{b} = (\cos\Delta\theta\ \cos\theta\ \cos\phi - \sin\Delta\theta\ \sin\theta\ \cos\phi)\ \underset{\sim}{i} + (\cos\Delta\theta\ \cos\theta\ \sin\phi - \sin\Delta\theta\ \sin\theta\ \sin\phi)\ \underset{\sim}{j} - (\sin\theta\ \cos\Delta\theta + \sin\Delta\theta\ \cos\theta)\ \underset{\sim}{k} \tag{28}$$

$$\underset{\sim}{c} = -\sin\phi\ \underset{\sim}{i} + \cos\phi\ \underset{\sim}{j} \tag{29}$$

The indicatrix is a tensor ellipsoid, that is, the geometrical representation of the impermeability tensor N which relates the electric and displacement vectors of the radiation field by the equation[16]

$$E = ND \tag{30}$$

The relation between the element N_{ij} and the principal refractive indices is as follows: if the indicatrix is referred to its principal axes, the matrix N becomes diagonal with elements which we shall denote by N_1, N_2 and N_3, where $N_1 = 1/n_1^2$, $N_2 = 1/n_2^2$, $N_3 = 1/n_3^2$ and n_1, n_2 and n_3 are principal refractive indices.

$$N = \begin{pmatrix} 1/n_2^2 & 0 & 0 \\ 0 & 1/n_3^2 & 0 \\ 0 & 0 & 1/n_1^2 \end{pmatrix} \tag{31}$$

Now when the indicatrix is rotated with respect to fixed coordinate axes, a rotated indicatrix N' instead of N shall be used:

$$N' = R^{-1} NR \tag{32}$$

R, the matrix operator describing the rotation, is defined as

$$\begin{pmatrix} \underset{\sim}{b} \\ \underset{\sim}{c} \\ \underset{\sim}{a} \end{pmatrix} = (R) \begin{pmatrix} \underset{\sim}{x} \\ \underset{\sim}{y} \\ \underset{\sim}{z} \end{pmatrix} \tag{33}$$

The desired ellipse of section in the YZ plane is determined by only three elements of N', which are N_{22}', N_{23}' and N_{33}' respectively. Its equation is

$$N_{22}' y^2 + 2N_{23}' yz + N_{33}' z^2 = 1 \tag{34}$$

In general, an ellipse with principal axes oriented at angle β relative to OY, OZ axes and principal refractive indices a and b, as shown in Figure 28, can be written as

$$\left(\frac{\cos^2\beta}{b^2} + \frac{\sin^2\beta}{a^2}\right) y^2 + 2 \sin\beta \cos\beta \left(\frac{1}{b^2} - \frac{1}{a^2}\right) yz + \left(\frac{\cos^2\beta}{a^2} + \frac{\sin^2\beta}{b^2}\right) z^2 = 1 \tag{35}$$

Comparing Eqn. (34) and Eqn. (35), we obtain

$$\beta = \frac{1}{2} \tan^{-1} \left(\frac{2N_{23}'}{N_{22}' - N_{33}'}\right) \tag{36}$$

$$a = \left[\frac{N_{22}' - \cos^2\beta\ (N_{22}' + N_{33}')}{(1 - 2\cos^2\beta)}\right]^{-1/2} \tag{37}$$

$$b = \left[(N_{22}' + N_{33}') - \frac{N_{22}' - \cos^2\beta\ (N_{22}' + N_{33}')}{(1 - 2\cos^2\beta)}\right]^{-1/2} \tag{38}$$

Each division with thickness t can be considered as a single retardation plate and can be represented mathematically by a two by two complex matrix called a Jones matrix:[17]

$$(A_j) = \begin{pmatrix} \cos^2\beta_j\ e^{i\delta j/2} + \sin^2\beta_j\ e^{-i\delta j/2} & \cos\beta_j\ \sin\beta_j\ 2i\ \sin\delta_j/2 \\ \cos\beta_j\ \sin\beta_j\ 2i\ \sin\delta_j/2 & \cos^2\beta_j\ e^{-i\delta j/2} + \sin^2\beta_j\ e^{i\delta j/2} \end{pmatrix} \tag{39}$$

where β_j is the angle of the fast axis relative to the OY axis, and δ_j is the retardation, $= 2\pi\ t/\lambda\ |(a - b)|$.

For m divisions, there are m matrices (A_1), (A_2), $\cdots\cdots\cdots(A_m)$ with respective orientations β_1, β_2, $\cdots\cdots\cdots\beta_m$. Suppose that the light passes through the elements in the order in which they are numbered; we then have

$$
\begin{aligned}
E_1 &= (A_1)\, E_0 \\
E_2 &= (A_2)\, E_1 \\
E_3 &= (A_3)\, E_2 \\
&\vdots \\
E_m &= (A_m)\, E_{m-1}
\end{aligned}
\tag{40}
$$

where E_0 is the light vector of the incident beam and E_i is the light vector as it emerges from the ith retardation plate. By substituting each of the equations (40) in the one following it, we have at once the relation between E_m and E_0:

$$E_m = (A_m)\,(A_{m-1}) \cdots\cdots (A_3)\,(A_2)\,(A_1)\, E_0 = (B)\, E_0 \tag{41}$$

and

$$(B) = (A_m)\,(A_{m-1}) \cdots\cdots (A_2)\,(A_1) \tag{42}$$

It has been proved[18] that for the light of a given wavelength, an optical system which contains any number of retardation plates and rotators is optically equivalent to a system containing only two plates --one a retardation plate, and the other a rotator. Eqn. (42) can be written in an equivalent form:

$$(B) = \begin{pmatrix} B_{11} & B_{12} \\ B_{21} & B_{22} \end{pmatrix}$$

$$= \begin{pmatrix} \cos^2\gamma_Q \, e^{i\delta_Q/2} + \sin^2\gamma_Q \, e^{-i\delta_Q/2} & 2i \cos\gamma_Q \sin\gamma_Q \sin\delta_Q/2 \\ 2i \cos\gamma_Q \sin\gamma_Q \sin\delta_Q/2 & \cos^2\gamma_Q \, e^{-i\delta_Q/2} + \sin^2\gamma_Q \, e^{i\delta_Q/2} \end{pmatrix}$$

$$\times \begin{pmatrix} \cos\omega_Q & -\sin\omega_Q \\ \sin\omega_Q & \cos\omega_Q \end{pmatrix} \tag{43}$$

And by some mathematical manipulation, we can get

$$\gamma_Q = \frac{1}{2}\left[-\omega_Q + \tan^{-1}\frac{(B_{12} + B_{21})}{(B_{11} - B_{22})}\right] \tag{44}$$

$$\omega_Q = \tan^{-1}\frac{(B_{21} - B_{12})}{(B_{11} + B_{22})} \tag{45}$$

$$\delta_Q = 2\cos^{-1}\frac{(B_{11} + B_{22})}{2\cos\omega_Q} \tag{46}$$

where δ_Q is the retardation in radians for point Q in the YZ plane, and $(\gamma_Q + \omega_Q)$ is the angle of the fast direction relative to the OY axis for point Q.

We are also interested in the values of transmittance intensity at point Q. Since the matrix B is known, then the following relation can be obtained:

$$E_m = (B)\, E_0 \tag{41}$$

When the polarizer and analyzer are crossed, it can be written as

$$\begin{pmatrix} E_{ym} \\ E_{zm} \end{pmatrix} = (0 \quad 1) \begin{pmatrix} B_{11} & B_{12} \\ B_{21} & B_{22} \end{pmatrix} \begin{pmatrix} 1 \\ 0 \end{pmatrix} \tag{47}$$

So,

$$E_{ym} = 0 \qquad \text{and} \qquad E_{zm} = B_{21}$$

The transmittance intensity

$$I_t = K\, E_{zm}\, E_{zm}^* = K\, B_{21}\, B_{21}^* \tag{48}$$

By varying the values of r and α, the entire retardation contour

diagram, slow direction contour diagram and transmittance intensity contour diagram can be obtained. The computer program for carrying out these operations is given in Appendix III.

In Figures 29, 30, 31, 32, 33, 34, 35, 36 and 37, the theoretical slow direction contour diagrams, the theoretical retardation contour diagrams and the theoretical transmittance intensity contour diagrams for different elongations 0%, 8% and 20% are shown. In comparing with Figures 10, 11, 12, 13 and 14, good agreement was found between theory and experiments.

Conclusions

Light scattering studies and polarizing microscope studies provide new experimental techniques for analysis of stress distribution in filled elastomers. The polarizing microscope is useful to study a large single filler in the filled system. The light scattering technique can be applied to the system in which much smaller fillers are used in order to obtain information about average properties of the system. The authors hope that this work can be extended to any two-phase system in which the moduli of two phases are different, such as the stress induced crystallization of rubbers in which the crystallite is growing in the rubber matrix by stretching. An eight-lobe H_v pattern was obtained in the case of stress induced crystallization of rubber[19] in which crystals may grow in an ellipsoidal aggregate whose long axis is perpendicular to the stretching direction in the rubber matrix by stretching; the

contribution of strained amorphous polymer around crystallites may explain this phenomenon.

References

1. P. J. Flory, "Principles of Polymer Chemistry," Cornell University Press, Ithaca, New York, 1953, Chapter XI.
2. J. Scanlan, Rev. Gen. Gauoth, 41, 514 (1964).
3. T. Kotani and S. S. Sternstein, in "Polymer Networks: Structural and Mechanical Properties," A. J. Chompff and S. Newman, eds., Plenum Press, New York, New York.
4. R. S. Stein and G. L. Wilkes, J. Polymer Sci., A-2, 7, 1696 (1969).
5. C. Picot, M. Fukuda, C. Ong (Chou), and R. S. Stein, J. Macromol. Sci.-Phys., B6(1), 263 (1972).
6. J. N. Goodier, Appl. Mechanics (Trans. Am. Soc. Mech. Engrs.), 1, No. 2, 39 (1933).
7. M. B. Rhodes, D. A. Keedy, and R. S. Stein, J. Polymer Sci., 62, 73 (1962).
8. R. S. Stein, J. Polymer Sci., B7, 657 (1969).
9. J. N. Goodier, Appl. Mechanics (Trans. Am. Soc. Mech. Engrs.), 1, No. 2, 39 (1933).
10. M. Goldstein, J. Appl. Phys., 30, 501 (1959).
11. L. R. G. Treloar, "The Physics of Rubber Elasticity," Oxford Press, 1958.
12. E. M. Chamot and C. W. Mason, "Handbook of Chemical Microscopy, Vol. 1," John Wiley and Sons, New York, New York.
13. H. C. Van de Hulst, "Light Scattering by Small Particles," Wiley, New York, New York, 1957.

14. L. R. G. Treloar, "The Physics of Rubber Elasticity," Oxford Press, 1958.

16. J. F. Nye, "Physical Properties of Crystals," Oxford University Press, 1960.

17. R. C. Jones, Journal of Optical Society of America, 37, No. 2, 107 (1947).

18. H. Hurwitz, Jr. and R. C. Jones, J. O. S. A., 31, 493 (1941).

19. Y. Akana, M.S. Thesis, University of Massachusetts, 1973.

Captions for Figures

1. Schematic diagram of the apparatus for photographic light scattering.
2. Film calibration curve. Ordinate is shown as transmission, abscissa is shown as exposure time.
3. The variation in H_v light scattering patterns with strain for filled sample.
4. The variation in H_v light scattering patterns with strain for unfilled sample.
5. The variation in V_v light scattering patterns with strain for filled sample.
6. H_v light scattering pictures of the sample with (a) 0-5 μm beads and (b) 29 μm beads at 28% elongation.
7. H_v light scattering pictures of the sample with (a) 0.002 g/g and (b) 0.0002 g/g at 28% elongation.
8. H_v light scattering pictures of the sample with (a) silane coated beads and (b) uncoated beads at 28% elongation.
9. The variation in V_v light scattering patterns with strain for the sample without silane.
10. Photomicrographs of filled sample elongated at different strain ratios.
11. Contour plot of the measured retardations in radians at 6% elongation.

12. Contour plot of the measured retardations in radians at 12% elongation.
13. Contour plot of measured angles of slow directions relative to the stretching direction at 6% elongation.
14. Contour plot of the measured angles of slow directions relative to the stretching direction at 12% elongation.
15. The coordinate system for the calculation of orientations and magnitudes of normal stresses and shear stresses around beads.
16. The variations of normal stresses and shear stresses as a function of azimuthal angle at reduced distance r/a = 1.1.
17. The polar plot of radial stress and tangential stress as a function of azimuthal angle at reduced distance r/a = 1.1.
18. A simple diagram to explain a rotation is required to get the principal stresses from normal and shear stresses.
19. The angular coordinates of one point in the rubber matrix.
20. The comparison of calculated and measured retardations as a function of reduced distance at 0% elongation.
21. The calculated small angle light scattering pattern in the polar coordinates (θ', μ) at 0% elongation.
22. The calculated small angle light scattering pattern in the polar coordinates (θ', μ) at 8% elongation.
23. The calculated small angle light scattering pattern in the polar coordinates (θ', μ) at 20% elongation.
24. The calculated small angle light scattering pattern in the polar coordinates (θ', μ) at 30% elongation.

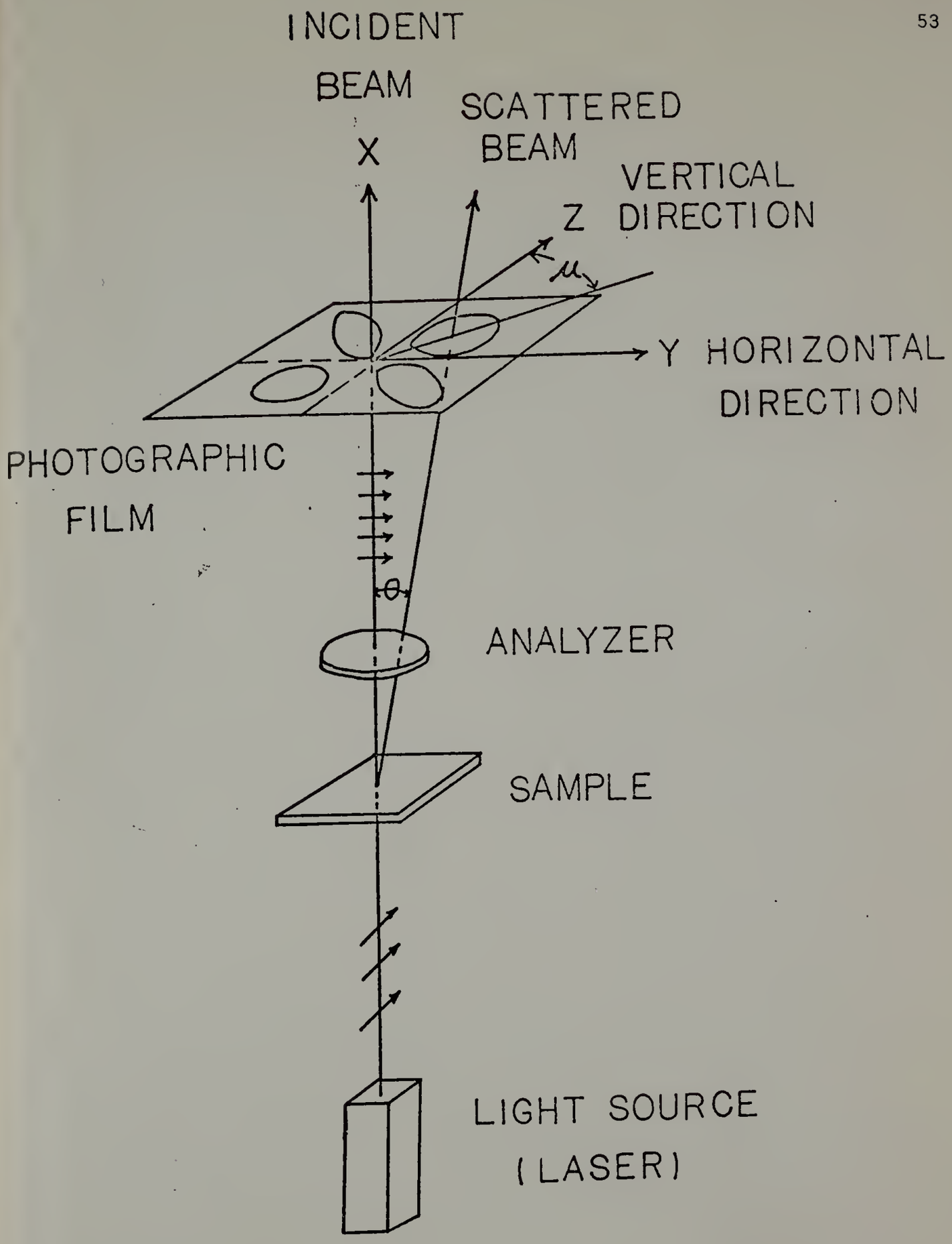
INCIDENT
BEAM
SCATTERED
BEAM
X
VERTICAL
Z DIRECTION
Y HORIZONTAL
DIRECTION
PHOTOGRAPHIC
FILM
ANALYZER
SAMPLE
LIGHT SOURCE
(LASER)

Fig. 1

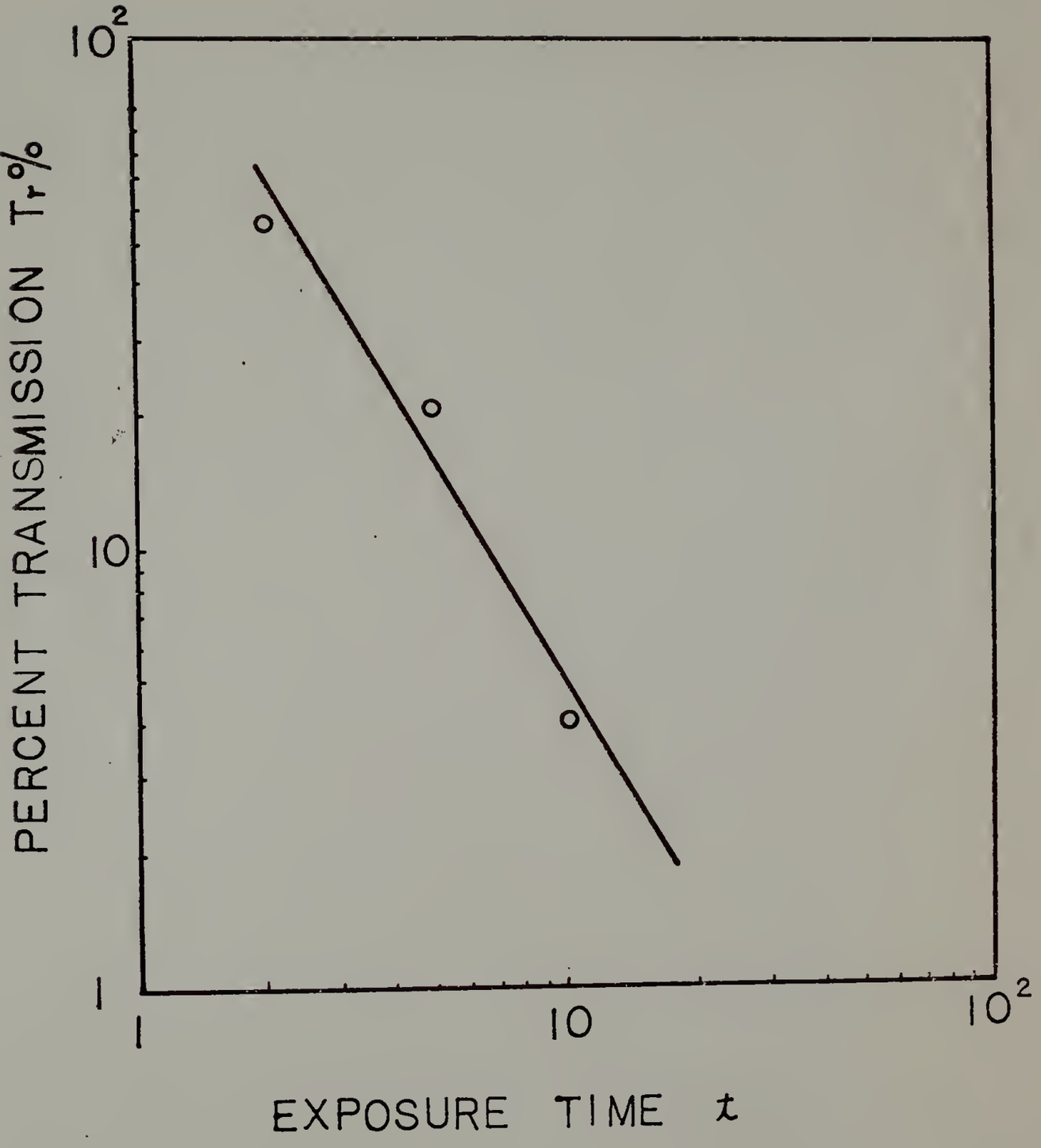

Figure 2

Figure 3

Hv

0%

S.D.

6 %

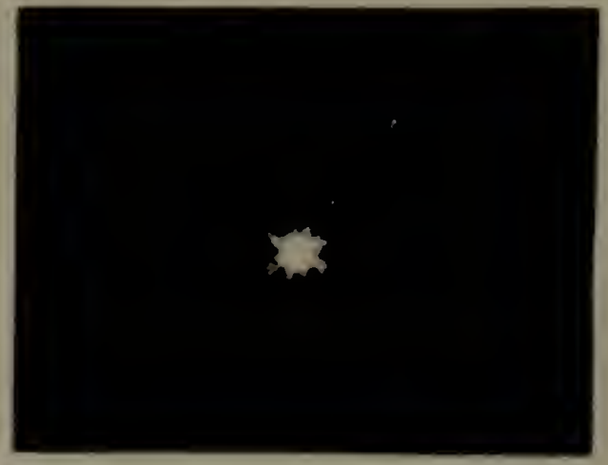

17%

28%

36%

Figure 4

H_V

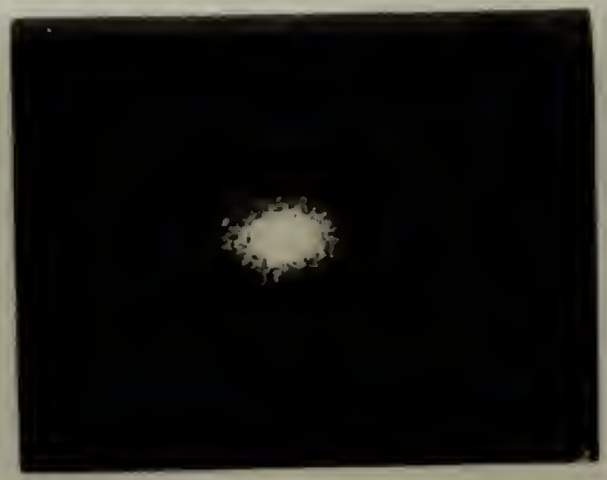

0%

S.D.

3%

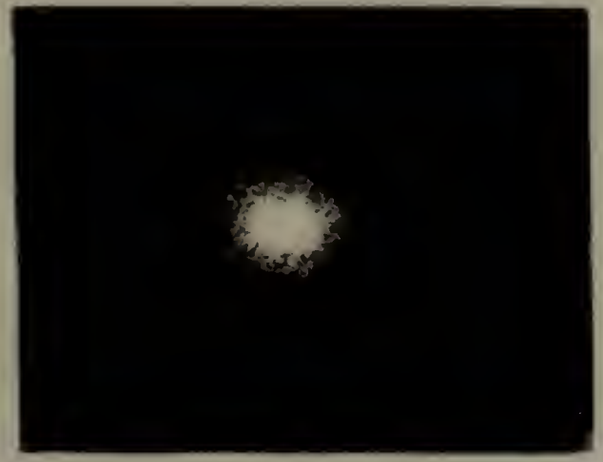

9%

15%

19%

Figure 5

S.D.

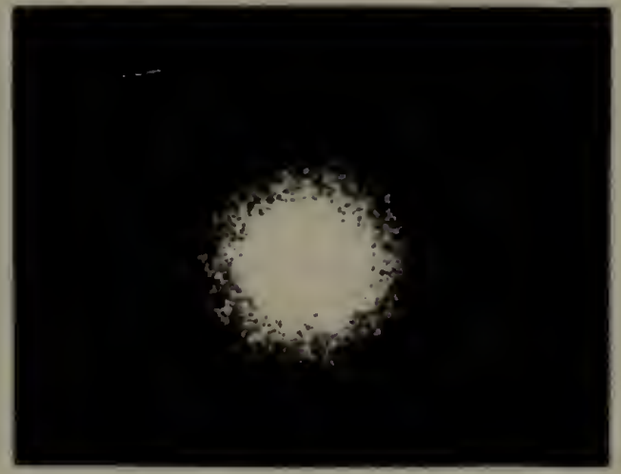

28%

Figure 6

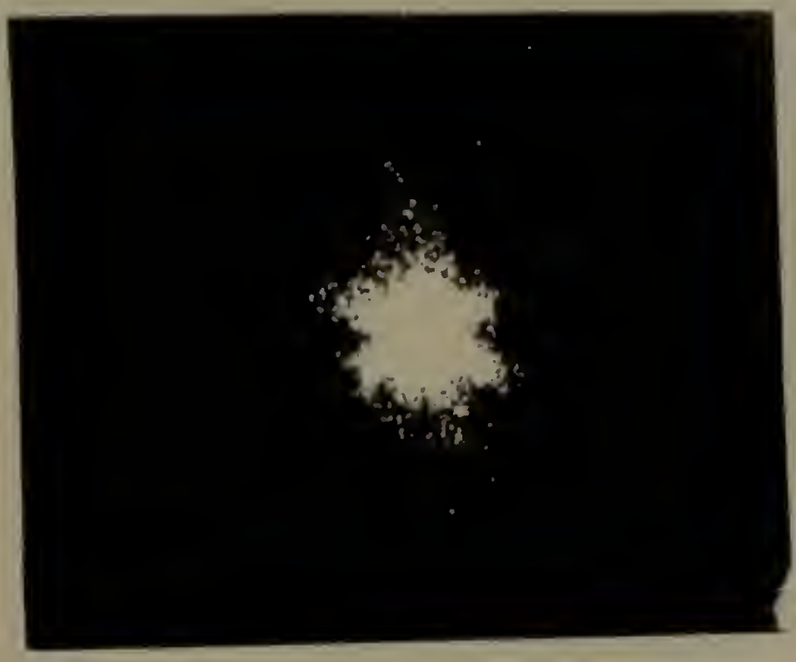

(a)

Figure 7

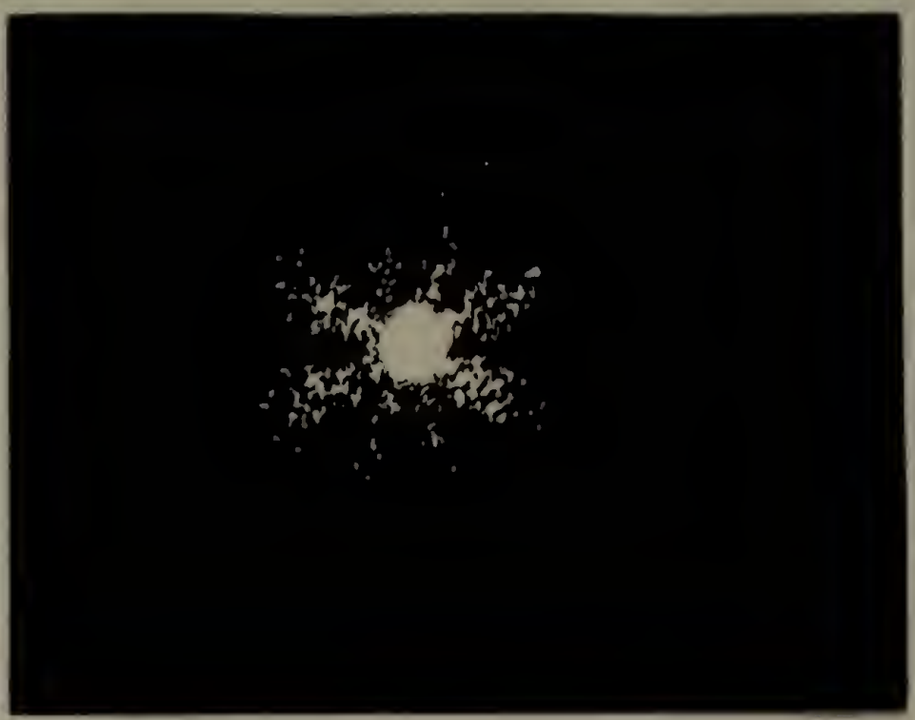

(a)

(b)

Figure 8

(a)

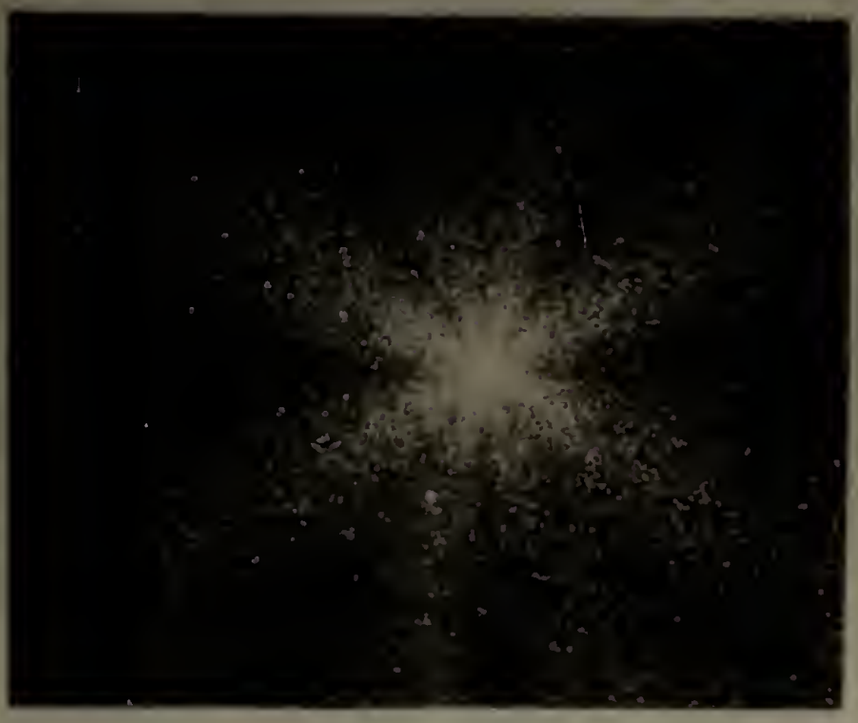

(b)

Figure 9

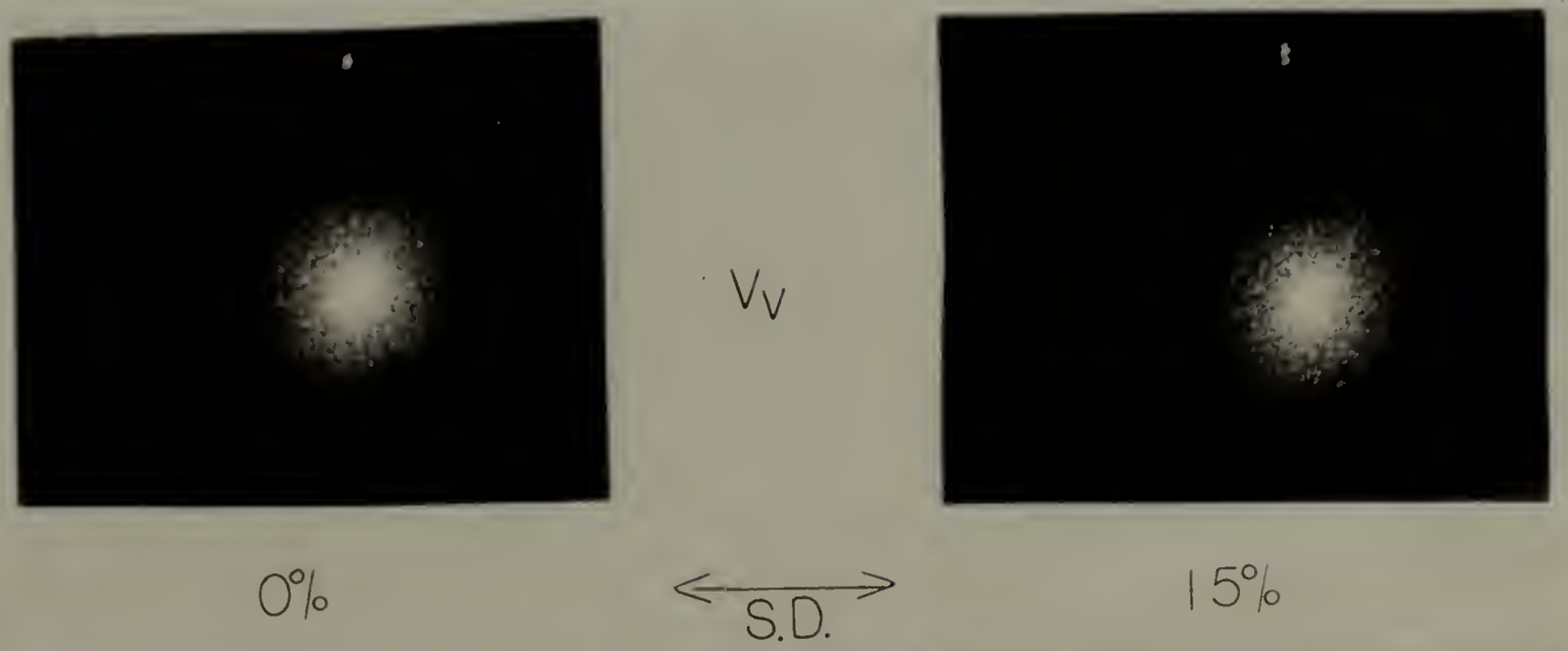
V_V
0%
S.D.
15%
23%
30%

Figure 10

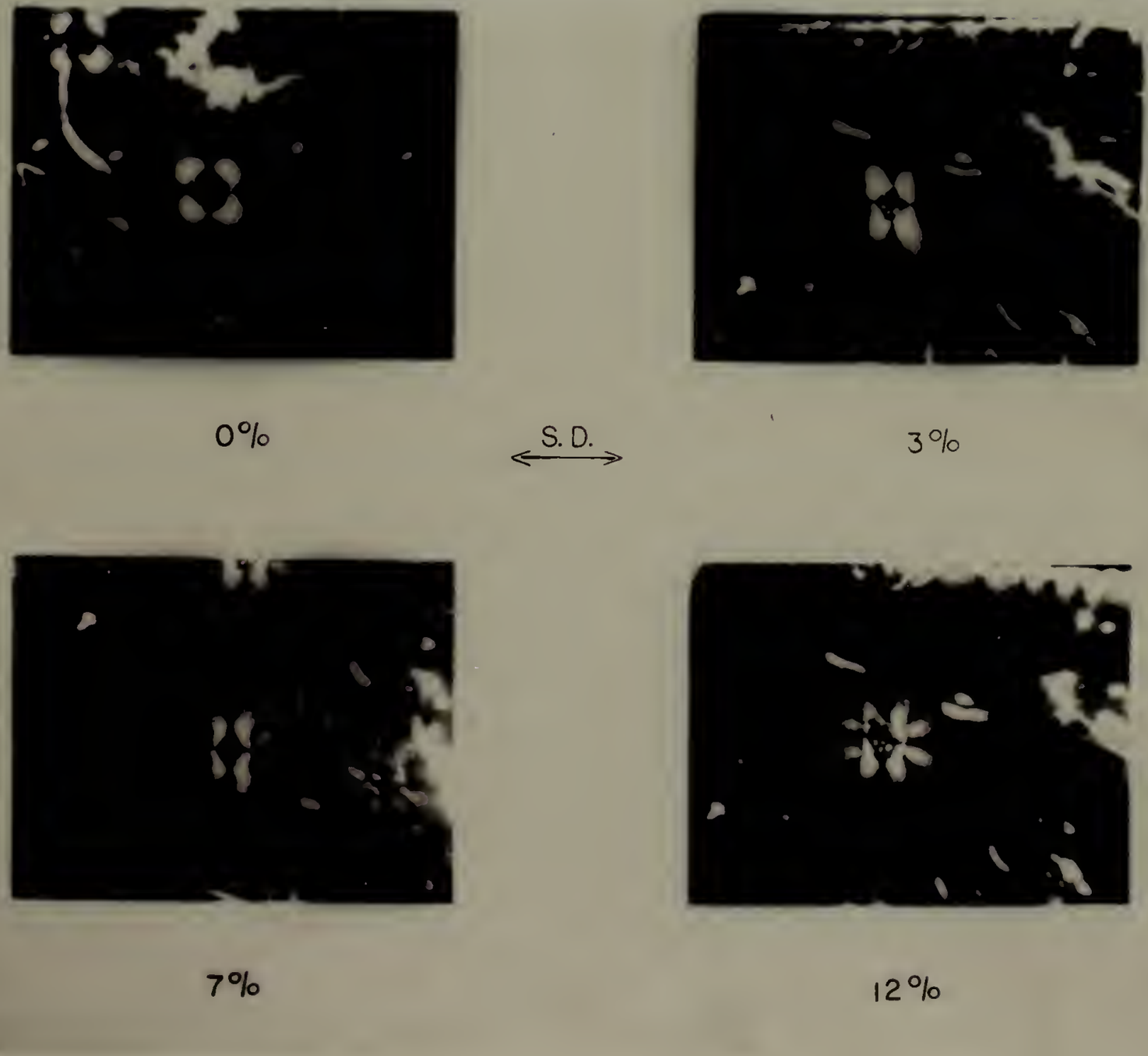
0%
S. D.
3%
7%
12%

MEASURED RETARDATION CONTOUR PLOT

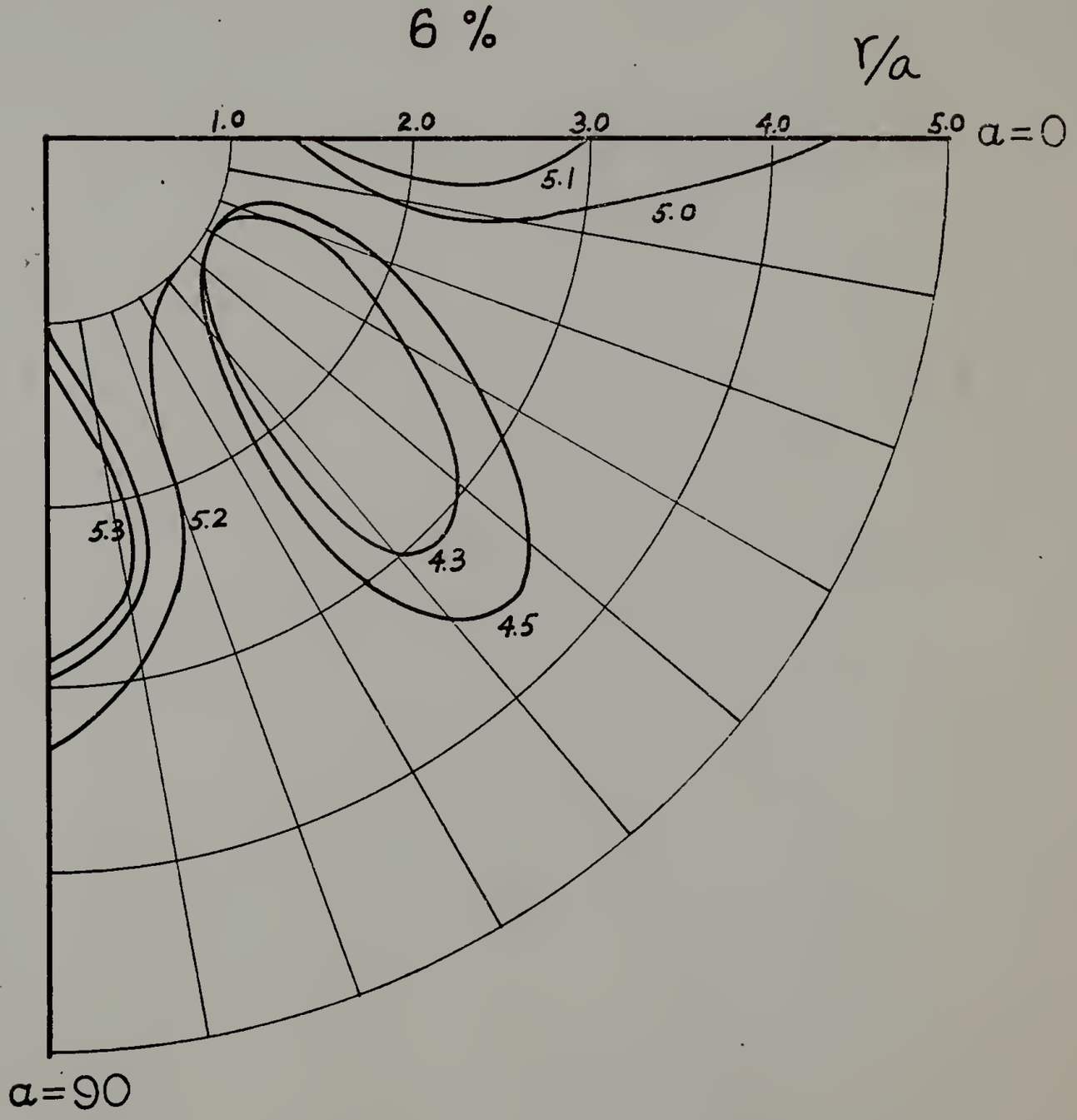

Figure 11

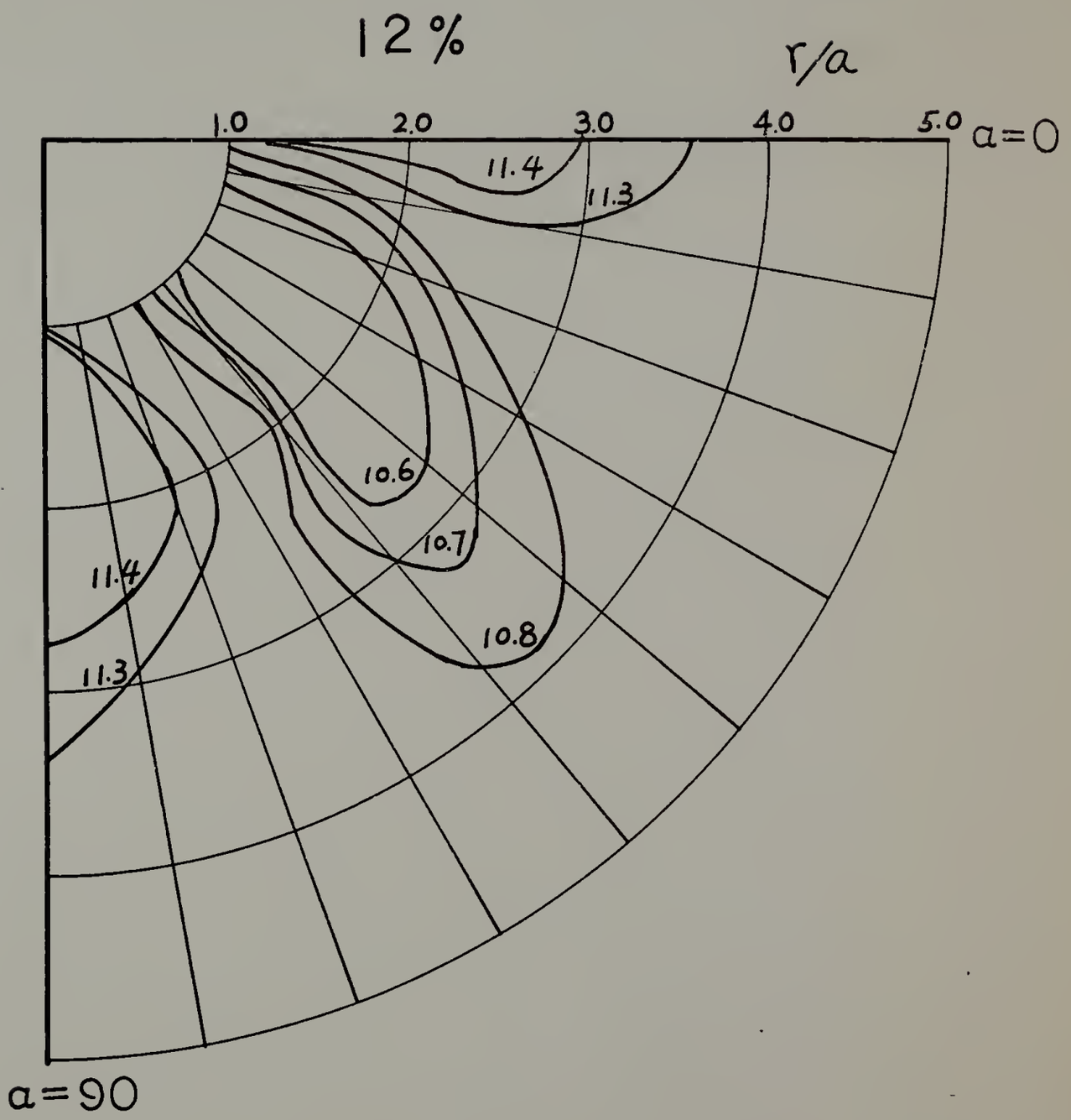

Figure 12

MEASURED SLOW DIRECTION CONTOUR PLOT

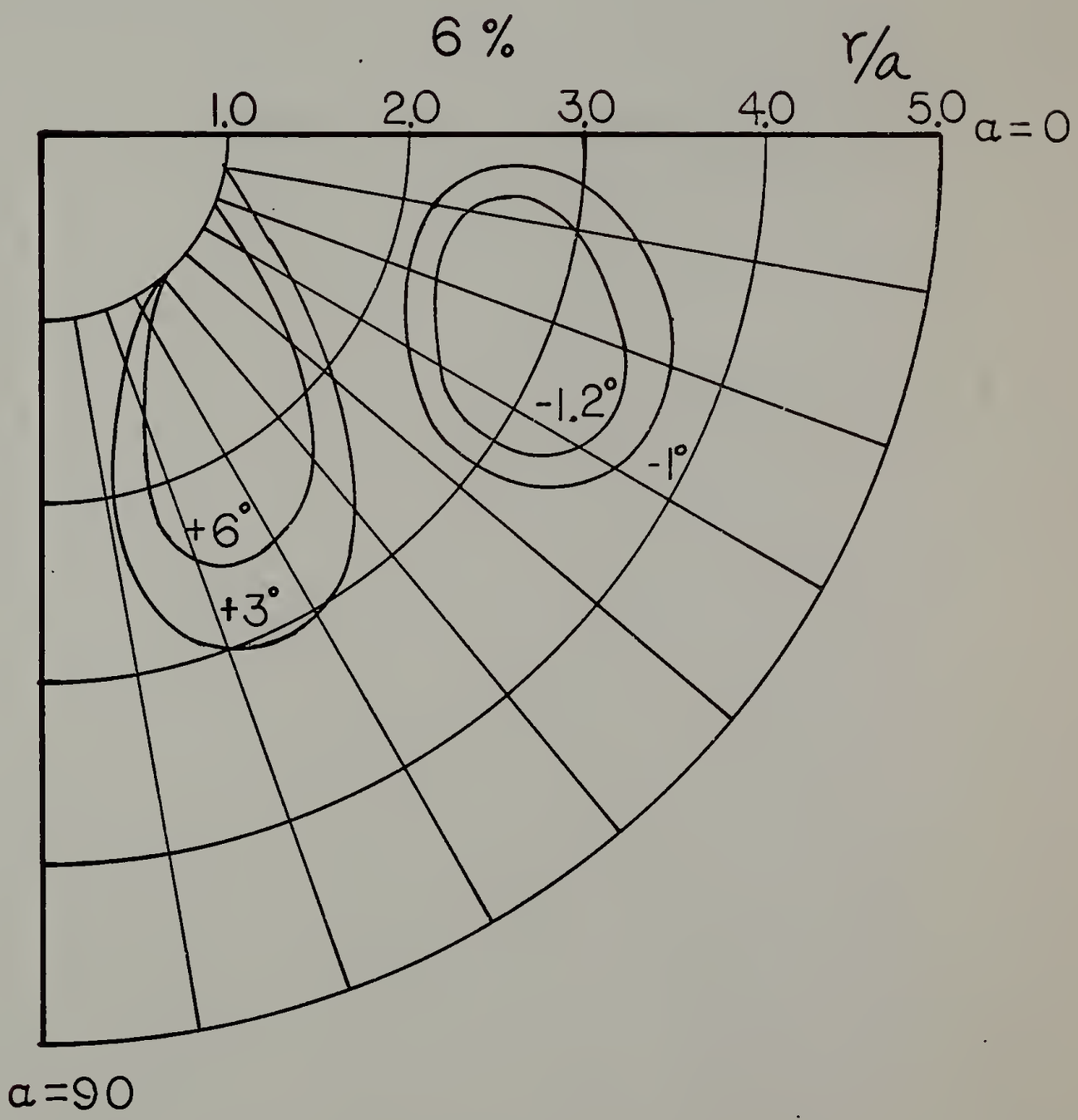

Figure 13

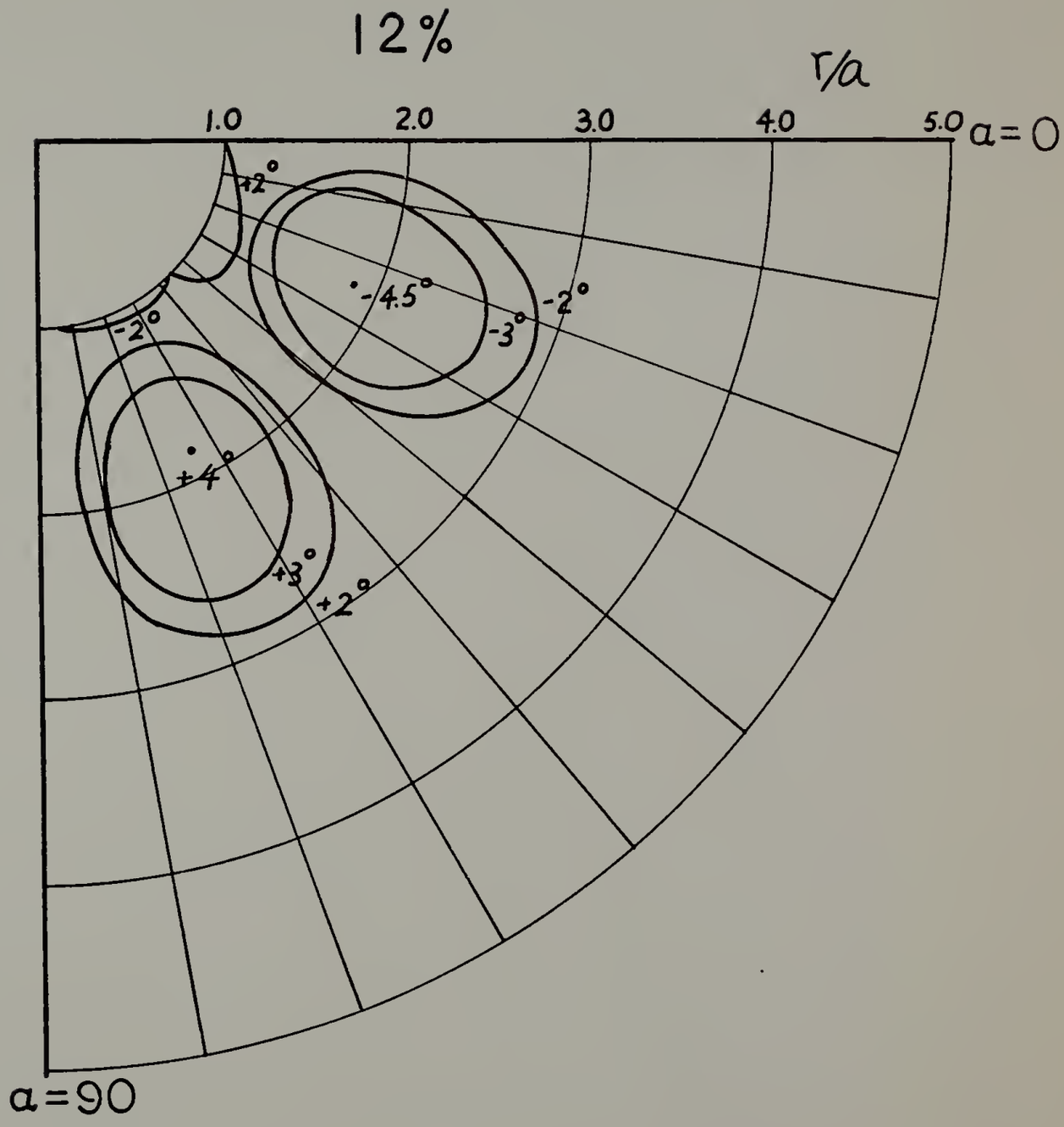

Figure 14

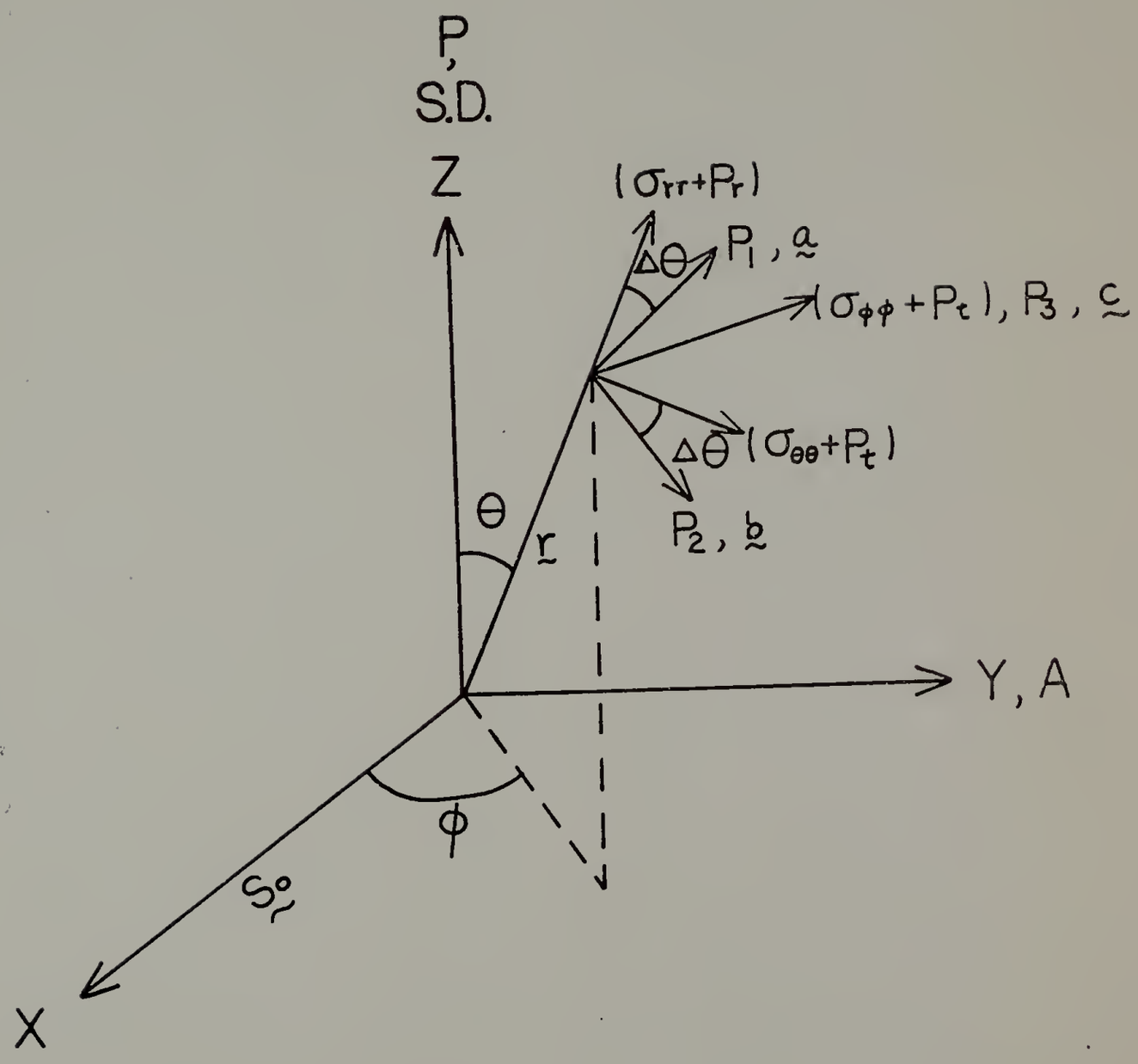
P,
S.D.
Z
$(\sigma_{rr}+P_r)$
$\Delta\theta$
P_1, $\underset{\sim}{a}$
$(\sigma_{\phi\phi}+P_t)$, P_3, $\underset{\sim}{c}$
$\Delta\theta$
$(\sigma_{\theta\theta}+P_t)$
P_2, $\underset{\sim}{b}$
θ
$\underset{\sim}{r}$
Y, A
ϕ
$S^o_{\sim}$
X

Figure 15

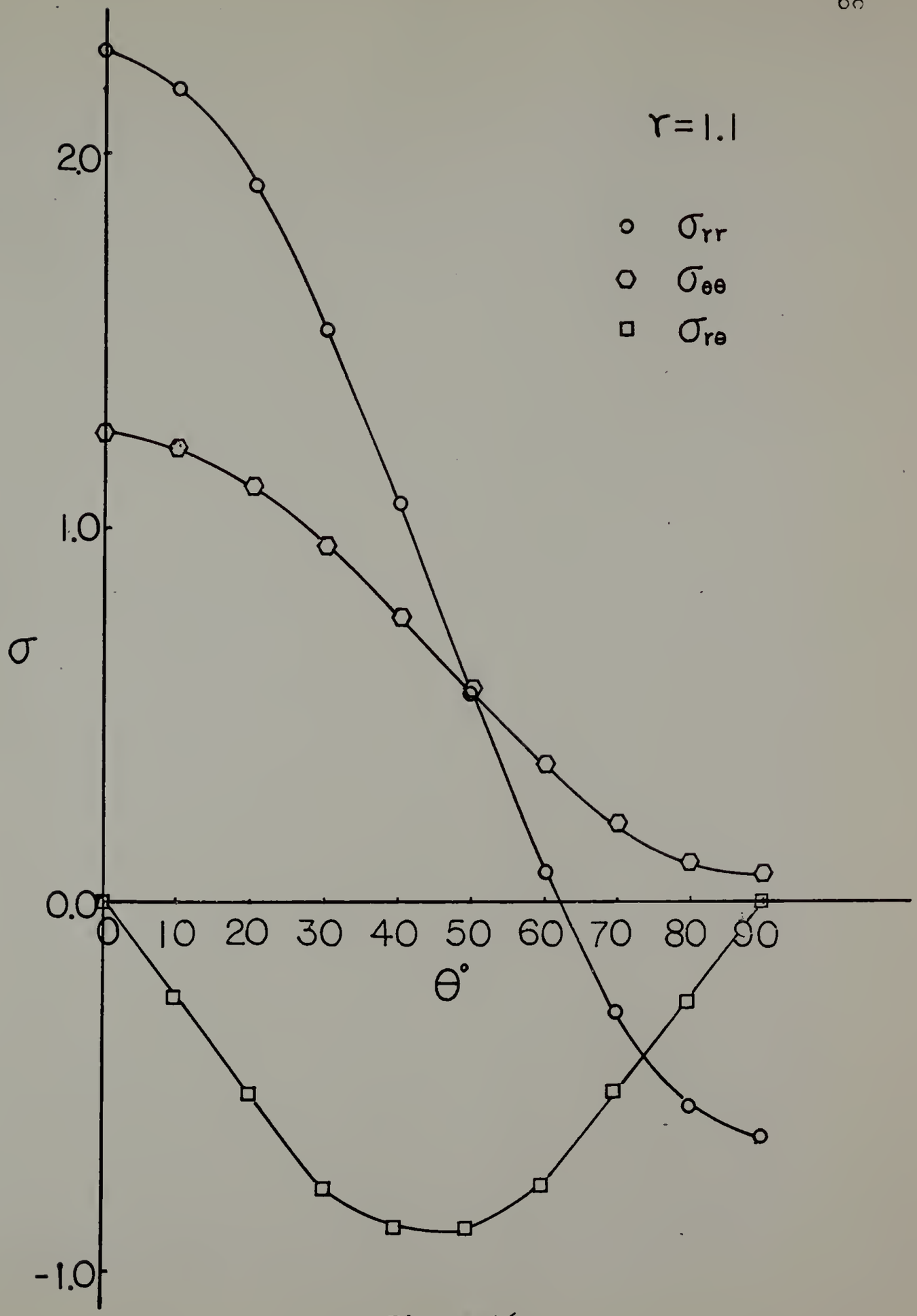

Figure 16

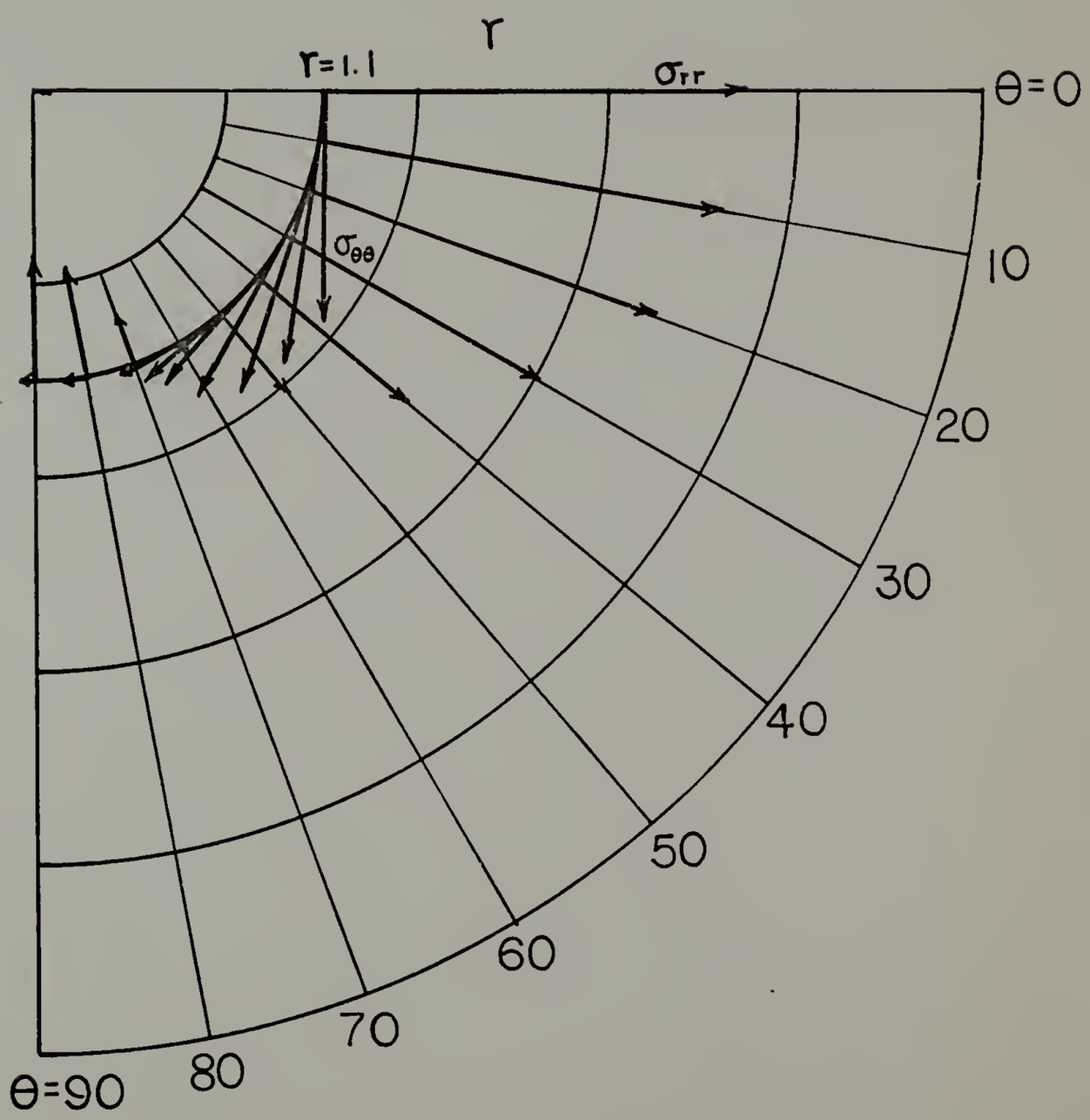

Figure 17

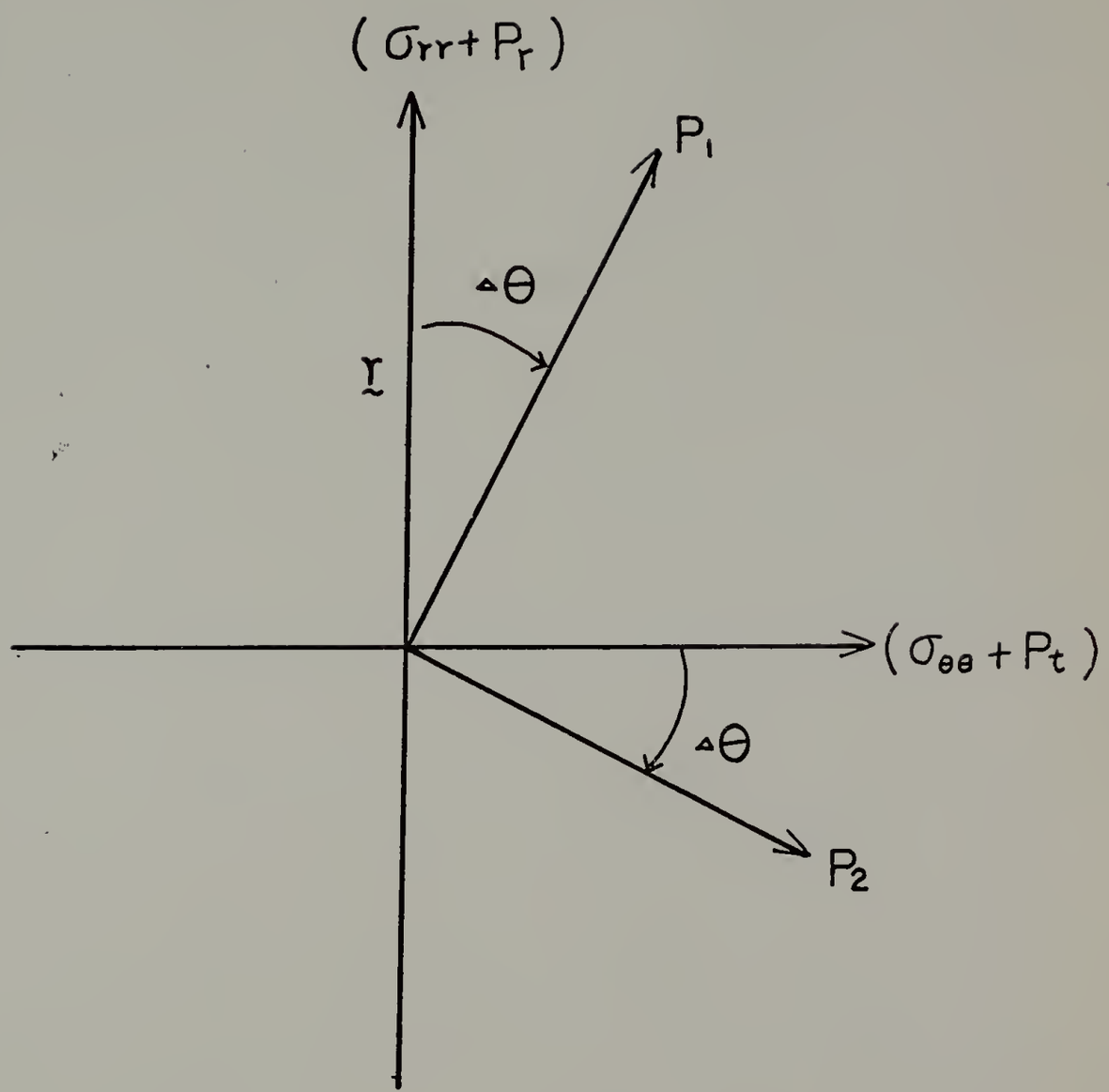
$(\sigma_{rr}+P_r)$
P_1
$\Delta\theta$
$\underset{\sim}{r}$
$(\sigma_{\theta\theta}+P_t)$
$\Delta\theta$
P_2

Figure 18

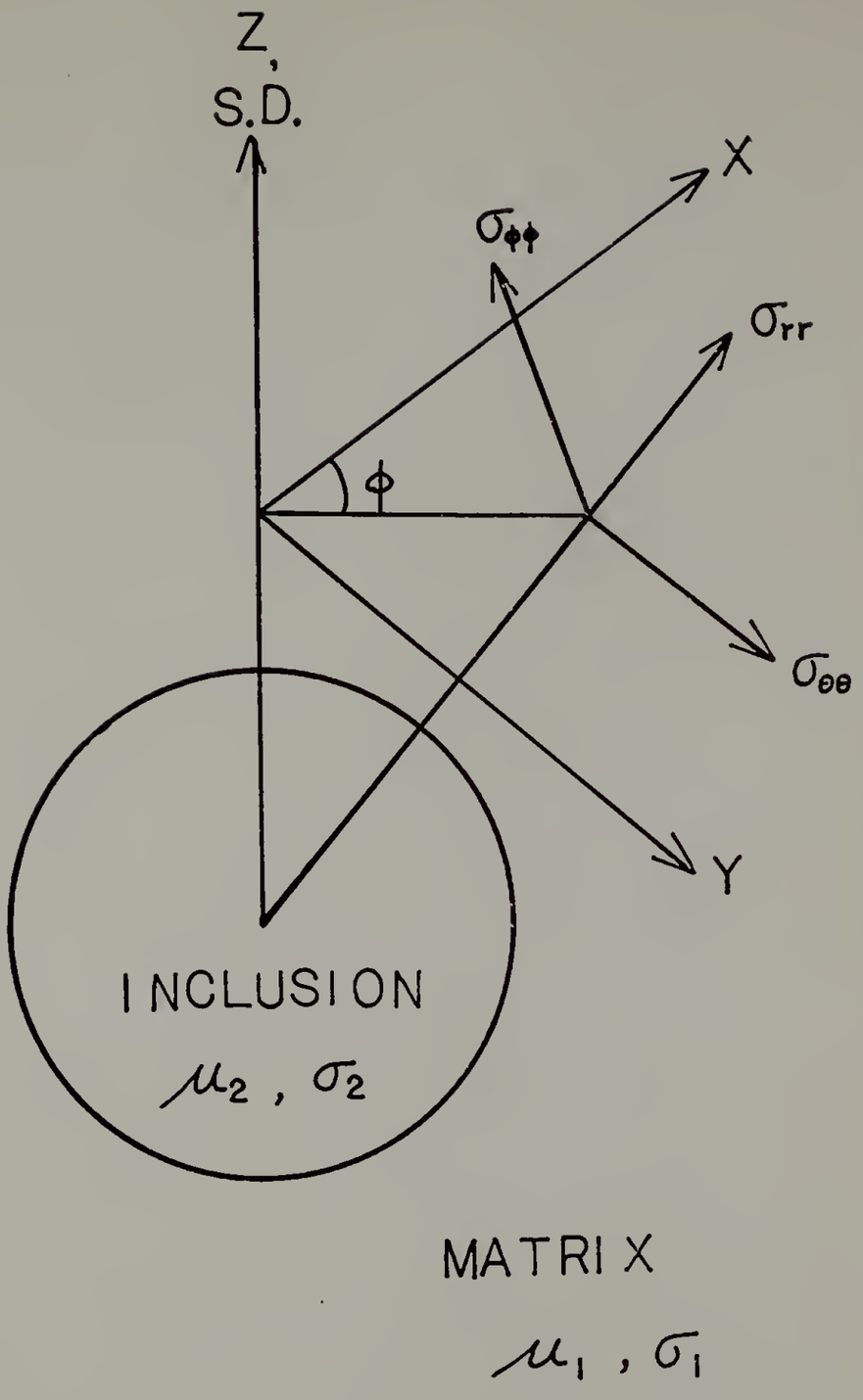
Z,
S.D.
X
$\sigma_{\phi\phi}$
σ_{rr}
ϕ
$\sigma_{\theta\theta}$
Y
INCLUSION
μ_2 , σ_2
MATRIX
μ_1 , σ_1

Figure 19

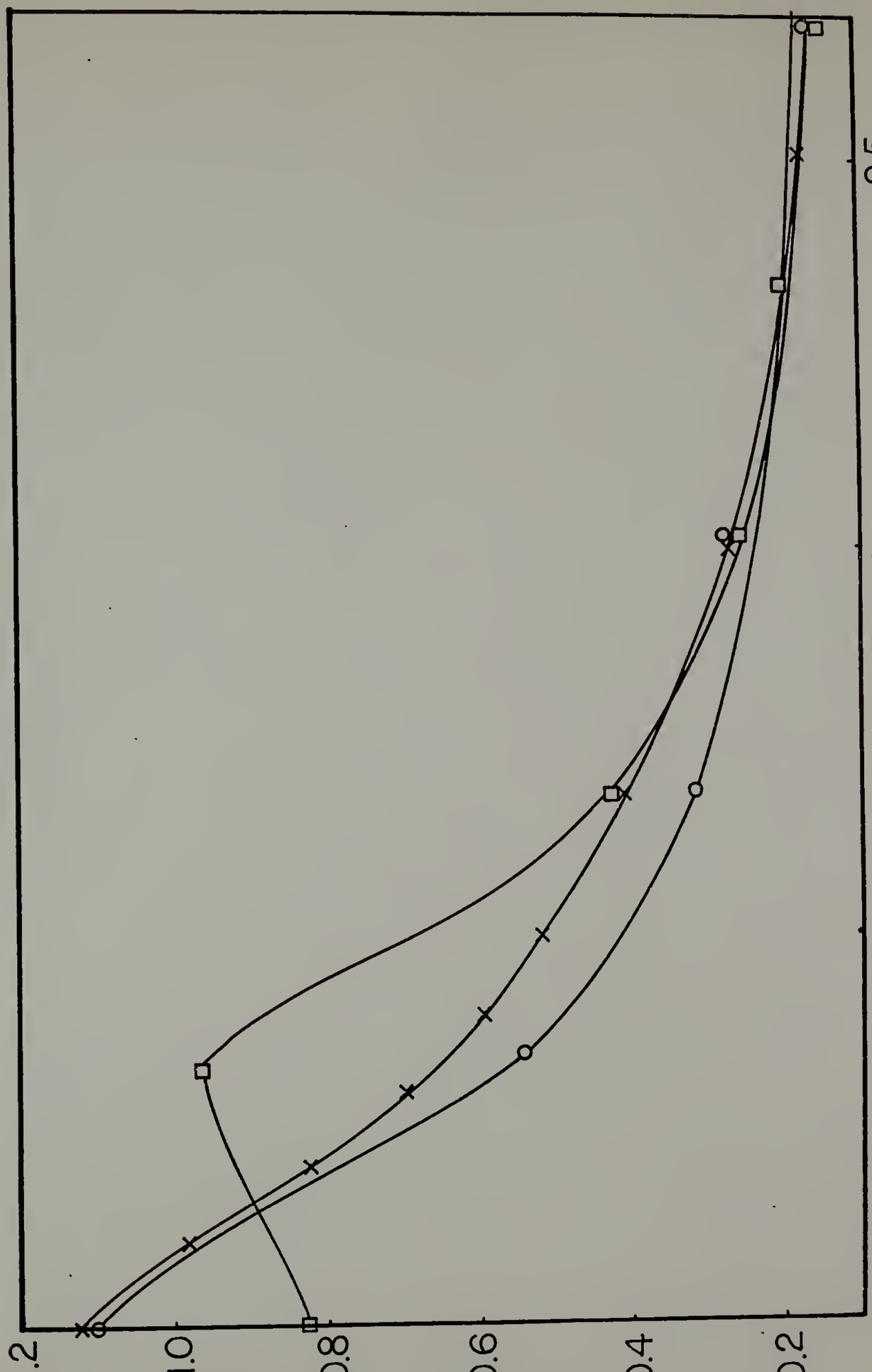

Figure 20

0 %

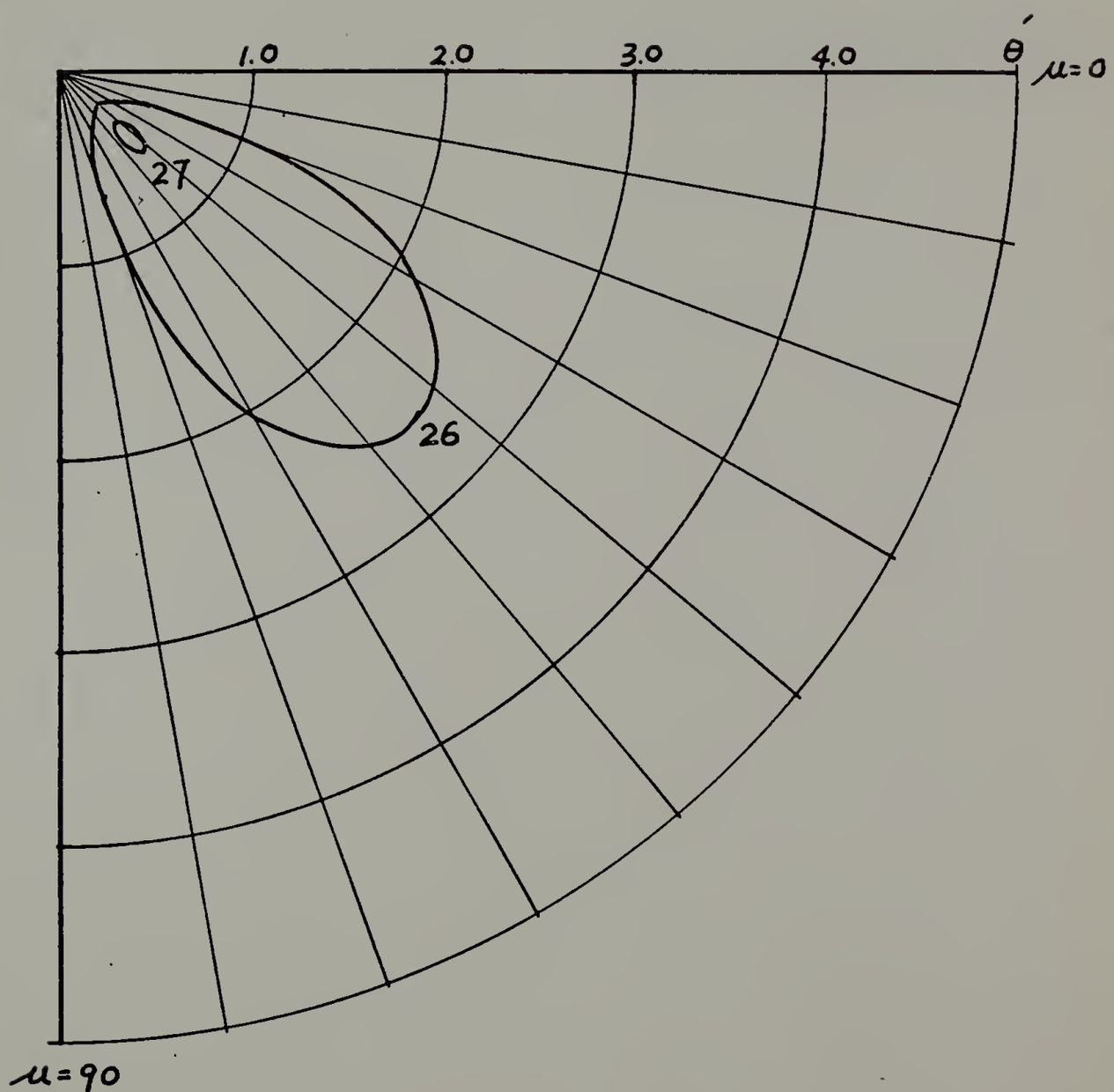

Figure 21

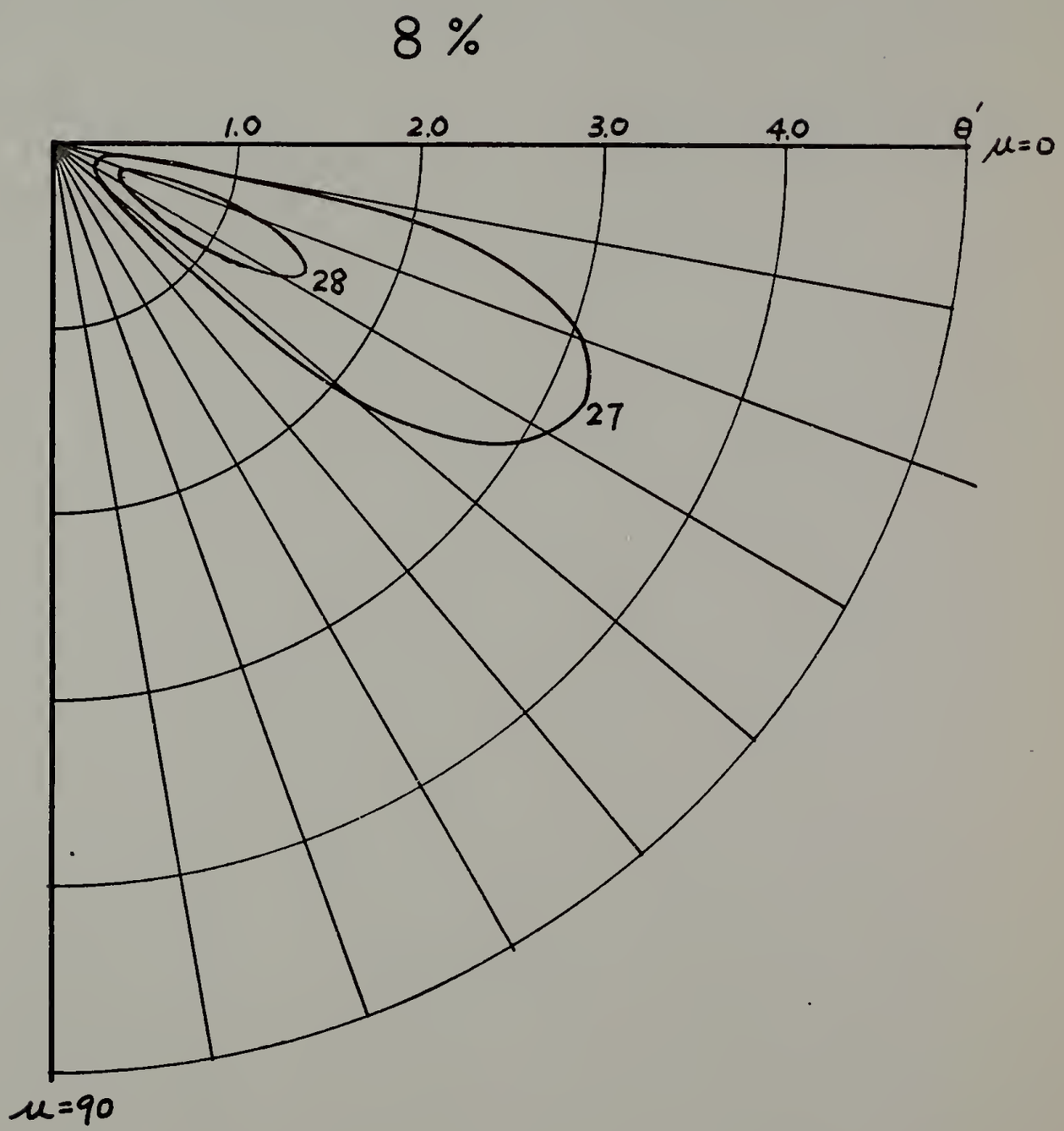

Figure 22

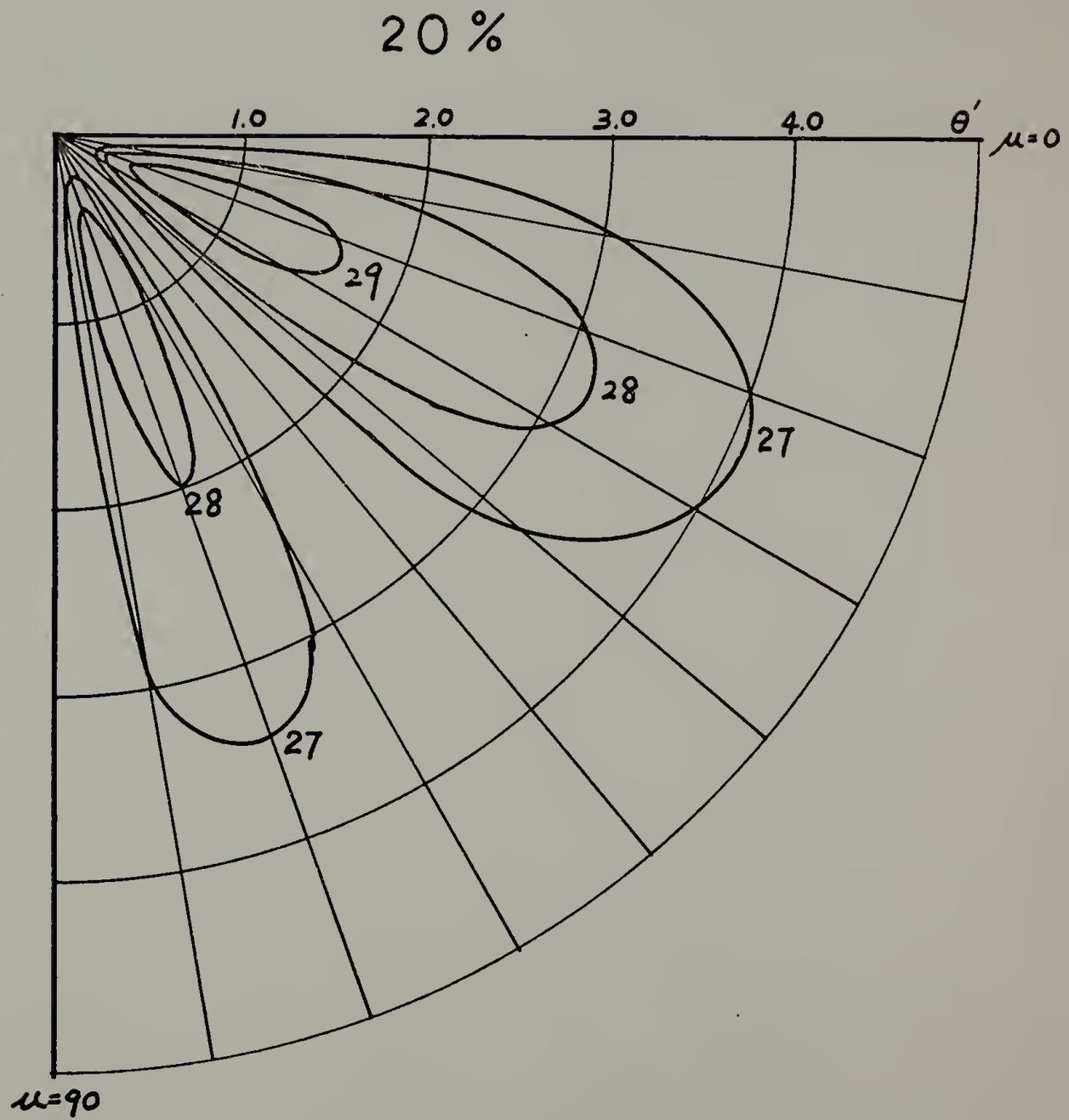

Figure 23

CALCULATED LIGHT SCATTERING PATTERN

30%

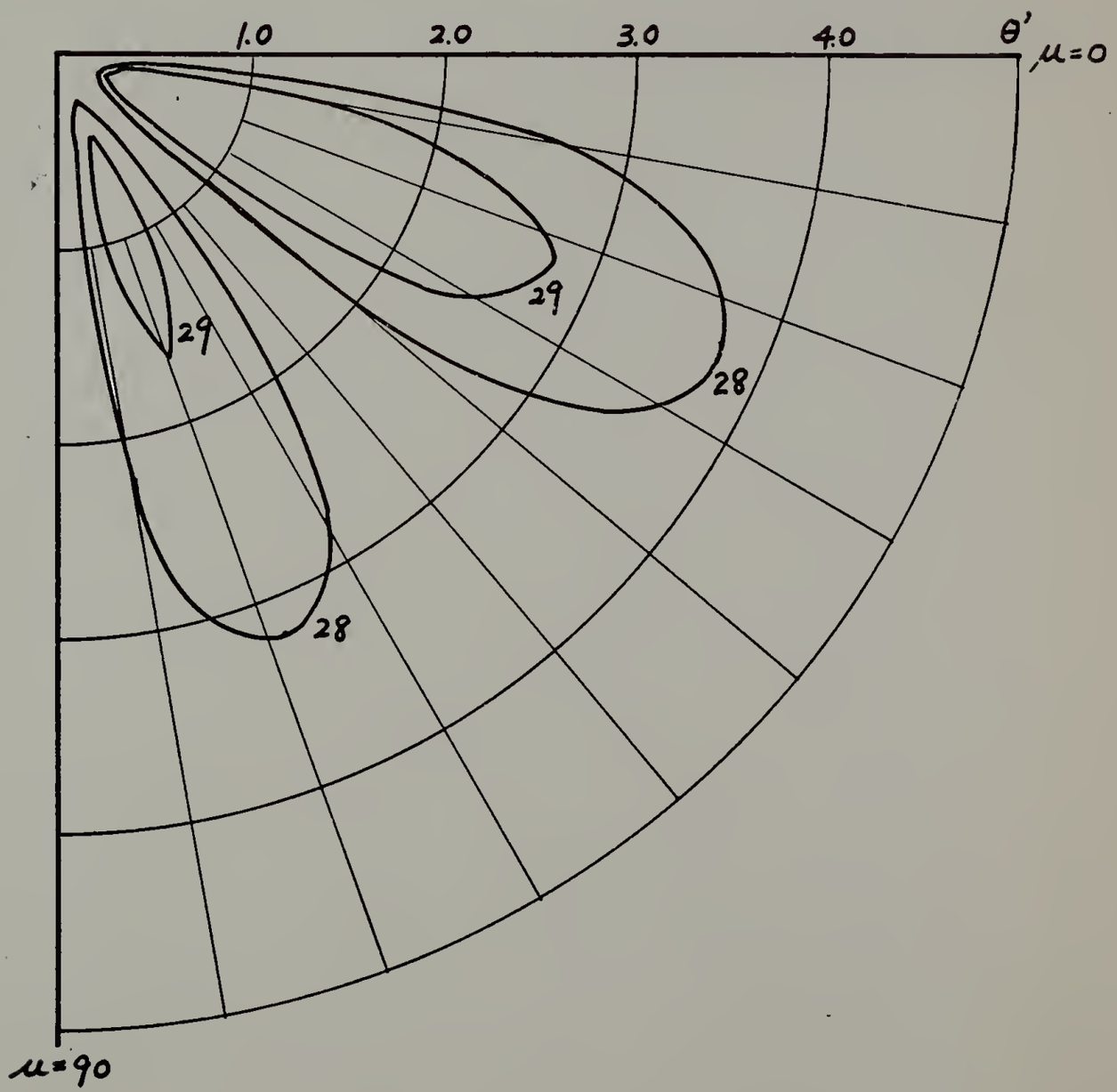

Figure 24

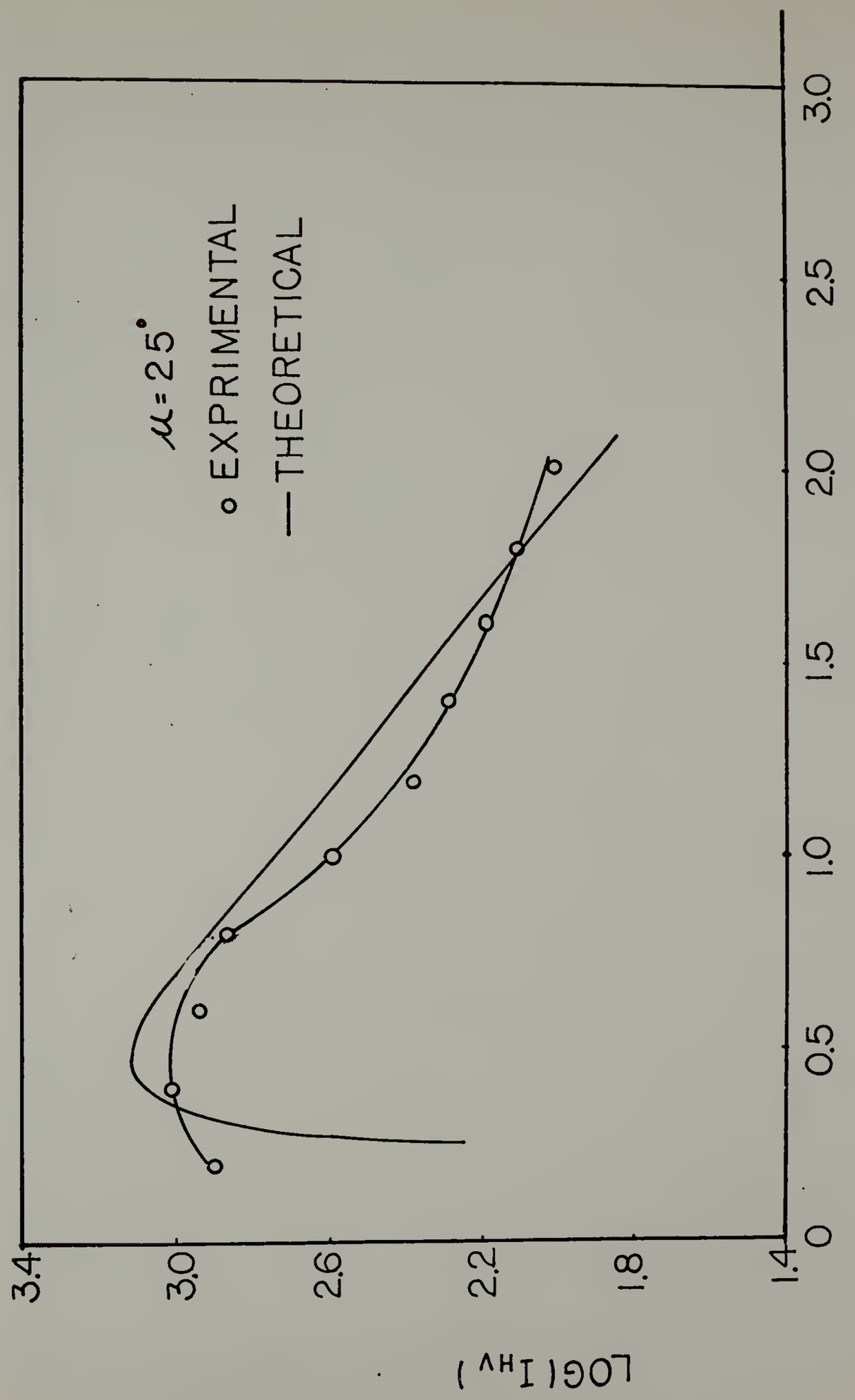
μ = 25°
o EXPRIMENTAL
— THEORETICAL
LOG(I_Hv)
θ′
3.4
3.0
2.6
2.2
1.8
1.4
0
0.5
1.0
1.5
2.0
2.5
3.0

Figure 25

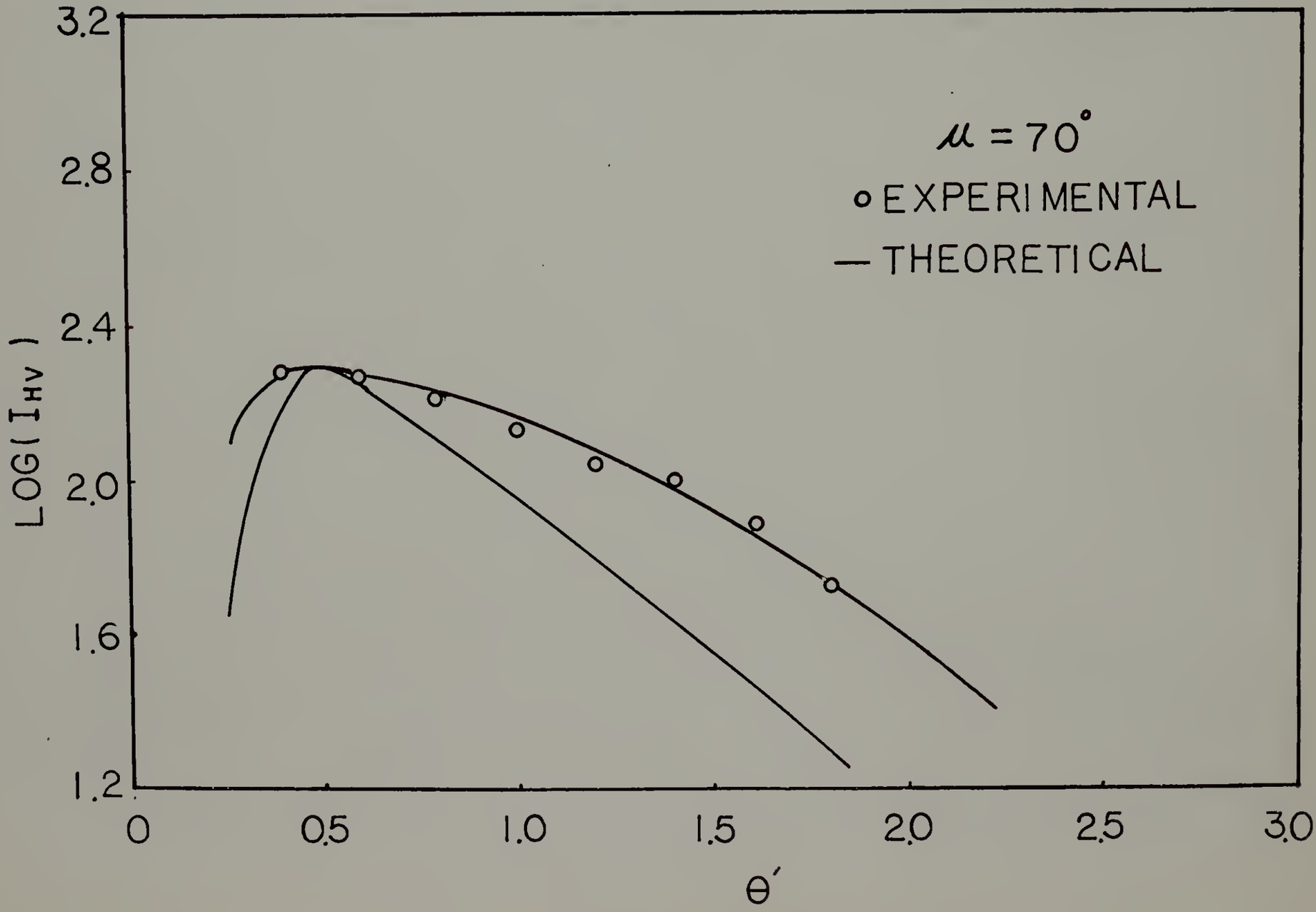
3.2
2.8
2.4
2.0
1.6
1.2
LOG(I_{HV})
0
0.5
1.0
1.5
2.0
2.5
3.0
θ′
μ = 70°
o EXPERIMENTAL
— THEORETICAL

Figure 26

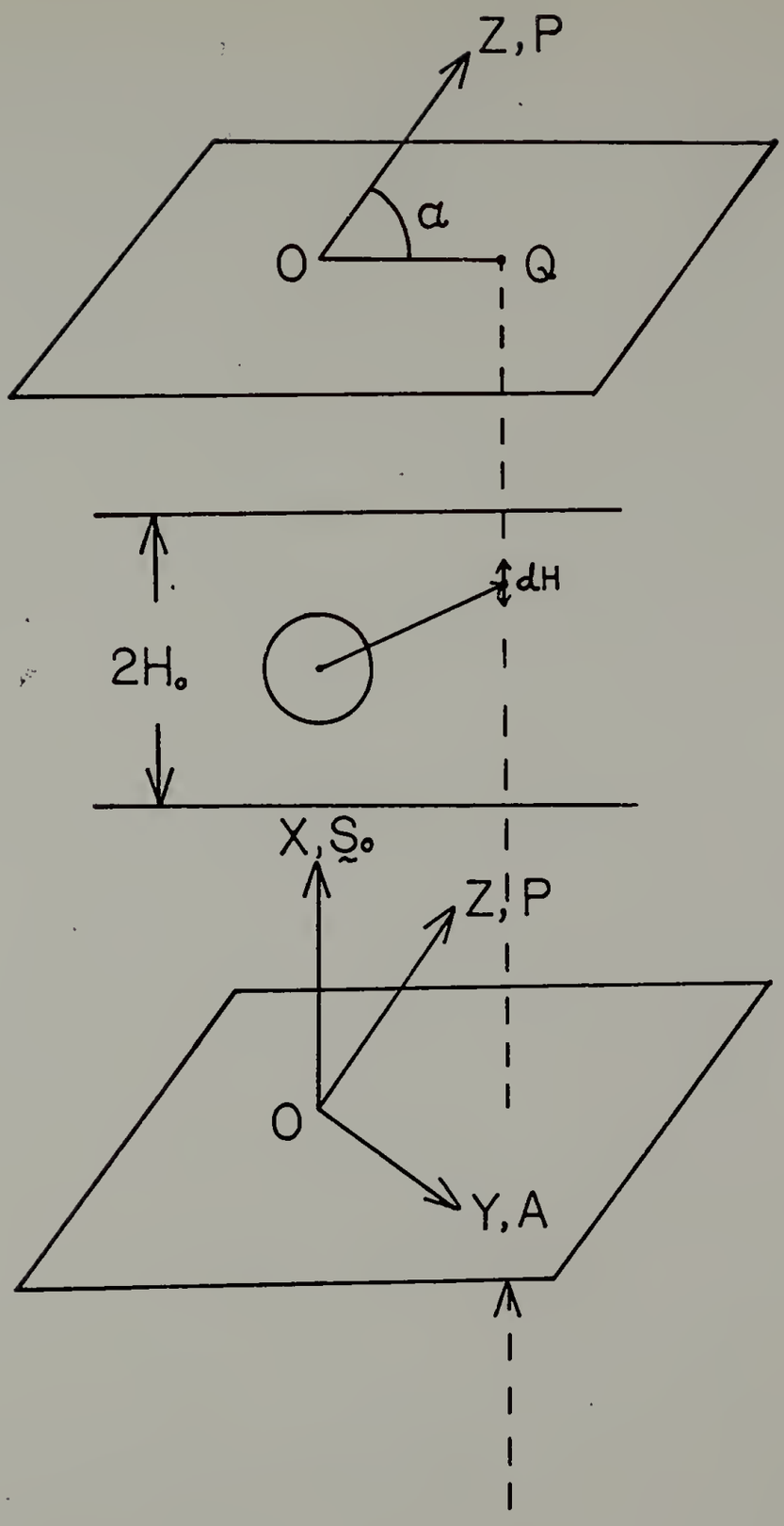

Figure 27

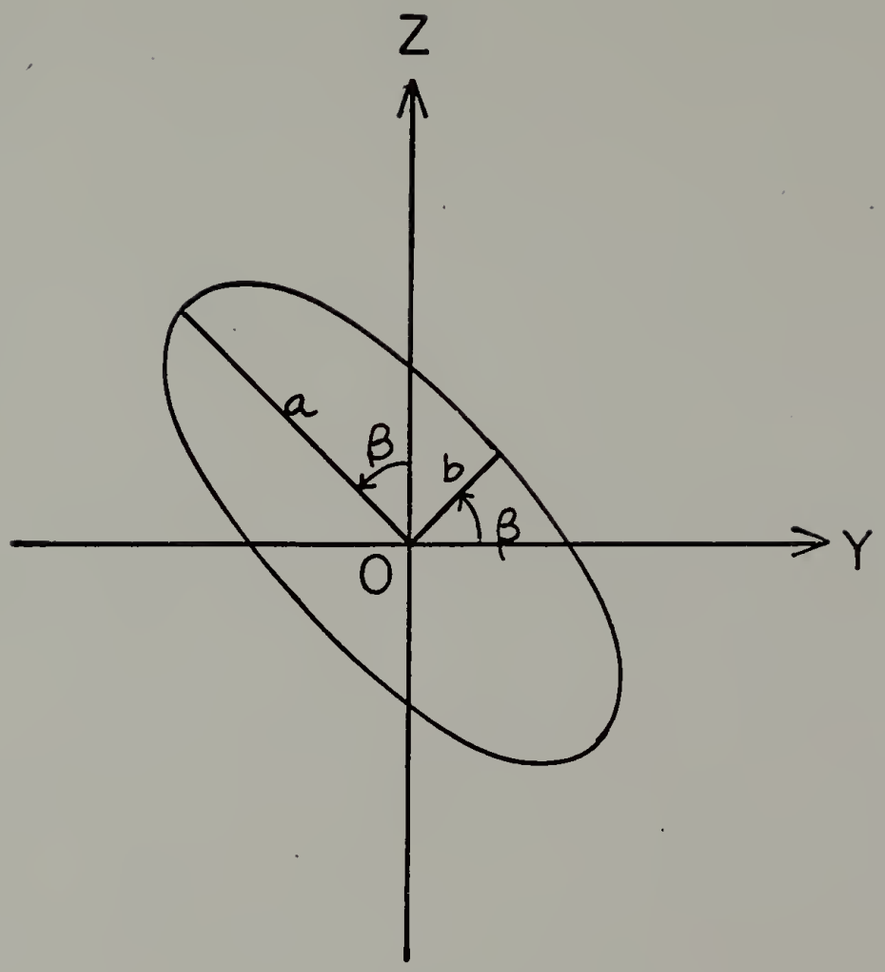

Figure 28

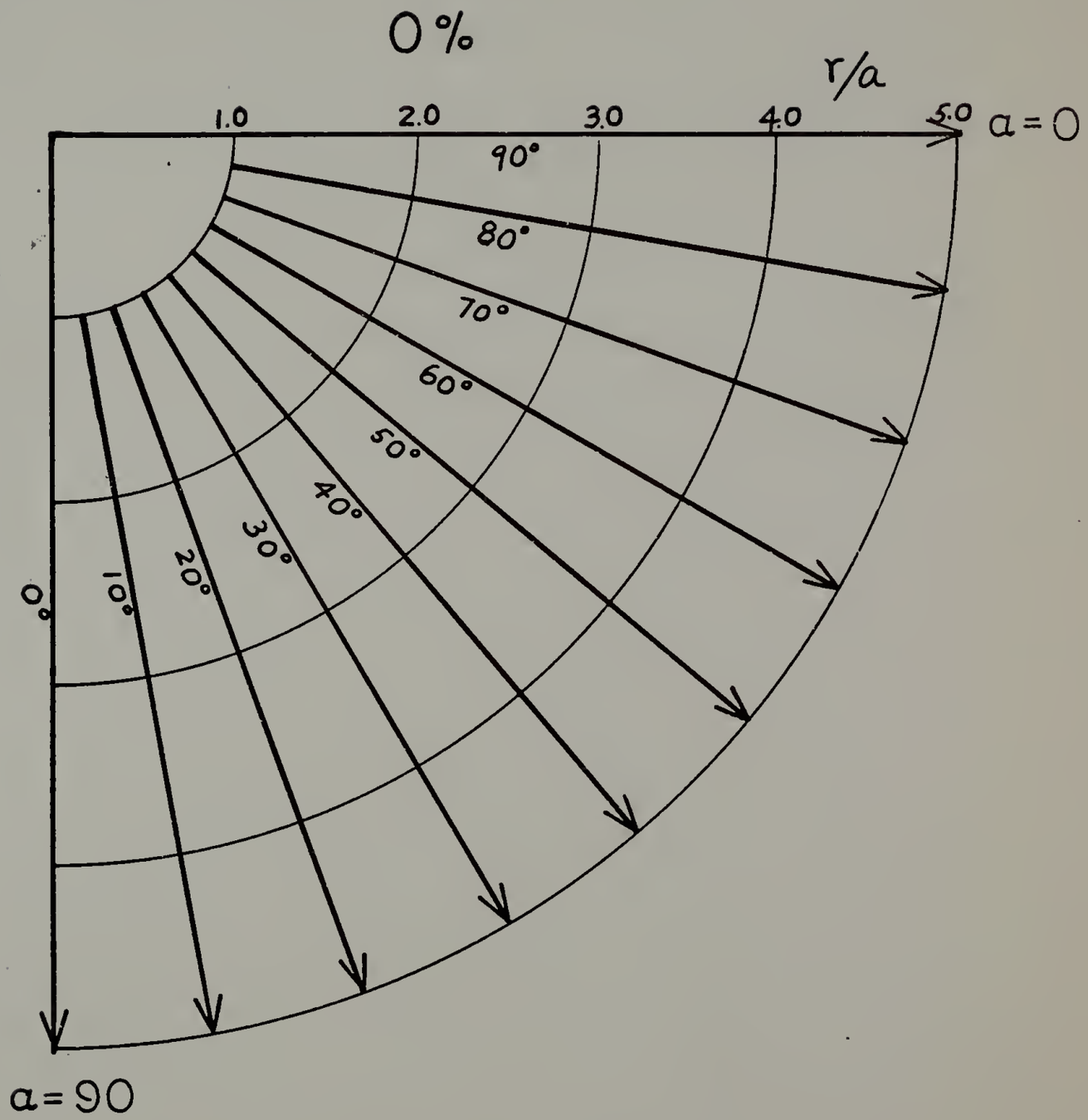

Figure 29

CALCULATED SLOW DIRECTION CONTOUR PLOT

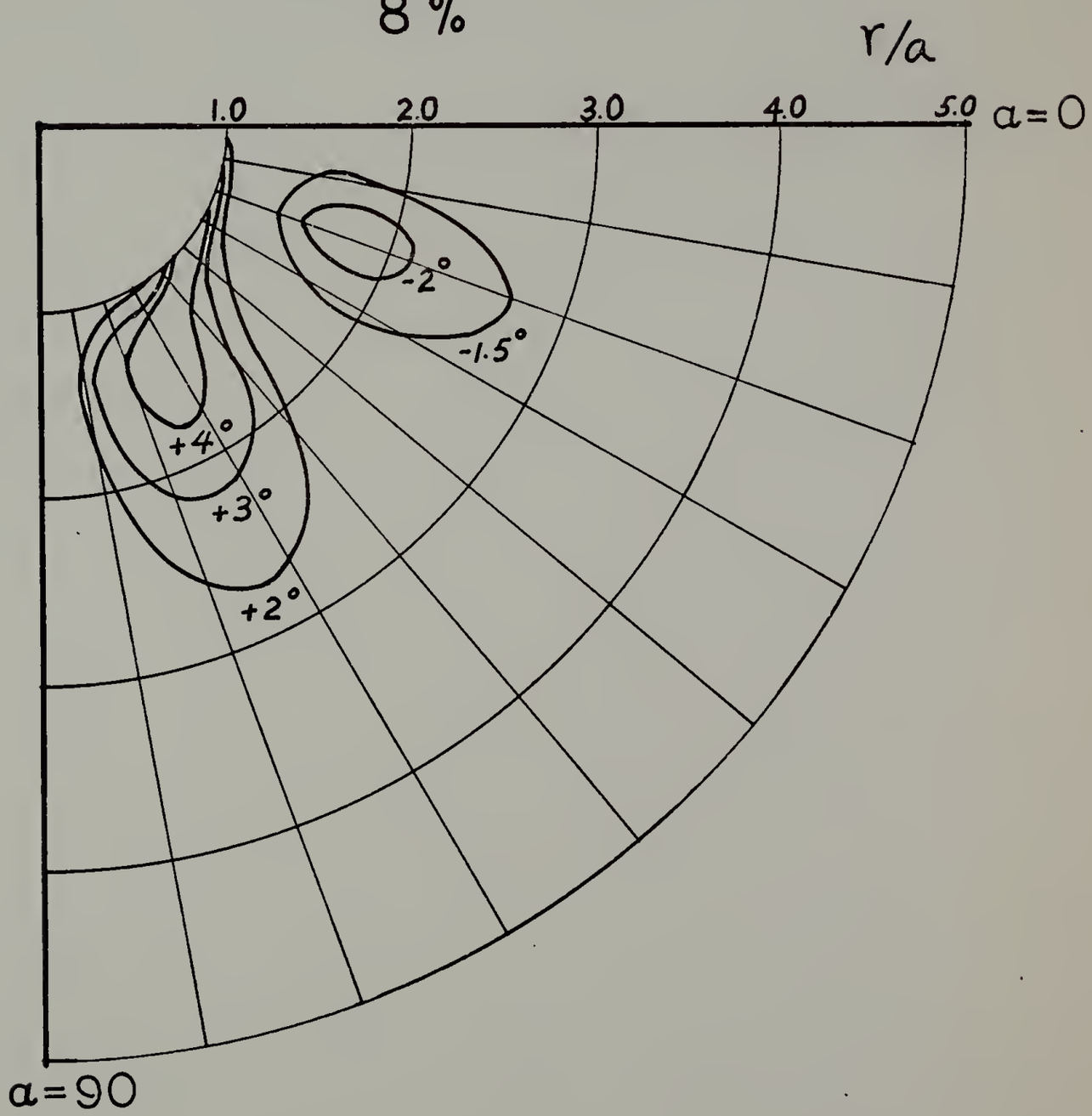

Figure 30

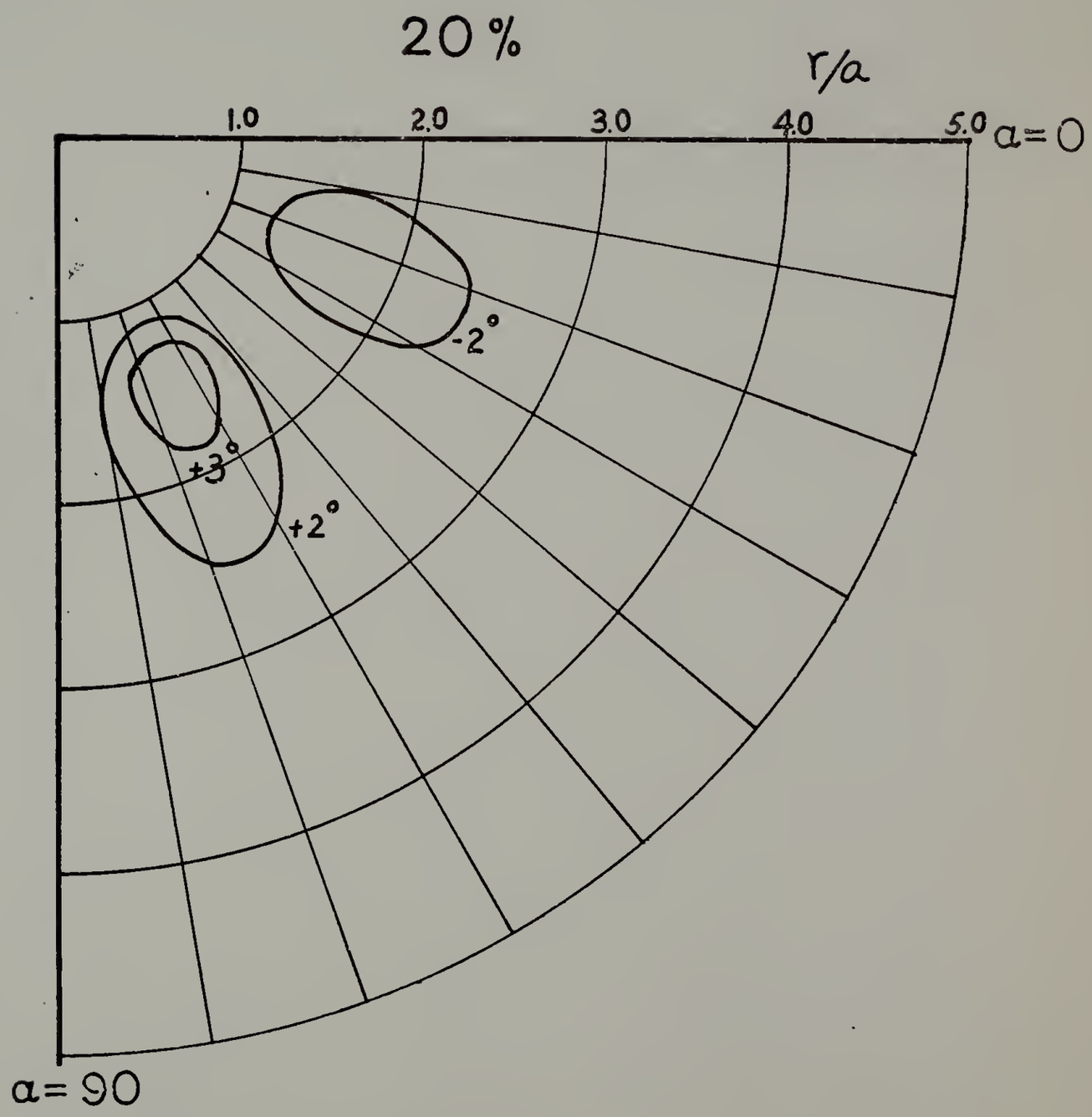

Figure 31

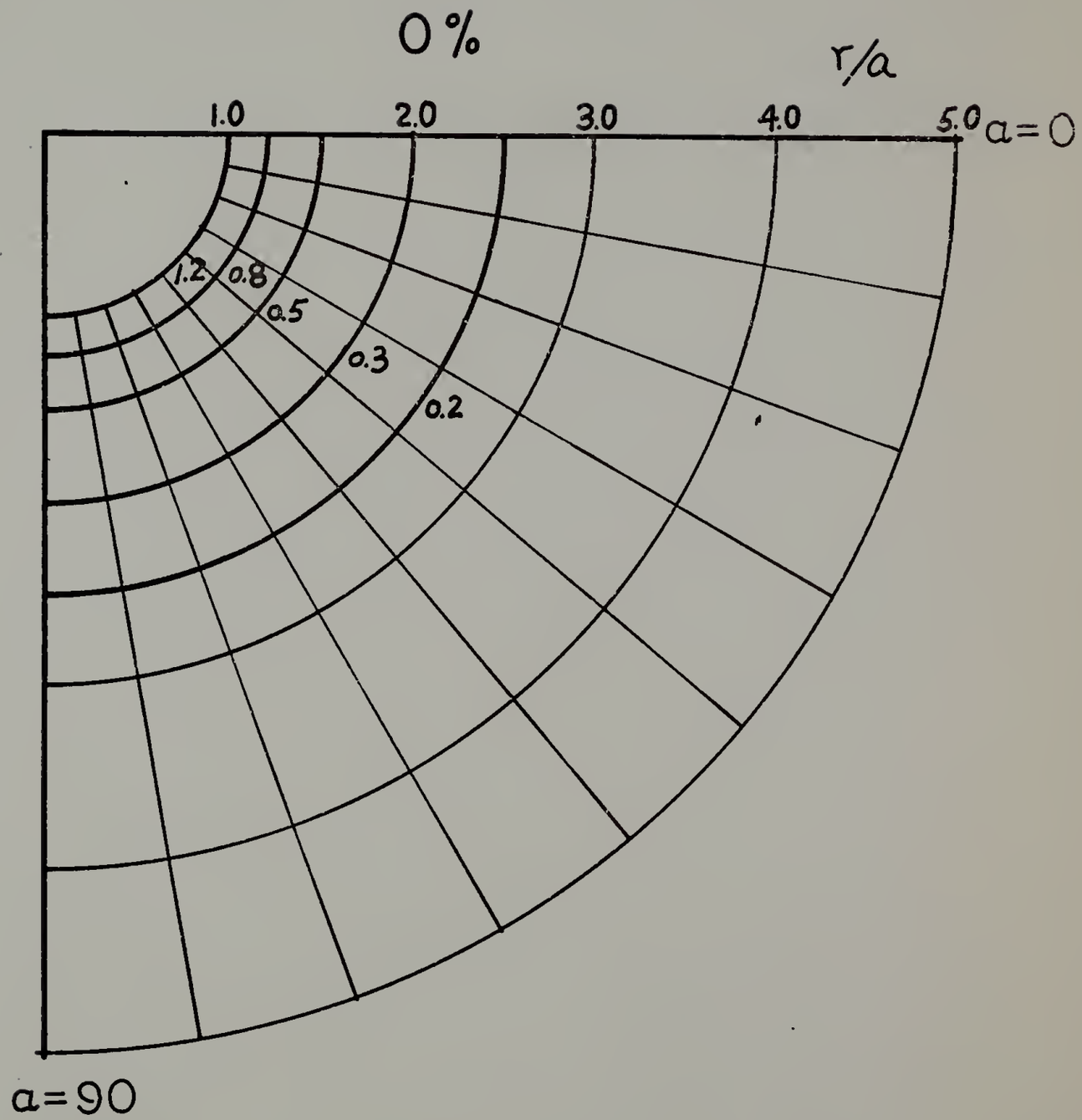

Figure 32

CALCULATED RETARDATION CONTOUR PLOT

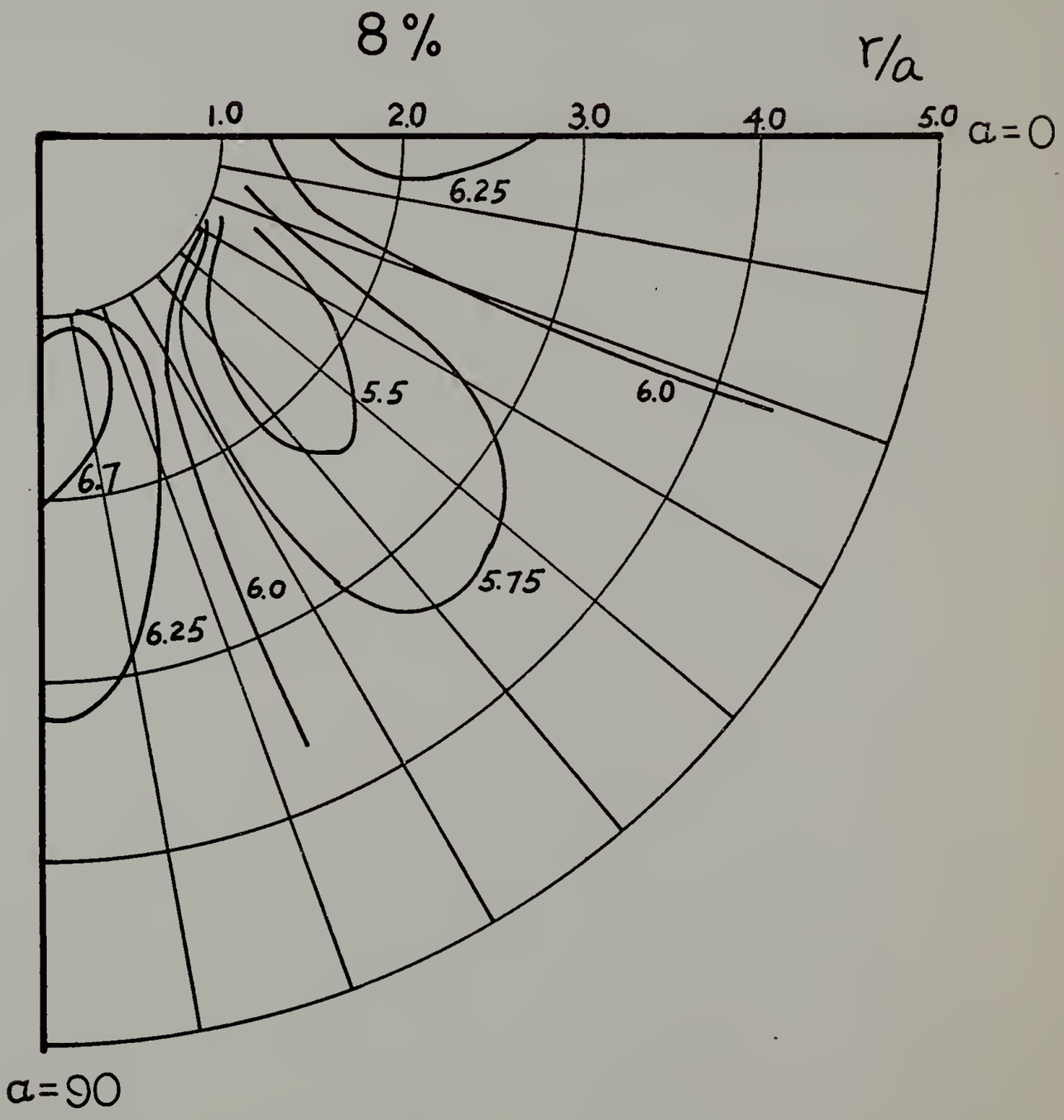

Figure 33

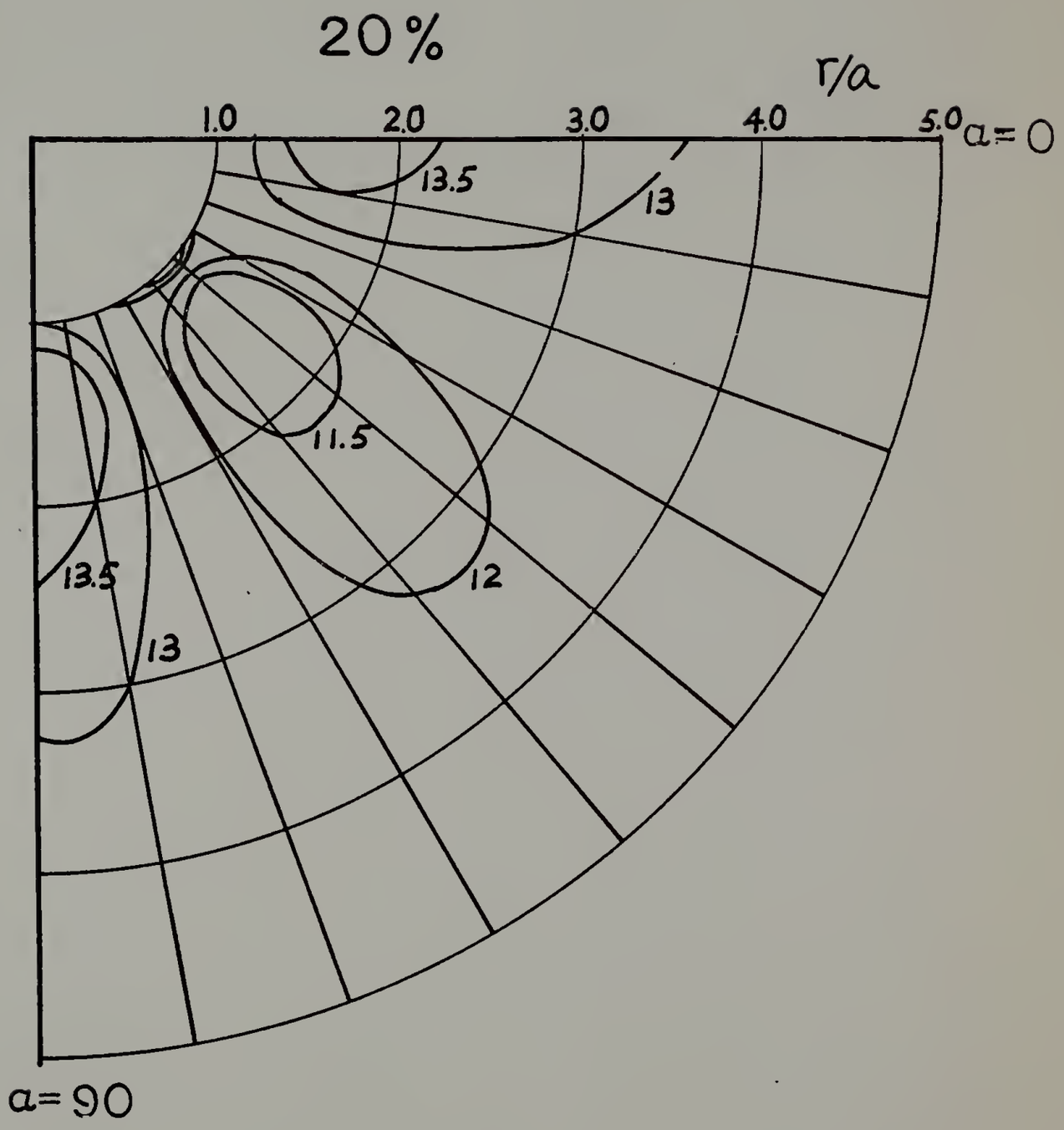

Figure 34

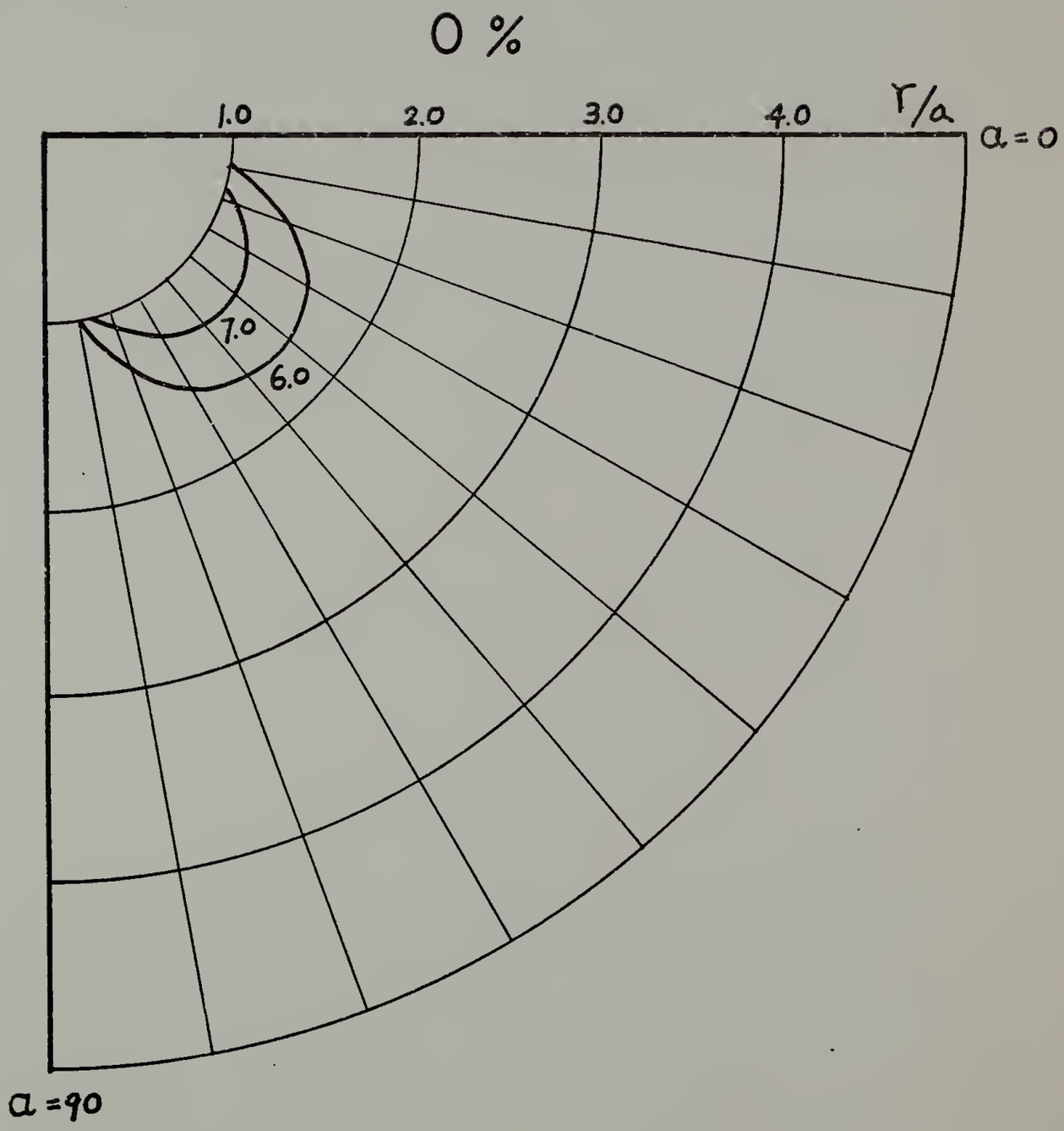

Figure 35

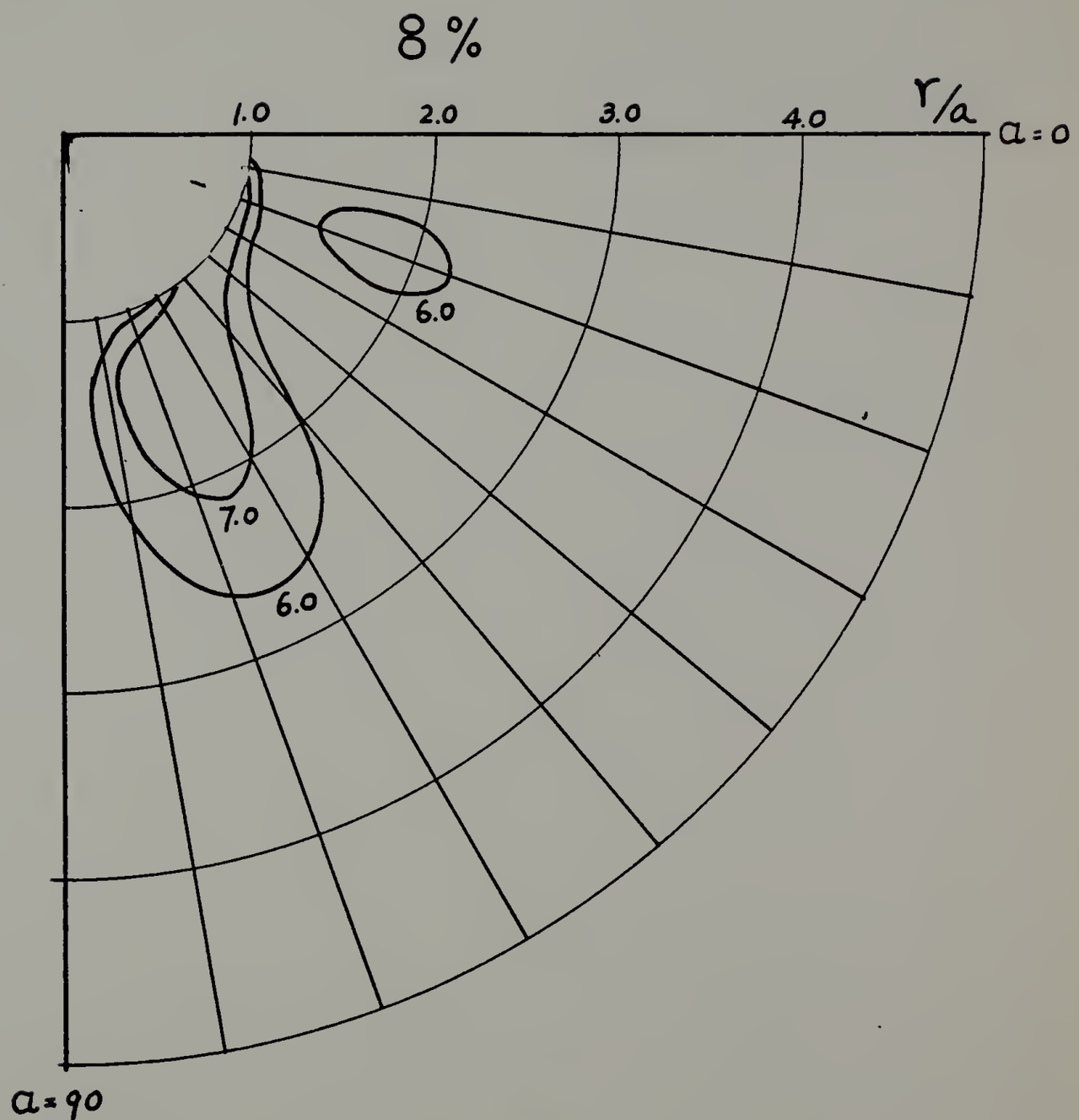

Figure 36

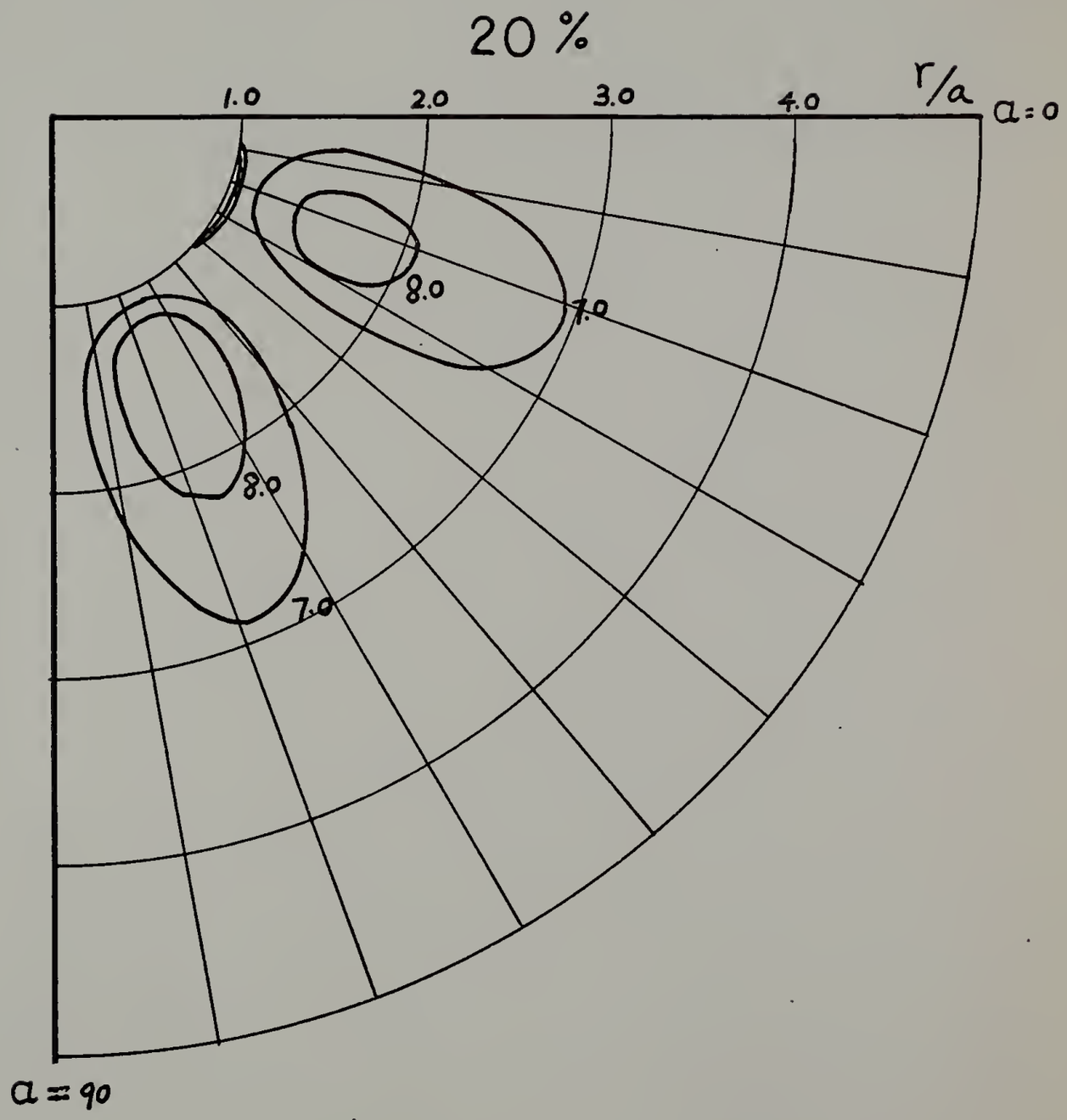

Figure 37

CHAPTER III

THE CORRECT MEASUREMENT OF BIREFRINGENCE IN A NON-UNIFORM MEDIUM

Introduction

Birefringence is often used for the characterization of the orientation distribution in a spherulite or fiber or the stress distribution around a crack or filler particle in a polymer system.[1,2] This is often done[3-5] by measuring the retardation using a compensator. The retardation, δ, is (in units of number of waves of path difference) given by

$$\delta = d\,\Delta/\lambda \tag{1}$$

where d is the thickness of the sample, Δ is the birefringence (in refractive index units), and λ is the wavelength of the light in vacuum, measured in the same units as d. This relationship presumes that the birefringence is constant over the optical path. In the event that it is not, it must be replaced by the integral relationship

$$\delta = (1/\lambda) \int_0^d \Delta(x)\, dx \tag{2}$$

assuming that the optic direction remains constant over the path length. This variation in birefringence along the path length is sometimes neglected, in which case the value of the birefringence which is obtained

is an average, as is the case in the measurements by Samuels[5] for starch granules, isotactic polystyrene and polypropylene, and Benoit, et al.,[4] for isotactic polystyrene. The meaning of this average is dependent upon the distribution in the absolute value and direction of optic axis orientation and is analyzed in this note.

Theory

When a light wave characterized by a wave normal, $\underset{\sim}{\ell}$, propagates, through an optically anisotropic crystal, it divides into two rays plane polarized in mutually perpendicular planes travelling with different phase velocities. The indicatrix serves to determine these planes of polarization and phase velocities in the following way: A diametral section of the indicatrix normal to $\underset{\sim}{\ell}$ is an ellipse having axes lying in the allowed polarization planes. The length of the major axis of this ellipse is proportional to the refractive index for the slow ray whose electric vector vibrates along it while the length of the minor axis is proportional to the refractive index of the fast ray.

As a specific example of a system of variable birefringence, let us consider the propagation of light through a spherulite of diameter D, for which the principal axes lie along and perpendicular to the radius shown in Figure 1. Consider a point Q after the transmitted ray has passed through the spherulite which is a distance r from the projection of the center of the spherulite, O, measured in a plane perpendicular to the transmitted ray. The line OQ makes an angle α with respect to

the plane of polarization. The retardation at Q is the sum of retardations along the path through the spherulite. At any point P along this path, the optical properties of the spherulite may be represented by the indicatrix tensor[6]

$$N = \begin{pmatrix} \frac{1}{n_2^2} & 0 & 0 \\ 0 & \frac{1}{n_3^2} & 0 \\ 0 & 0 & \frac{1}{n_1^2} \end{pmatrix} \tag{3}$$

where n_1, n_2 and n_3 are the principal refractive indices. We shall assume a uniaxial spherulite with its principal axis along the radius so that $n_3 = n_2 = n_t$ and $n_1 = n_r$, where n_r and n_t are the radial and tangential refractive indices of the spherulite. The polarizer and analyzer have their electric vector axes parallel to the Y and Z axes shown in Figure 1, where the light wave propagates along the X axis. In terms of this coordinate system the indicatrix is

$$N' = R^{-1} NR \tag{4}$$

where R is the rotation matrix given by

$$R = \begin{pmatrix} \cos\theta & 0 & -\sin\theta \\ 0 & 1 & 0 \\ \sin\theta & 0 & \cos\theta \end{pmatrix} \begin{pmatrix} \cos\phi & \sin\phi & 0 \\ -\sin\phi & \cos\phi & 0 \\ 0 & 0 & 1 \end{pmatrix} \tag{5}$$

$$= \begin{pmatrix} \cos\theta\cos\phi & \cos\theta\sin\phi & -\sin\theta \\ -\sin\phi & \cos\phi & 0 \\ \sin\theta\cos\phi & \sin\theta\sin\phi & \cos\theta \end{pmatrix}$$

The angles θ and ϕ are defined in Figure 2 and define the orientation of $\underset{\sim}{r}$ within the spherulite. The section of the indicatrix ellipsoid in the YZ plane is determined by any three elements of N', N_{22}', N_{23}' and N_{33}' and is given by the equation

$$N_{22}' y^2 + 2 N_{23}' yz + N_{33}' z^2 = 1 \tag{6}$$

and its principal axis is inclined to the OY axis by an angle β where

$$\tan^2\beta = 2 N_{23}'/(N_{22}' - N_{33}') \tag{7}$$

and its principal refractive indices are

$$a = \left[\frac{N_{22}' - \cos^2\beta\ (N_{22}' + N_{33}')}{1 - 2\cos^2\beta}\right]^{-1/2} \tag{8}$$

and

$$b = \left[(N_{22}' + N_{33}') - \frac{N_{22}' - \cos^2\beta\ (N_{22}' + N_{33}')}{1 - 2\cos^2\beta} \right]^{-1/2} \qquad (9)$$

The effect of a thin layer of the anisotropic medium on the light wave can be represented by a two-by-two complex Jones matrix[7]

$$A_j = \begin{pmatrix} \cos^2\beta_j\ e^{i\delta_j/2} + \sin^2\beta_j\ e^{-i\delta_j/2} & 2i\ \sin\beta_j\ \cos\beta_j\ \sin(\delta_j/2) \\ 2i\ \sin\beta_j\ \cos\beta_j\ \sin(\delta_j/2) & \sin^2\beta_j\ e^{i\delta_j/2} + \cos^2\beta_j\ e^{-i\delta_j/2} \end{pmatrix} \qquad (10)$$

where β_j is the angle between the fast axis of the ellipse of section and the OY axis. β_j is either β or $\beta - 90°$, depending upon the orientation of the ellipse of section. δ_j is the retardation produced by the j^{th} layer of the medium, given by $\delta_j = |a_j - b_j|(2\pi/\lambda)(D/m)$. D is the total thickness of the sample, which is divided into m thin layers within which the refractive index is assumed constant. The effect of the entire thickness of the sample is obtained by taking the product for the matrices for the m layers, giving the matrix B as

$$B = (A_m)\ (A_{m-1})\ (A_{m-2}) \cdots (A_2)\ (A_1) \qquad (11)$$

From the matrix B, the path difference and optic axis direction at point Q can be calculated as follows: It has been shown[8] that an optical system containing any number of retardation plates and rotators is optically equivalent to a system containing only two plates--one a retardation plate and the other a rotator. Eqn. (11) can be written in an equivalent form:

$$B = \begin{pmatrix} \cos\omega_Q & -\sin\omega_Q \\ \sin\omega_Q & \cos\omega_Q \end{pmatrix}$$

$$\begin{pmatrix} \cos^2\gamma_Q\, e^{i\delta_Q/2} + \sin^2\gamma_Q\, e^{-i\delta_Q/2} & 2i\sin\gamma_Q\cos\gamma_Q\sin(\delta_Q/2) \\ 2i\sin\gamma_Q\cos\gamma_Q\sin(\delta_Q/2) & \sin^2\gamma_Q\, e^{i\delta_Q/2} + \cos^2\gamma_Q\, e^{-i\delta_Q/2} \end{pmatrix}$$

$$= \begin{pmatrix} B_{11} & B_{12} \\ B_{21} & B_{22} \end{pmatrix} \tag{12}$$

from which it follows that

$$\gamma_Q = (1/2)\,\{-\omega_Q + \tan^{-1}\,[(B_{12} + B_{21})/(B_{11} - B_{22})]\} \tag{13}$$

$$\omega_Q = \tan^{-1}\,[(B_{21} - B_{12})/(B_{11} + B_{22})] \tag{14}$$

and

$$\delta_Q = 2\cos^{-1}\left[(B_{11} + B_{22})/(2\cos\omega_Q)\right] \qquad (15)$$

The retardation in radians at point Q is then given by δ_Q, and the angle between the fast axis and the OY axis in the YZ plane at this point is given by $\gamma_Q + \omega_Q$. Thus from a knowledge of the refractive indices at every point j within the medium, the matrix N may be determined from Eqn. (3), which may be transformed to N' using Eqns. (4) and (5). From the components of N', a, b and β may be determined using Eqns. (8), (9) and (7), from which the Jones matrix A_j can be obtained using Eqn. (8). These are then multiplied together to give matrix B, using Eqn. (9). From the components of this, δ_Q and $\gamma_Q + \omega_Q$ are obtained using Eqns. (13), (14) and (15), giving the retardation and optic axis orientation at any point of the field of view. A computer program for carrying out these operations can be devised.[9]

A Typical Calculation

For purposes of illustration, the retardation pattern arising from a single spherulite was considered, where the thickness of the film D equalled the diameter of the spherulite. A spherulite birefringence $n_r - n_t = -2.0 \times 10^{-4}$, a sample thickness D = 15μm, and a wavelength in vacuum λ = 0.55μm were assumed. The retardation δ_Q was calculated as a function of the distance OQ from the center of the projection of the

spherulite in the YZ plane and is plotted in Figure 3. Because of spherical symmetry, δ_Q is independent of the azimuthal angle α. The observed birefringence $\Delta n'$ equal to $\delta_Q \lambda/D$ was compared with the value that would have been obtained had the sample birefringence been assumed equal to the spherulite birefringence. The percent difference is plotted in Figure 4. This, of course, depends upon the distance from the center of the spherulite.

It is seen that an appreciable error results if the average birefringence of the sample is assumed equal to the spherulite birefringence, as has been done by some workers. A correction for this error can be obtained through use of Figure 4. Because of the symmetry of the spherulite, the slow axis direction will be at a fixed angle (90°) to the projection of the spherulite radius.

The approach described here is a general one which can be applied not only to that case in which the optical indicatrix is uniaxial and arranged with spherical symmetry, as with a spherulite, but also to the more complicated case in which the optical indicatrix is biaxial, as with the strain pattern in a stretched rubber containing spherical filler particles.[9,10] In this case the birefringence and optic axis orientation depend upon both radial and angular coordinates about the filler particle in a known way. Consequently, both the retardation and the slow axis direction depend upon radial and angular coordinates in the plane of observation. These serve as independent variables which may be measured and compared with theory.[9,10]

It follows that in order to relate a measured distribution of

retardation and slow axis direction to a local birefringence and optic axis orientation, one must have available some model which describes the spacial distribution of these variables. If this is available, the procedures described here may be employed to relate the parameters describing the local birefringence to the measured optical properties.

References

1. C. Picot, M. Fukuda, C. Ong (Chou), and R. S. Stein, J. Macromol. Sci., B6(1), 263 (1972).
2. T. Kotani and S. S. Sternstein, in "Polymer Networks: Structural and Mechanical Properties," A. J. Chompff and S. Newman, eds., Plenum Press, New York, New York.
3. F. J. Padden, Jr. and H. D. Keith, J. Appl. Phys., 36, 14701 (1959).
4. C. Picot, G. Weill, and H. Benoit, J. Polymer Sci., C, 6, 3973 (1968).
5. R. J. Samuels, J. Polymer Sci., A2, 9, 2165 (1971).
6. H. D. Keith and F. J. Padden, Jr., J. Polymer Sci., 39, 101 (1959).
7. R. C. Jones, J. Opt. Soc. Amer., 37, 107 (1947).
8. H. Hurwitz, Jr. and R. C. Jones, J. Opt. Soc. Amer., 31, 493 (1941).
9. C. Ong, Ph.D. Thesis, University of Massachusetts (Amherst), 1973.
10. C. Ong and R. S. Stein, in preparation.

Captions for Figures

1. The coordinates describing the passage of a light beam through a sample containing an anisotropic spherulite.
2. The angular coordinates of point P within a spherulite.
3. The variation of the retardation, δ_R, with distance from the center of the projection of the spherulite, OQ.
4. The percentage difference between the calculated average birefringence and the actual spherulite birefringence.

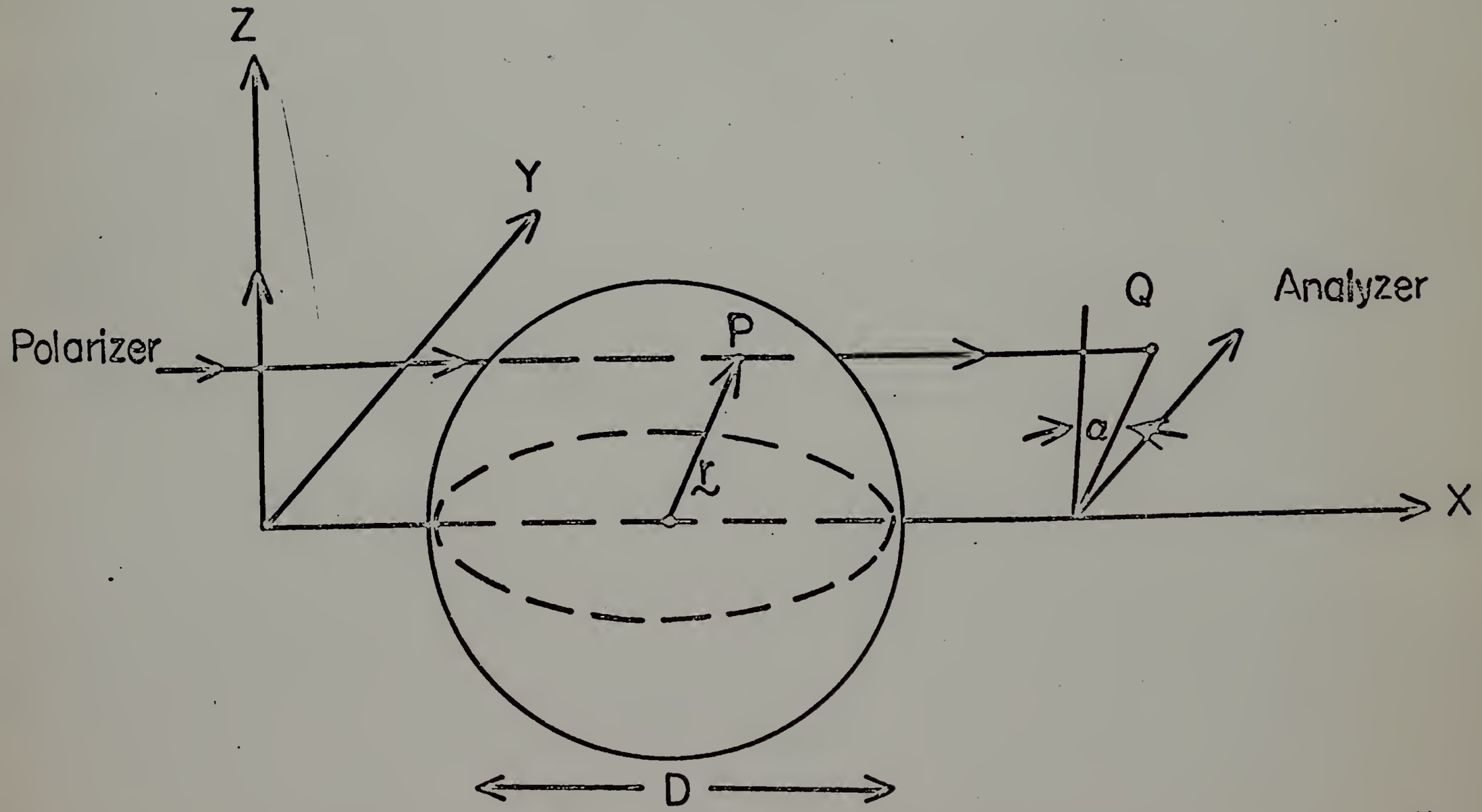

Figure 1

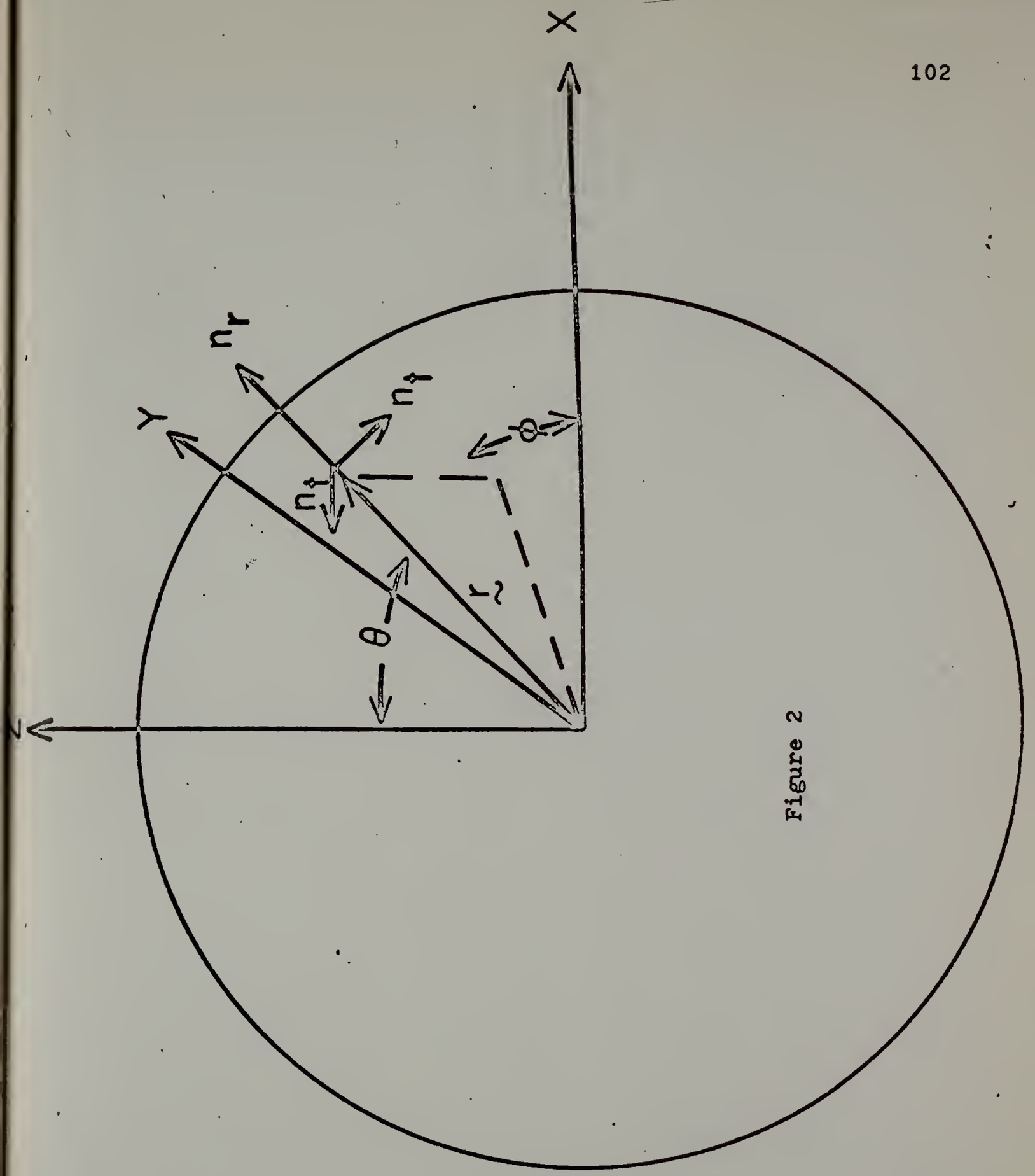

Figure 2

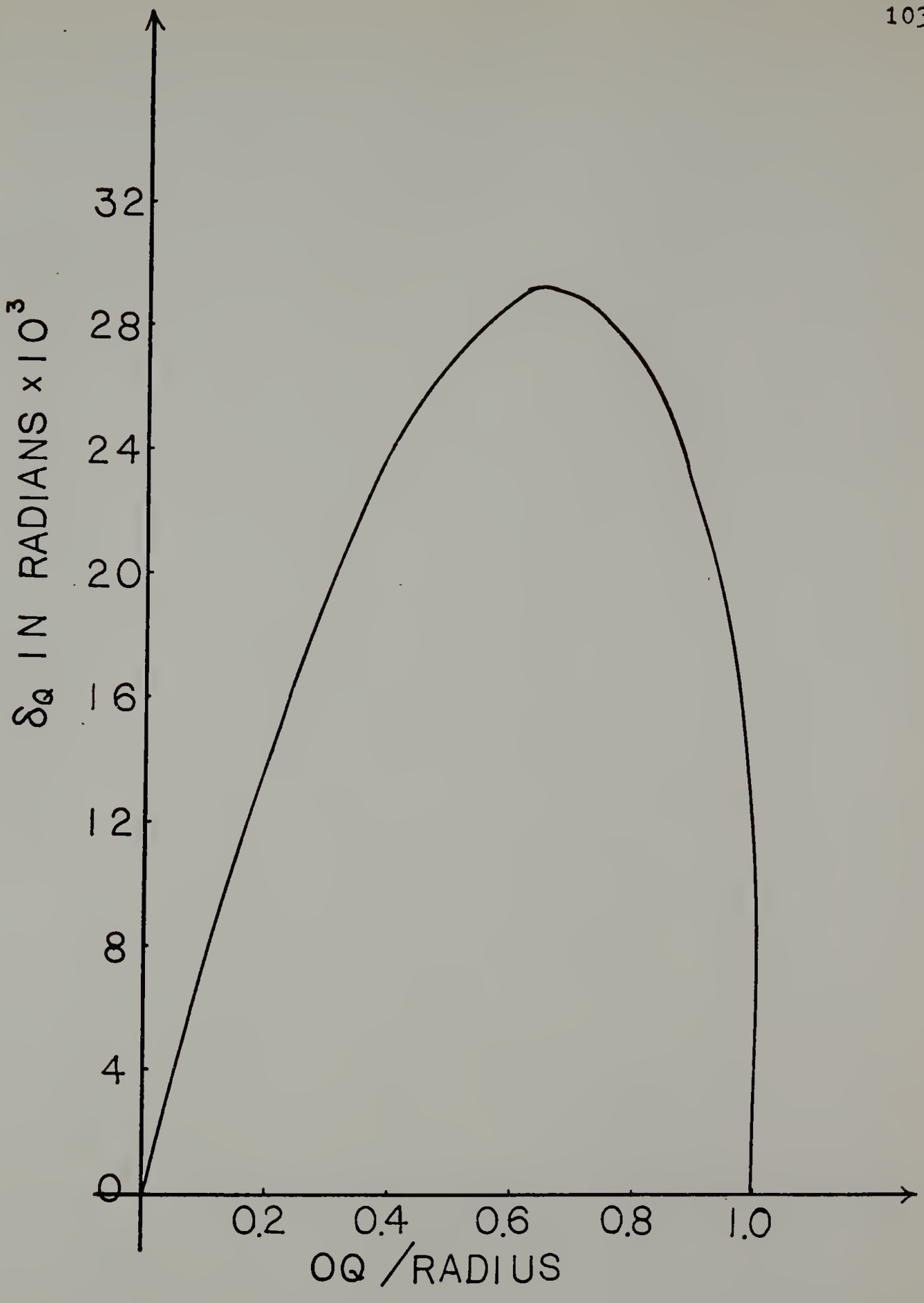
δ_Q IN RADIANS x 10^3
32
28
24
20
16
12
8
4
0
0.2
0.4
0.6
0.8
1.0
OQ / RADIUS

Figure 3

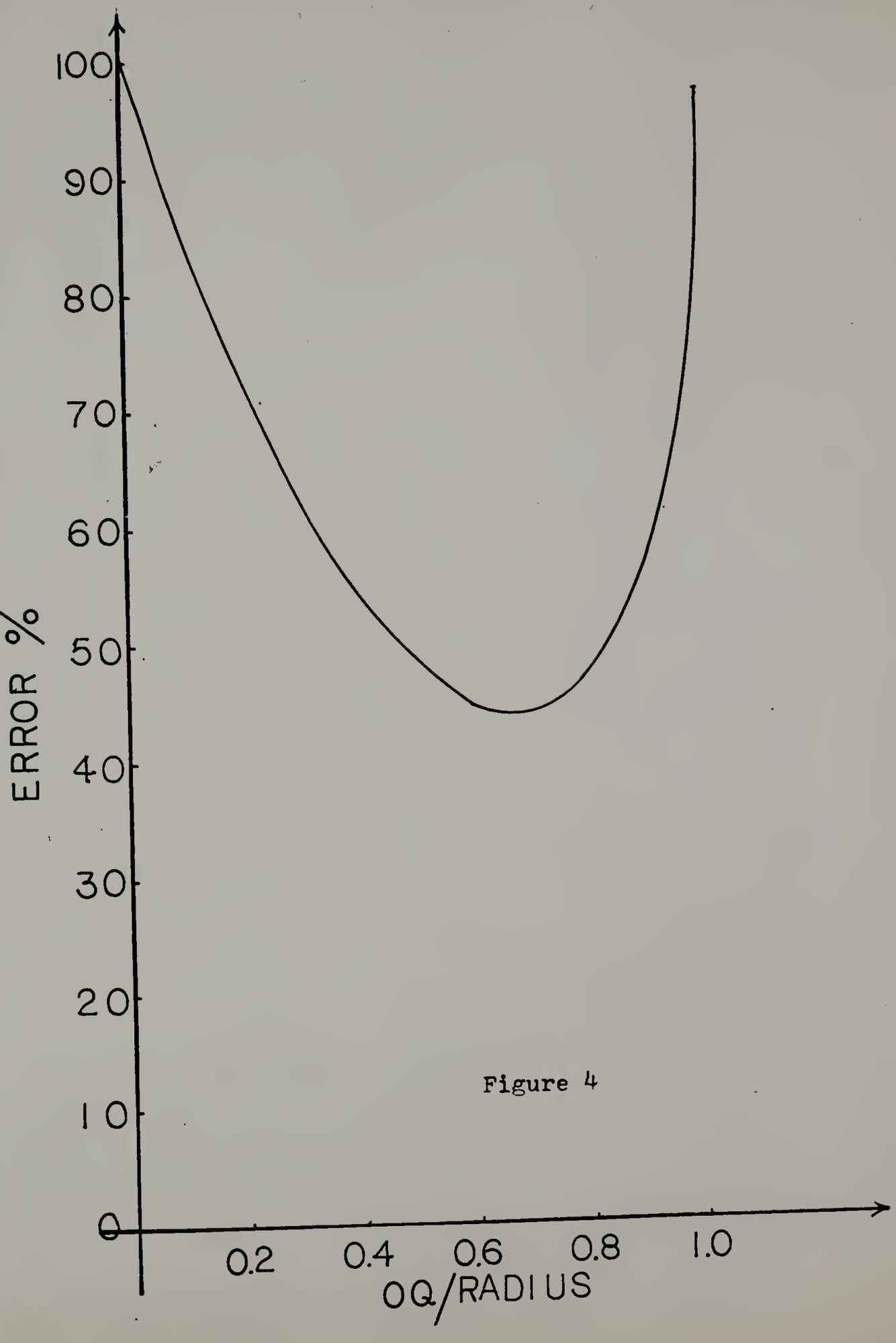

Figure 4

CHAPTER IV

STRESS, STRAIN AND BIREFRINGENCE RELATIONS OF SWOLLEN CIS-1,4-POLYBUTADIENE CROSSLINKED IN SOLUTION

Summary

Stress-strain-birefringence relations are measured for a series of unswollen and swollen networks of cis-1,4-polybutadienes which differ both in the degree of crosslinking and in the volume fraction of rubber present during crosslinking. The stress optical coefficient (SOC), the Mooney-Rivlin constants C_1, C_2 and B_1, B_2 are calculated. Results show that the unswollen solution vulcanized polymers have very low values of C_2 and B_2, but high SOC. Upon swelling with CCl_4, the stress optical coefficients decrease considerably and agree well with the values obtained by Fukuda, Wilkes and Stein and by Ishikawa and Nagai. The networks prepared in solution exhibit different behaviors from those crosslinked in dry state, suggesting that in order to understand the origin of deviations from kinetic rubber elasticity theory and Kuhn-Grün's birefringence theory, more consideration must be given to the effect of overall network topology on stress-strain-birefringence behavior.

Introduction

Stress, strain and birefringence measurements have been carried out on swollen and unswollen networks of cis-1,4-polybutadiene

polymers.[1,2] Neither stress-strain nor birefringence-strain relations of unswollen specimens obey the Gaussian network theory, but both can be fitted by the Mooney-Rivlin equations

$$\sigma_o/(\lambda - \lambda^{-2}) = 2\ C_1 + 2\ C_2\lambda^{-1} \tag{1}$$

$$\Delta n/(\lambda^2 - \lambda^{-1}) = B_1 + B_2\lambda^{-1} \tag{2}$$

where σ_o is the stress referred to the unswollen, unstretched cross section; Δn is the birefringence referred to the stretched thickness; λ is the elongation ratio $\lambda = 1/l_0$, l and l_0 being the lengths in the presence and in the absence of applied load, respectively; and C_1, C_2 and B_1, B_2 are constants independent of λ.

The stress optical coefficient of cis-1,4-polybutadiene polymers or, equivalently, the optical anisotropy $\Delta\Gamma$ of Kuhn's statistical segment has also been measured. The stress optical coefficient of a rubber network may be described in terms of the statistical segment model of Kuhn-Grün[3] and Treloar[4] as

$$C = \frac{\Delta n}{\sigma} = \frac{2\pi}{45kT} \cdot \frac{(\bar{n}^2 + 2)^2}{\bar{n}} \Delta\Gamma \tag{3}$$

where Δn is the birefringence of the uniaxially stretched rubber subjected to a stress σ (on unit area in the stretched state), k is Boltzmann's constant, T is the absolute temperature, and $\bar{n}$ is the

average refractive index of the rubber. The anisotropy of the statistical segment $\Delta\Gamma$ is given by

$$\Delta\Gamma = (b_1 - b_2)_s \tag{4}$$

where b_1 and b_2 are the polarizabilities parallel and perpendicular, respectively, to the axes of the segment.

The stress optical coefficient of unswollen networks does not obey Eqn. (3) and can be represented by

$$C = \frac{\Delta n}{\sigma} = \frac{B_1 + B_2\lambda^{-1}}{2(C_1 + C_2\lambda^{-1})} \tag{5}$$

Deviations from the Gaussian network theory and the Kuhn-Grün birefringence theory are found which are reduced upon swelling. The magnitudes of C_2 and B_2 are large in dry rubbers and decrease to zero at high degrees of swelling. The anisotropy of the statistical segment depends on the nature of swelling solvent and has its lowest value when the network is swollen with an isotropic solvent, CCl_4. The dependence of $\Delta\Gamma$ on the nature of the swelling solvent is believed to result from the effect of the internal field from anisotropy solvent molecules.[1] The $\Delta\Gamma$ obtained in CCl_4 is believed to represent that of an isolated segment.

There is as yet no satisfactory quantitative explanation for the

observed deviations from the Gaussian network theory and the Kuhn-Grün birefringence theory. Many of the difficulties associated with the problem have clearly been due to the lack of basic information concerning the behavior of C_2 and B_2. Many attempts have been made to analyze the assumptions underlying the ideal theory; Blokland[5] has reviewed all these theories and concluded that all except the theories of Dimarzio[6] and Jackson[7] c. s. are unsatisfactory. These two theories were based on the space-filling character of real polymer molecules. However, the calculated effects from these two theories seem to be insufficient in magnitude--at least, too small to explain the observed deviations between Gaussian network theory and experiment. Again, Blokland's bundle structure theory was found unsatisfactory by Prins and Dusek,[8] but they believe the concept of a certain structure in the network is capable of explaining the deviations.

Recently, Price[9] and Mark[10] have reported that rubber crosslinked in the presence of a diluent had much lower values of C_2 after removing the diluent than those vulcanized in dry state, and had considerably smaller non-equilibrium relaxation effects. These results seem to support the contentions that networks prepared by crosslinking a polymer in solution have very different topologies from those prepared in the bulk, undiluted state. They also pointed out that successful revision of the theory of polymer networks must explicitly take into account the topology of the network structure.

It is the purpose of this research to study the stress, strain and birefringence relations of swollen cis-1,4-polybutadiene crosslinked in

solution. This information may provide a better understanding of the discrepancy between theory and experiment.

Experimental

Sample Preparation

A high cis-1,4-(93%)polybutadiene sample was obtained from the Phillips Petroleum Company. Two series of samples were prepared. Series A, which differs in ϕ_r, was crosslinked in solution. (ϕ_r is the volume fraction of rubber present during crosslinking.) Series B, which differs in the concentration of curing agent used, was crosslinked conventionally. For Series A, the polymer, which was purified by precipitation from benzene solution by methanol, was dissolved in a solution of dicumyl peroxide in a relatively inert, high boiling point solvent, decalin. It was stirred carefully until equilibrium was reached. The solution was then transferred to a Teflon coated pan (in order to obtain a thin film with thickness of about 20 mils). After all the bubbles had disappeared from the solution, the Teflon pan was sealed in a desiccator under nitrogen. The system was then heated to 140°C for $1\frac{1}{2}$ hrs. The desiccator was opened and was cooled to room temperature. A small amount of methanol was added in order to deswell the gel, which then came away cleanly from the pan. The gel was extracted with gently stirred benzene at room temperature for 24 hrs., and was then deswelled with methanol and dried under vacuum about 12 hrs. The samples with three different ϕ_r values (0.10, 0.16 and 0.20)

were designated as A-1, A-2 and A-3 when they were measured in the dry state.

For Series B, the conventional dry state crosslink method was used. A curing agent, dicumyl peroxide, was added to the rubber-benzene solution, and then films 10-25 mils thick were cast on a Teflon pan. These were crosslinked at 140°C at 3000 psi for 40 min. in a small laboratory press. The samples with different concentrations of dicumyl peroxide 0.1%, 0.3% and 0.5% by weight relative to rubbers were designated as B-1, B-2 and B-3 when they were measured in the dry state.

The corresponding samples which were measured in the swollen state were designated as A-1', A-2', A-3' and B-1', B-2', B-3'.

Stress-Strain-Birefringence Measurements

The relations between stress, strain and birefringence were investigated in both the dry and the swollen states. The samples measured in their dry state were mounted between two clamps in an Instron, where the samples were stretched by an automatic mechanical stretching device, and the retardations were read using a Babinet compensator. Stresses were also measured simultaneously by using an Instron table model tensile tester.[11] The samples used were about 0.5 cm in width, 2.5 cm in length and 10-20 mils in thickness. The length between two reference marks was measured to ±0.002 cm with a cathetometer. The dimensions of the samples in the stretched state were calculated on the bases of the attained cross-sectional area and the thickness in this state. For each sample, six elongations, from $\lambda = 1.2$ to 1.7, were measured.

For the measurements carried out in the swollen state, the isotropic solvent CCl_4 was used and samples were swollen to equilibrium. A cell which has glass windows on two sides was used. It was mounted in the Instron, and the stress and birefringence were measured in the same way as described above. The volume fraction of rubber in the swollen polymer, v_r, was measured by quickly removing the sample from the swelling bath, wiping it off and weighing.

Results and Discussion

Stress-strain and birefringence-strain relations on the swollen and unswollen specimens of solution vulcanized cis-1,4-polybutadiene are shown in Figure 1 and Figure 2. The data were taken at room temperature and plotted in accordance with the Mooney-Rivlin relations

$$\sigma v_r^{1/3} / (\lambda - \lambda^{-2}) = 2\ C_1 + 2\ C_2\lambda^{-1} \tag{6}$$

$$\Delta n\ v_r^{1/3} / (\lambda^2 - \lambda^{-1}) = B_1 + B_2\lambda^{-1} \tag{7}$$

where v_r is the volume fraction of polymer.

Similar plots for dry state vulcanized cis-1,4-polybutadiene are shown in Figure 3 and Figure 4.

Calculated values of SOC, C_1, C_2 and B_1, B_2 for solution vulcanized and dry state vulcanized elastomers are given in Table I and Table II. The stress optical coefficients are calculated from slopes of

birefringence-stress curves. The constants C_1, C_2 and B_1, B_2 are calculated as intercepts and slopes of straight lines shown in Figures 1 through 4. The least square method was used to determine the locations of the straight lines.

As seen in Table II, both stress and birefringence exhibit significant deviations from kinetic elasticity and birefringence theory when the rubber was crosslinked in the dry state. The noted decrease in C_2 was attributed by Prins and Dusek[8] to the disappearance of the original structure (bundles or correlated regions) upon swelling. However, this explanation is controversial. The decrease of $\Delta\Gamma$ is mainly due to the internal field effect suggested by Stein.[1]

For the unswollen solution vulcanized rubber as seen in Table I, it is noted that the slopes of the MR plots, C_2 and B_2 are either very low or zero. C_2 and B_2 approach zero when $\phi_r < 0.16$ (where ϕ_r is the volume fraction of rubber present during crosslinking) and increase with increasing ϕ_r. The stress optical coefficients (SOC) obtained are the same magnitude as those of unswollen conventional vulcanizates (compare with Table II).

On swelling the solution vulcanized rubbers, the values of C_2 and B_2 decrease slightly; however, both C_1 and B_1 decrease substantially. The SOC obtained are about the same magnitude as those of swollen conventional vulcanizates.

Viewing the data as a whole, two different types of behavior for these two polymers vulcanized in different conditions were observed. In the unswollen state, the photoelastic behavior of the solution

vulcanized elastomers appears to be in much closer agreement with the theories than is the case for vulcanizates prepared in the dry state. Ir the swollen state, the behavior of both rubbers agrees well with the theories. These results suggest that the concept of an original structure to account for the origin of C_2 is in doubt, and that more emphasis should be put on the overall network topology to account for the deviations from the theories.

References

1. M. Fukuda, G. L. Wilkes, and R. S. Stein, J. Polymer Sci., A-2, 9, 1417 (1971).
2. T. Ishikawa and K. Nagai, J. Polymer Sci., A-2, 7, 1123 (1969).
3. W. Kuhn and F. Grün, Kolloid Z., 101, 248 (1942).
4. L. R. G. Treloar, "The Physics of Rubber Elasticity," 2nd ed., Oxford University Press, 1967.
5. R. Blokland, "Elasticity and Structure of Polyurethane Networks," Rotterdam University Press, 1968.
6. E. A. Dimarzio, J. Chem. Phys., 36, 1563 (1962).
7. J. L. Jackson, M. C. Shen, and D. A. McQuarrie, J. Chem. Phys., 44, 2388 (1966).
8. K. Dusek and W. Prins, Fortschr. Hochpolym. Fosch., 6, 1 (1969).
9. C. Price, G. Allen, F. De Candia, M. C. Kirkham, and A. Subramanian, Polymer, 11, 486 (1970).
10. J. E. Mark, J. Am. Chem. Soc., 7252, December (1970).
11. D. A. Keedy, R. V. Volungis, and H. Kawai, Rev. Sci. Inst., 32, 415 (1961).

Captions for Figures

1 Mooney-Rivlin plots for stress-strain relations for solution vulcanized cis-1,4-polybutadiene.

2. Mooney-Rivlin plots for birefringence-strain relations for solution vulcanized cis-1,4-polybutadiene.

3. Mooney-Rivlin plots for stress-strain relations for dry state vulcanized cis-1,4-polybutadiene.

4. Mooney-Rivlin plots for birefringence-strain relations for dry state vulcanized cis-1,4-polybutadiene.

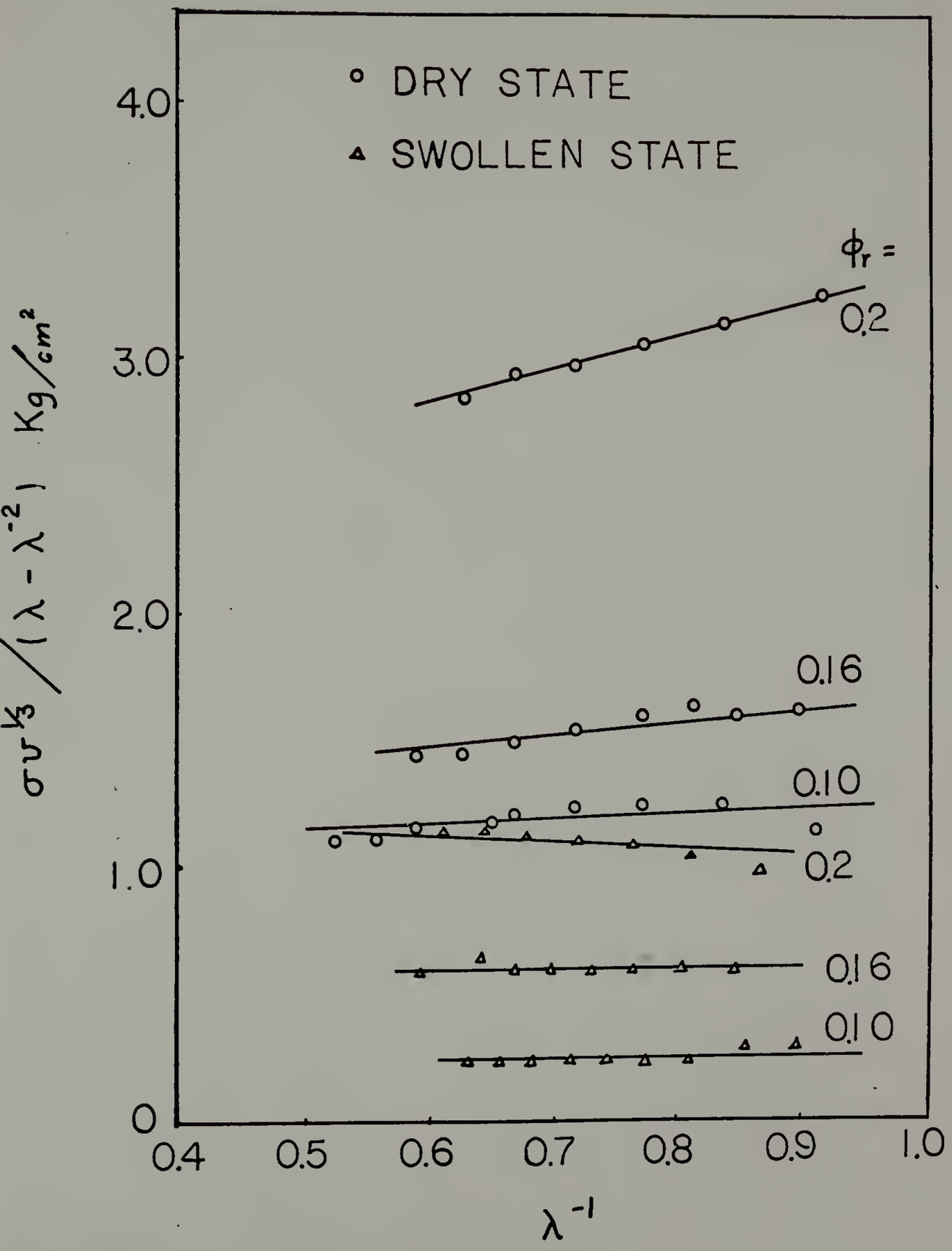
DRY STATE
SWOLLEN STATE
ϕ_r =
0.2
0.16
0.10
0.2
0.16
0.10
$\sigma v^{1/3} / (\lambda - \lambda^{-2})$ Kg/cm²
λ^{-1}
4.0
3.0
2.0
1.0
0
0.4
0.5
0.6
0.7
0.8
0.9
1.0

Figure 1

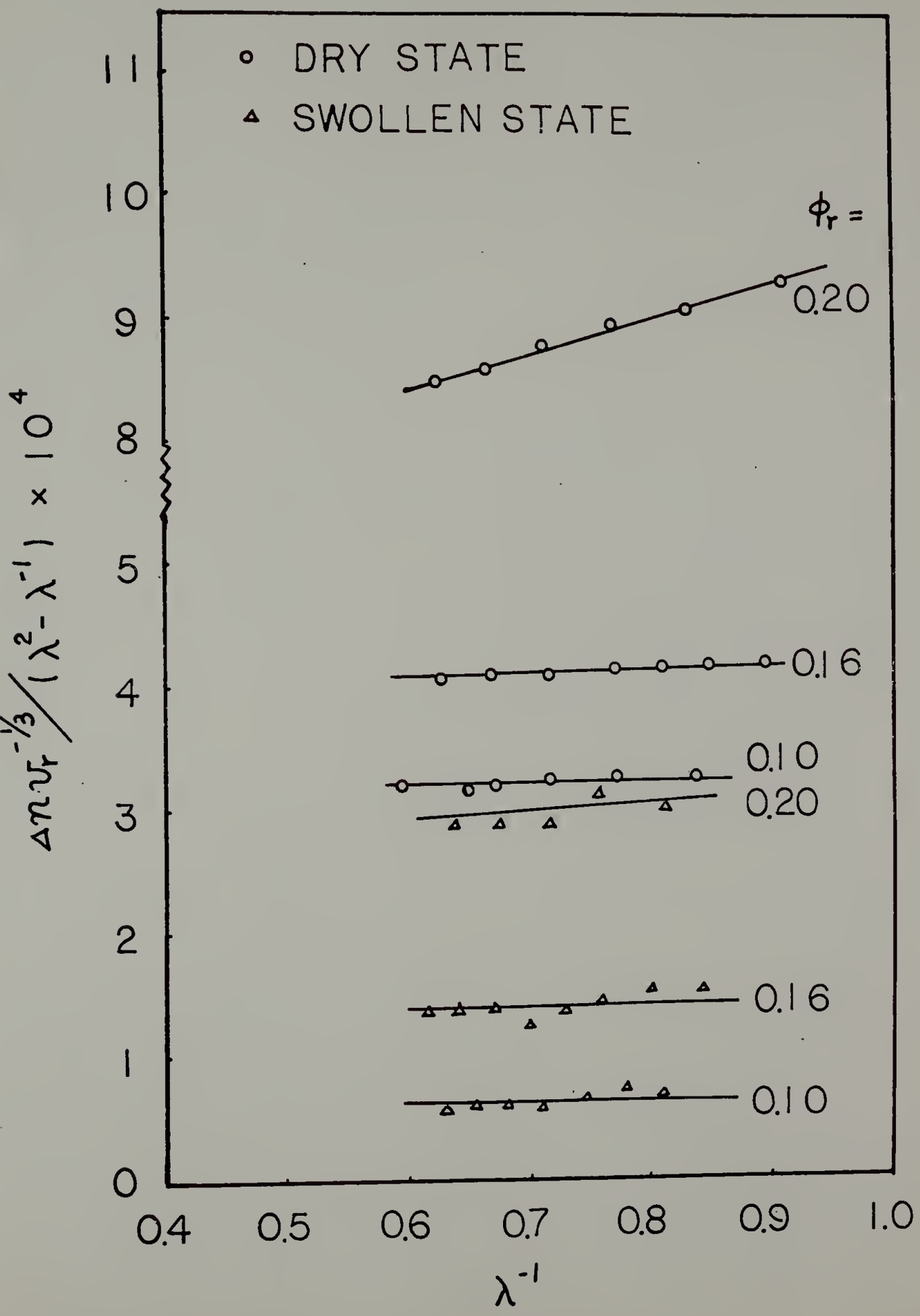
DRY STATE
SWOLLEN STATE
ϕ_r =
0.20
0.16
0.10
0.20
0.16
0.10
$\Delta n v_r^{-1/3} / (\lambda^2 - \lambda^{-1}) \times 10^4$
λ^{-1}
0
1
2
3
4
5
8
9
10
11
0.4
0.5
0.6
0.7
0.8
0.9
1.0

Figure 2

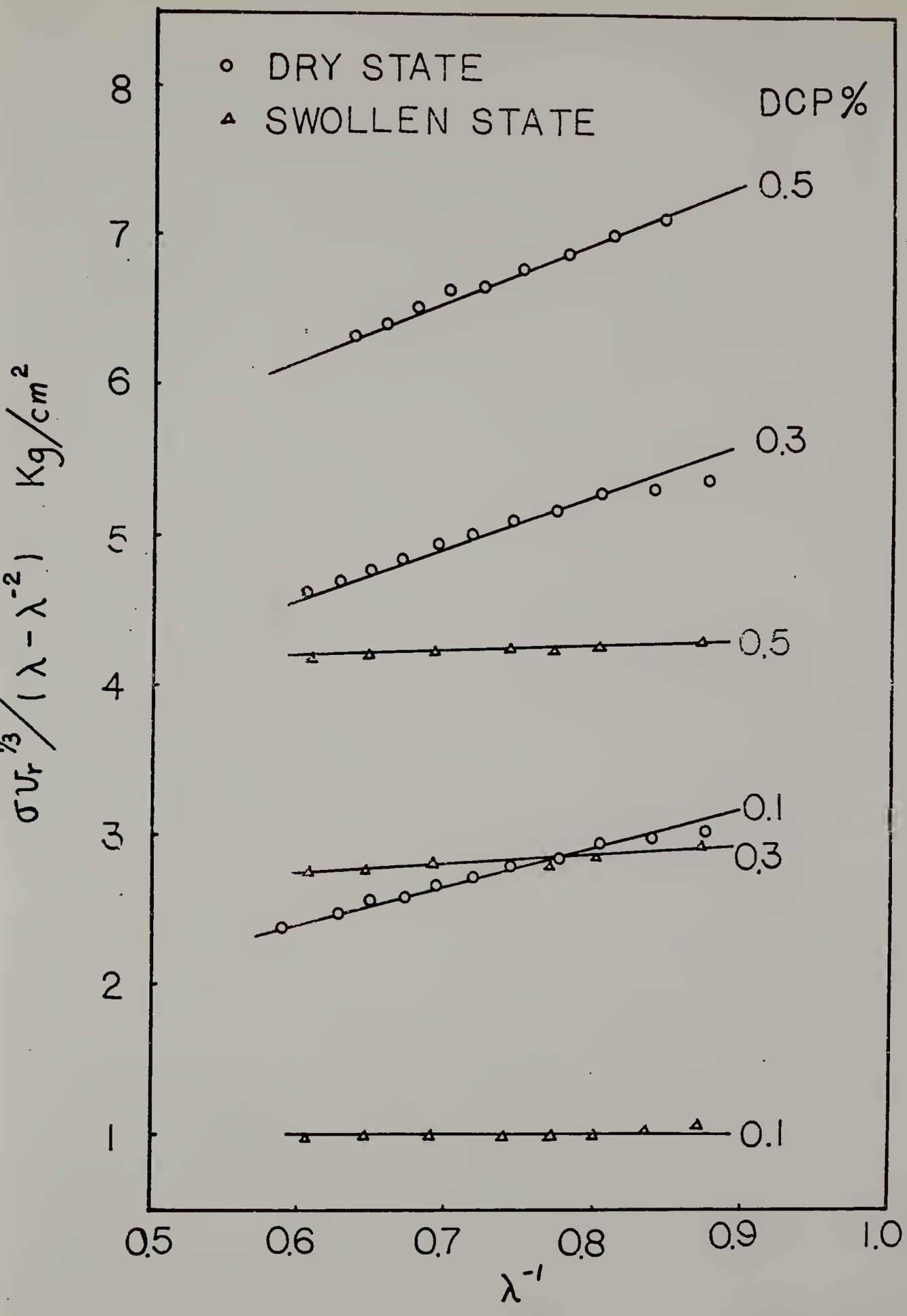
DRY STATE
SWOLLEN STATE
DCP%
0.5
0.3
0.5
0.1
0.3
0.1
8
7
6
5
4
3
2
1
0.5
0.6
0.7
0.8
0.9
1.0
λ^{-1}
$\sigma V_r^{1/3}/(\lambda-\lambda^{-2})$ Kg/cm²

Figure 3

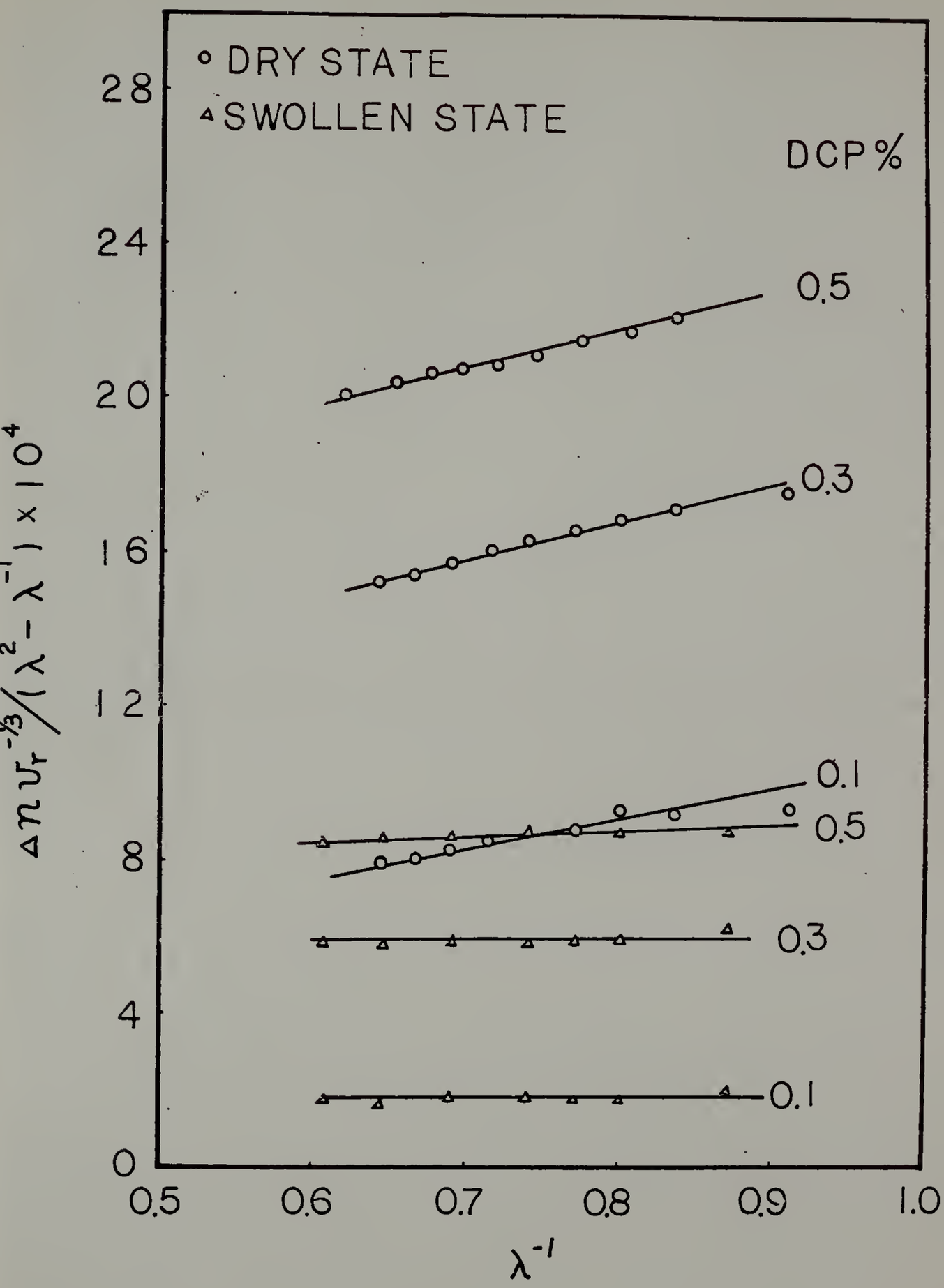
DRY STATE
SWOLLEN STATE
DCP %
0.5
0.3
0.1
0.5
0.3
0.1
28
24
20
16
12
8
4
0
0.5
0.6
0.7
0.8
0.9
1.0
λ^{-1}
$\Delta n\, v_r^{-1/3}/(\lambda^2-\lambda^{-1})\times 10^4$

Figure 4

TABLE II

SAMPLE	ϕ_r	DCP %	V_r	SOC $\times 10^{+7}$	$2C_1$ kg/cm^2	$2C_2$ kg/cm^2	B_1 $\times 10^{+4}$	B_2 $\times 10^{+4}$
A-1	1.0	0.1	1.0	3.1	0.87	2.1	2.65	8.0
A-2	1.0	0.3	1.0	3.2	2.46	3.5	9.2	9.1
A-3	1.0	0.5	1.0	3.2	3.92	3.84	14.9	8.45
A-1′	1.0	0.1	0.091	2.04	1.0	0.019	1.8	0.6
A-2′	1.0	0.3	0.134	2.10	2.32	0.69	4.8	1.46
A-3′	1.0	0.5	0.16	2.06	3.91	0.44	7.95	0.92

CONVENTIONAL VULCANIZED RUBBERS

TABLE I

SAMPLE	ϕ_r	DCP%	V_r	SOC $\times 10^{+7}$	$2C_1$ kg/cm^2	$2C_2$ kg/cm^2	B_1 $\times 10^{+4}$	B_2 $\times 10^{+4}$
B-1	0.10	3	1.0	3.14	1.0	0.3	3.1	0.3
B-2	0.16	3	1.0	3.2	1.17	0.5	4.0	0.2
B-3	0.20	3	1.0	3.18	1.95	0.96	7.1	2.1
B-1′	0.10	3	0.04	2.15	0.25	0.038	0.6	0.02
B-2′	0.16	3	0.06	2.03	0.61	0.005	1.25	0.03
B-3′	0.20	3	0.09	2.1	1.25	-0.2	2.25	0.5

SOLUTION VULCANIZED RUBBERS

CHAPTER V

SUGGESTIONS FOR FUTURE STUDIES

(1) In Chapters I and II, the light scattering and birefringence patterns arising from deformed regions surrounding inclusions in crosslinked cis-1,4-polybutadiene have been described. The H_v small angle light scattering patterns were shown to arise from the birefringence patterns associated with the inhomogeneous stress field which is induced by swelling and stretching. If the filled rubber were swollen to equilibrium and then stretched to different extents, the behavior of the stress field around the fillers would be different from those cases presented in Chapters I and II. The interpretation of the light scattering pattern, the birefringence pattern and the stress distribution around the fillers would be very interesting to obtain.

It would also be very interesting to extend this work to the case in which glass fibers rather than glass spheres are used as the filler. This would be a good approximation to the effect of growing crystallites in a polymer sample.

(2) In Chapter II, the observation of no change in the shape and the intensity of V_v patterns during stretching indicates that there is no failure occurring at the interface of the beads and the matrix up to 40% elongation. The sample breaks beyond 40% elongation, due to the high crosslink density of the sample. In order

to detect any failure occurring at the interface, a lower concentration of crosslinking agent should be used so that the sample could be extended to high elongations.

(3) Eight-lobe H_v light scattering patterns were observed in the case of stress-induced crystallization of rubbers in which crystals may grow in an ellipsoidal aggregate whose long axis is perpendicular to the stretching direction in the rubber matrix by stretching. The contribution of strained amorphous polymer around crystallites may explain this phenomenon. Theoretical calculations of light scattering patterns of this polymer system can be performed in order to compare with experimental results.

(4) Inhomogeneity in crosslink density leads to local stress concentrations which serve as incipient regions of failure or fatigue. Presumably, a more homogeneously crosslinked rubber possesses greater tensile strength and fatigue resistance. When an inhomogeneous crosslinked network is swollen or stretched, the local strain may differ from the external strain. The strain of more highly crosslinked regions will be less than that of more lightly crosslinked regions. This variation will lead to variations in the local birefringence and optic axis orientation, which will result in an enhanced scattering. The theory for the enhanced V_v intensity of scattering resulting from swelling has been published by Stein;[2] the enhanced scattering is proportional to the

mean square fluctuation in crosslink density, and the angular variation in this scattered intensity is related to the size of the region in which fluctuation occurs. It would be interesting to study, both experimentally and theoretically, the enhanced H_v scattering intensity arising from the inhomogeneity of strains during swelling and stretching. For this purpose, the elastomers crosslinked by three different methods--radiation, sulfur, peroxide--and crosslinked at different diluent contents could be used.

(5) In a recent publication of Fukuda, Wilkes and Stein,[3] it is found that the stress optical coefficient of cis-1,4-polybutadiene depends upon the swelling solvent. It is believed to result from the effect of internal field from anisotropic solvent molecules. The stress optical coefficient obtained in the isotropic solvent CCl_4, which has the least solvent effect, has the lowest value. Usually, the solvent effect as explained by Stein will depend on (1) the correlation of orientation of solvent molecules with the segment axis and (2) the distribution of centers of solvent molecules. The first contribution is of no consequence for an isotropic solvent, but a solvent effect resulting from the second contribution may still persist. Although a solvent effect may be small for CCl_4, the SOC obtained in CCl_4 might still be different from that obtained in CBr_4, due to the second contribution. It would be interesting to obtain the SOC from crosslinked cis-1,4-PBE swollen with CBr_4 to compare with that obtained with CCl_4.

(6) As discussed in Chapter IV, the solution crosslinked rubbers behave ideally, as predicted by the kinetic theory of rubber elasticity and Kuhn-Grün's birefringence theory. It would be interesting to extend the work to a wider range of ϕ_r (where ϕ_r is the volume fraction of rubber present during crosslinking) to obtain the variations of Mooney-Rivlin constant $2C_2$ with ϕ_r.

References

1. Y. Akana, M.S. Thesis, University of Massachusetts (Amherst), 1972.

2. R. S. Stein, J. Polymer Sci., B7, 657 (1969).

3. M. Fukuda, G. H. Wilkes, and R. S. Stein, J. Polymer Sci., A-2, 9, 1417 (1971).

A P P E N D I X

APPENDIX I

Procedures of Retardation and Slow Direction Measurements by Microscope

1. A Carl Zeiss polarizing microscope with relative positions of polarizer, analyzer, the stretching direction of sample and the slow direction of rotary compensator shown in Figure 1 was used.
2. The sample was fastened in place with its stretching direction along 0°-180° direction on the stage. The stage was rotated and the centering screw was adjusted so as to bring the center of revolution to coincide with the intersection of the crosshairs.
3. The point of interest was moved to the intersection of the crosshairs by moving the mechanical stage either horizontally or vertically or both.
4. The stage was rotated to the position of maximum darkness (extinction position); it was repeated several times, and the graduated scale was read each time so that the average position of maximum darkness was obtained.
5. The stage was rotated ±45° from the average position of maximum darkness. An Ehringhaus rotary compensator with its slow direction parallel to the longitudinal direction of the whole instrument at a -45°-135° direction was inserted, and it was decided whether there was compensation of retardation occurring or not. The slow direction of this point was then determined.

6. An arithmetic mean of two readings toward both sides of the rotary compensator was taken as the retardation of this point.

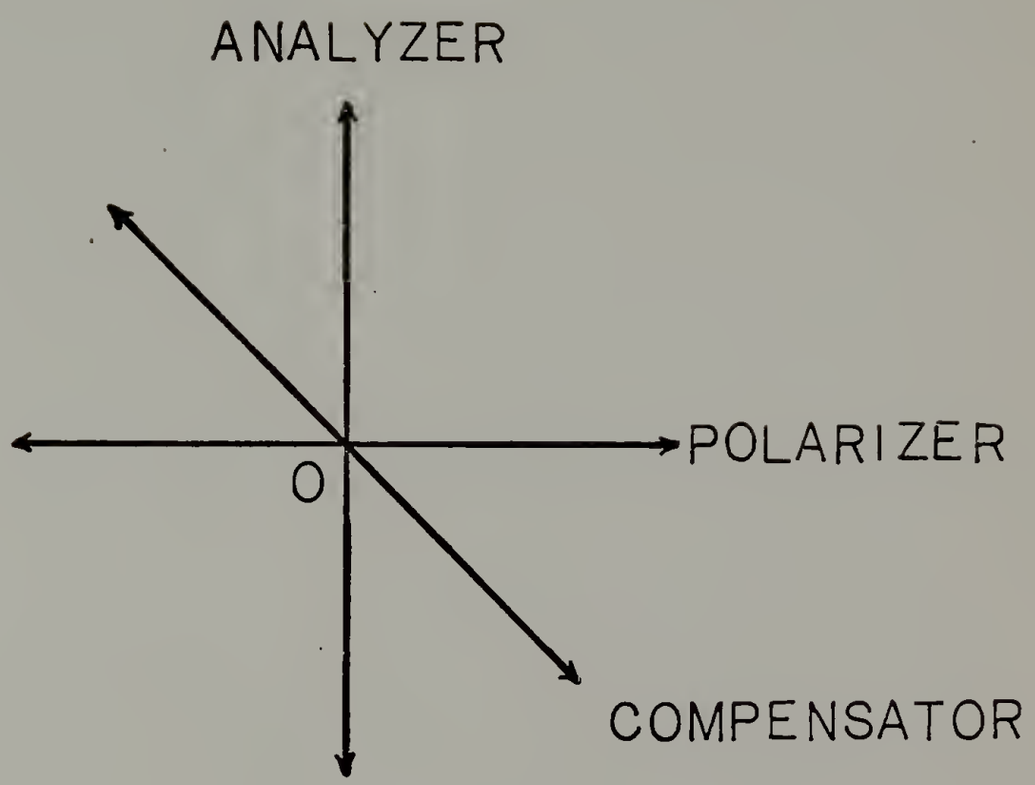

Figure 1

Appendix II

Computer Program for Light Scattering Calculations

```
10 PROGRAM SCATT
20 DIMENSION Y(101),Z(91), S(200)
22 NC=1
25 SØC=2.8E-10
30 T=1.2E6
35 PA=1.23E6
38 X3=1.05
39 X2=(1./X3)**0.5
40 PI=3.141592654
50 AN=1.519
60 XLAM=.000063/1.519
70 R1=3.E-4
80 P2=15.*R1
90 DR=(R2-R1)/20.
100 CT=.5/180.*PI
110 CTMA=10./180.*3.141592654
120 DC=CTMA/20.
130 AZ=0.0
140 DAZ=10./180.*3.141592654
150 AZMA=PI/2.
250 AL=0.0
260 DA=5.0/180.*3.141592654
270 DO 700 I=1,37
280 R=R1
290 DO 600 J=1,21
300 X=2.*PI/XLAM*SIN(CT)*SIN(AZ)*R*SIN(AL)
320 CALL BES(NO,X,0,AJ1,S)
400 PR=-PA*(R1/R)**3*((X2*SIN(AL))**2+(X3*COS(AL))**2)**(-1.5)
410 PT=.5*PA*(R1/R)**3*((X2*SIN(AL))**2+(X3*COS(AL))**2)**(-1.5)
465 RR=T*(5./4.*(R1/R)**3-(R1/R)**5+(-3.*(R1/R)**5+15./4.*
466C(R1/R)**3)*COS(2.*AL)+.5*(1.+COS(2.*AL)))
467C+PR
470 CC=T*(.25*(R1/R)**5+7./4.*(R1/R)**5*COS(2.*AL)+.5*(1.-
471CCOS(2.*AL)))+PT
472 RC=T*(5./4.*(R1/R)**3-2.*(R1/R)**5)*SIN(2.*AL)-T*.5*SIN
473C(2.*AL)
474 IF (RC .EQ. 0.0) GO TO 477
475 DCT=0.5*ATAN2((RR-CC),2.*RC)
476 GO TO 478
477 DCT=0.0
478 P=RR*(2.*COS(DCT)**2-1.)+4.*RC*SIN(DCT)*COS(DCT)+CC*(1.-2.
479C*COS(DCT)**2)
480 Y(J)=2.*P*(COS(DCT)**2*COS(AL)*SIN(AL)+COS(AL)**2*SIN(DCT)
481C*COS(DCT)-COS(AL)*SIN(AL)*SIN(DCT)**2-SIN(AL)**2*SIN(DCT)*
482CCOS(DCT))*SIN(AL)*SIN(2.*PI/XLAM*SIN(CT)*COS(AZ)*R*COS(AL)
483C)*AJ1*R**2*1.0E20
600 R=R+DR
610 SUMY=0.0
```

```
LIST 620,940

620 DO 640 M=1,9
640 SUMY=SUMY+4.*Y(2*M)+2.*Y(2*M+1)
660 AMP=DR/3.*(Y(1)+SUMY+4.*Y(20)+Y(21))
680 Z(I)=AMP
700 AL=AL+DA
720 SUMZ=0.0
740 DO 760 N=1,17
760 SUMZ=SUMZ+4.*Z(2*N)+2.*Z(2*N+1)
780 AHVZ=DA/3.*(Z(1)+SUMZ+4.*Z(36)+Z(37))
800 XIH=(-2.*S0C*9./2.*AN/(AN**2+2.)**2)**2*AHVZ**2
810 ALXIH=ALOG(XIH)
820 PRINT 840,CT,AZ,XIH,ALXIH
840 FORMAT(2F7.3,E15.5,F10.4)
860 AZ=AZ+DAZ
880 IF (AZ-AZMA) 140,140,900
900 CT=CT+DC
920 IF (CT-CTMA) 110,110,940
940 END


 00  SUBROUTINE BES(NO,X,KODE,RESULT,T)
 110 DIMENSION T(40)
 115 FORMAT(55H1NEGATIVE ORDER NOT ACCEPTED IN BESSEL FUNCTION
 116C ROUTINE)
 120 KLAM = 1
 125 KO = NO + 1
 130 IF(X) 190,135,190
 135 IF(NO)155,140,160
 140 T(KO) = 1.0
 145 RESULT = 1.0
 150 RETURN
 155 IF(KO)180,170,160
 160 RESULT = 0
 165 RETURN
 170 RESULT = 9.999999999E200
 175 RETURN
 180 PRINT 115
 185 STOP
 190 IF(NO)180,195,195
 195 IF(KODE)200,205,200
 200 KLAM = KLAM + 1
 205 JO = 2*XFIXF(X)
 210 MO = NO
 215 IF(MO-JO)220,225,225
 220 MO = JO
 225 MO = MO + 11
 230 T(MO) = 0.
 235 LUB = MO-1
 240 T(LUB) = 1.0E-300
 245 GO TO (250,330),KLAM
 250 F = 2*LUB
 255 MO = MO-3
 260 I2 = MO
```

```
LIST 265,420


265 F = F-2.
270 T(I2+1) = F/X*T(I2+2) - T(I2+3)
275 IF(I2)280,290,280
280 I2 = I2 - 1
285 GO TO 265
290 SUM = T(1)
295 DO 300 J=3,M0,2
300 SUM = SUM + 2.*T(J)
305 F = 1./SUM
310 DO 315 J=1,K0
315 T(J) = T(J)*F
320 RESULT = T(K0)
325 RETURN
330 F = 2*LUB-2
340 I2 = M0
345 T(I2+1) = F/X*T(I2+2) + T(I2+3)
350 IF(I2)355,370,355
355 I2 = I2-1
365 GO TO 345
370 SUM = T(1)
375 DO 380 J=2,M0
380 SUM = SUM +2.*T(J)
385 F = 1./SUM*EXPF(X)
390 DO 395 J = 1,K0
395 T(J) = T(J)*F
400 RESULT = T(K0)
405 RETURN
410 END
420 ENDPROG
```

Appendix III

Computer Program for Birefringence Pattern Calculations

```
10 PROGRAM RETARD
20 DIMENSION A(61,2,2),B(2,2),W(61),C(61,3,3),AN1(61),AN3(61)
21 COMMON DCT(61),CT(61),P1,P2,T,AX,FF,PA,X2,X3
22 COMPLEX A,B
23 XLAM=.000055/1.52
24 PI=3.141592654
25 SOC=2.8E-10
26 PA=1.23E6
27 T=0.
28 X3=1.
29 X2=(1./X3)**0.5
30 R=1.0
32 DR=0.1
35 DO 645 II=1,11
40 DH=.1
50 DFAI=PI/18.
60 FAI=0.0
65 FAIMAX=PI/2.
70 H=-3.0
100 DO 390 I=1,61
102 AN2=1.
103 R2=R*R
104 H2=H*H
120 XAR=(R2+H2)**0.5
124 CF=COS(FAI)
125 CB=R*CF/XAR
126 IF (CB .GE. 1.0) GO TO 128
127 GO TO 130
128 CB=1.0
129 GO TO 130
130 CT(I)=ACOS(CB)
131 AT=ATAN(H/R)
132 CW=SIN(AT)/SIN(CT(I))
133 IF (CW .GE. 1.0) GO TO 136
134 IF (CW .LE. -1.0) GO TO 139
135 GO TO 142
136 CW=1.0
138 GO TO 142
139 CW=-1.0
142 W(I)=ACOS(CW)
143 IF (W(I) .GE. 3.141580) W(I)=PI
144 IF (W(I) .LE. 1.0E-04) W(I)=0.0
145 AX=1./XAR
```

```
150 CALL STRESS(I)
160 AN1(I)=1.+S0C/1.5*(P1-P2)
170 AN3(I)=1.-S0C/1.5*(P2-FF)
200 H=H+DH
204 A12=(COS(DCT(I))*COS(CT(I))*SIN(W(I))-SIN(DCT(I))*SIN(CT(I))
205C*SIN(W(I)))
208 A13=-(COS(DCT(I))*SIN(CT(I))+SIN(DCT(I))*COS(CT(I)))
210 A21=-SIN(W(I))
220 A2^=COS(W(I))
230 A23=0.0
240 A31=COS(DCT(I))*SIN(CT(I))*COS(W(I))+SIN(DCT(I))*COS(W(I))
241C*COS(CT(I))
245 A32=COS(DCT(I))*SIN(CT(I))*SIN(W(I))+SIN(DCT(I))*COS(CT(I))
246C*SIN(W(I))
250 A33=COS(DCT(I))*COS(CT(I))-SIN(DCT(I))*SIN(CT(I))
260 C(I,2,2)=A12**2/AN2**2+A22**2/AN3(I)**2+A32**2/AN1(I)**2
270 C(I,2,3)=A12*A13/AN2**2+A22*A23/AN3(I)**2+A32*A33/AN1(I)**2
280 C(I,3,3)=A13**2/AN2**2+A23**2/AN3(I)**2+A33**2/AN1(I)**2
282 CEC=C(I,2,2)-C(I,3,3)
290 D=2.*C(I,2,3)
292 IF (D .EQ. 0.0) GO TO 305
300 X=0.5*ATAN(D/CEC)
301 GO TO 310
305 X=0.0
310 X1=(C(I,2,2)-COS(X)**2*(C(I,2,2)+C(I,3,3)))/(1.0-2.*COS(X)
311C**2)
320 X2=C(I,2,2)+C(I,3,3)-X1
325 BP=SQRT(1.0/X2)
327 AP=SQRT(1.0/X1)
330 IF (AP .GE. BP) GO TO 365
335 IF (X .LT. 0.0) GO TO 350
338 IF (X .EQ. 0.0) GO TO 347
340 C1=SIN(X)
345 S1=-COS(X)
346 GO TO 355
347 C1=0.0
348 S1=1.0
349 GO TO 355
350 C1=-SIN(X)
352 S1=COS(X)
355 DT=2.*PI*DH*1.5E-4*(BP-AP)/XLAM
360 GO TO 381
365 C1=COS(X)
370 S1=SIN(X)
380 DT=2.*PI*DH*1.5E-4*(AP-BP)/XLAM
381 A(I,1,2)=CMPLX(0.0,C1*S1*2.*SIN(DT/2.))
382 A(I,2,1)=CMPLX(0.0,C1*S1*2.*SIN(DT/2.))
383 A(I,1,1)=CMPLX(COS(DT/2.),(2.*C1**2-1.0)*SIN(DT/2.))
386 A(I,2,2)=CMPLX(COS(DT/2.),-(2.*C1**2-1.0)*SIN(DT/2.))
390 CONTINUE
440 DO 550 I=1,60
450 I1=I+1
460 DO 475 J=1,2
465 DO 475 K=1,2
```

```
470 B(J,K)=CMPLX(0.0,0.0)
475 CONTINUE
490 DO 500 J=1,2
492 DO 500 K=1,2
493 DO 500 K1=1,2
495 B(J,K)=B(J,K)+A(I,J,K1)*A(I1,K1,K)
500 CONTINUE
510 DO 540 J=1,2
520 DO 540 K=1,2
530 A(I1,J,K)=B(J,K)
540 CONTINUE
550 CONTINUE
551 BB1=B(1,1)*B(2,2)
552 BB2=B(1,2)*B(2,1)
553 BB=BB1-BB2
554 AX3=B(2,1)-B(1,2)
555 AX4=B(1,1)+B(2,2)
557 IF (ABS(AX4) .LE. 1.0E-07) AX4=0.0
558 IF (ABS(AX3) .LE. 1.0E-07) AX3=0.0
560 AW=ATAN((B(2,1)-B(1,2))/(B(1,1)+B(2,2)))
565 BD=SQRT(BB)
570 DTT=2.*ACOS((B(1,1)+B(2,2))/(2.*BD*COS(AW)))
572 AX1=(B(1,2)+B(2,1))*CMPLX(0.,-1.0)
573 AX2=(B(1,1)-B(2,2))*CMPLX(0.,-1.0)
577 IF (ABS(AX1) .LE. 1.0E-07) AX1=0.0
578 IF (ABS(AX2) .LE. 1.0E-07) AX2=0.0
586 AL2=((AX1/AX2)-(AX3/AX4))
587 AL1=(1.+(AX1*AX3)/(AX2*AX4))
590 AF=.5*ATAN2(AX2,AX1)
591 IF (AF .GT. PI/2.) GO TO 594
592 IF (AF .LE. -PI/2.) GO TO 596
593 GO TO 597
594 AF=AF-3.141592654
595 GO TO 597
596 AF=AF+3.141592654
597 WF=(AW+AF)/3.141592654*180.
598 E=CABS(B(2,1))
600 XIT=1.0E8*E*E
602 ALI=ALOG(XIT)
605 PRINT 610,R,FAI,AW,DTT,AF,WF,ALI
610 FORMAT (2X,F3.1,2X,F6.4,2X,F5.2,3(2X,F7.3),2X,F10.4)
620 FAI=FAI+DFAI
630 IF (FAI-FAIMAX) 70,70,640
640 IF (II .GT. 5) DR=0.5
643 R=R+DR
645 CONTINUE
650 END
655 SUBROUTINE STRESS(I)
660 COMMON DCT(61),CT(61),P1,P2,T,AX,FF,PA,X2,X3
662 PR=-PA*AX**3*((X2*SIN(CT))**2+(X3*COS(CT))**2)**(-1.5)
664 PT=.5*PA*AX**3*((X2*SIN(CT))**2+(X3*COS(CT))**2)**(-1.5)
670 RR=T*(5./4.*AX**3-AX**5+(-3.*AX**5+15./4.*AX**3)*COS(2.*CT
671C(I))+0.5*(1.+COS(2.*CT(I))))
672C+PR
```

```
LIST 675,750


675 CC=T*(0.25*AX**5+1.75*AX**5*COS(2.*CT(I))+0.5*(1.-COS(2.*
676CCT(I))))
677C+PT
680 RC=T*(1.25*AX**3-2.*AX**5)*SIN(2.*CT(I))-0.5*SIN(2.*
681CCT(I))*T
685 FF=T*(3./4.*AX**5+5./4.*AX**5*COS(2.*CT(I)))
686C+PT
690 IF (RC .EQ. 0.0) GO TO 710
700 DCT(I)=0.5*ATAN2((RR-CC),2.*RC)
705 GO TO 720
710 DCT(I)=0.0
720 P1=RR*COS(DCT(I))**2+CC*SIN(DCT(I))**2+2.*RC*COS(DCT(I))
721C*SIN(DCT(I))
725 P2=RR*SIN(DCT(I))**2+CC*COS(DCT(I))**2-2.*RC*COS(DCT(I))
726C*SIN(DCT(I))
730 RETURN
740 END
750 ENDPROG
```

Appendix IV

Computer Program for Spherulite Birefringence

```
10 PROGRAM RETARD
20 DIMENSION A(61,2,2),B(2,2),W(61),C(61,3,3),AN1(61),AN3(61)
21 DIMENSION DCT(61),CT(61)
22 COMPLEX A,B
23 XLAM=.000055
24 PI=3.141592654
30 R=0.0
32 DR=0.05
35 DO 645 II=1,10
40 DH=0.5/30.
50 DFAI=PI/18.
60 FAI=0.0
65 FAIMAX=PI/2.
70 H=-0.5
100 DO 390 I=1,61
102 AN2=1.
103 R2=R*R
104 H2=H*H
120 XAR=(R2+H2)**0.5
124 CF=COS(FAI)
125 CB=R*CF/XAR
126 IF (CB .GE. 1.0) GO TO 128
127 GO TO 130
128 CB=1.0
129 GO TO 130
130 CT(I)=ACOS(CB)
131 AT=ATAN(H/R)
132 CW=SIN(AT)/SIN(CT(I))
133 IF (CW .GE. 1.0) GO TO 136
134 IF (CW .LE. -1.0) GO TO 139
135 GO TO 142
136 CW=1.0
138 GO TO 142
139 CW=-1.0
142 W(I)=ACOS(CW)
143 IF (W(I) .GE. 3.141580) W(I)=PI
144 IF (W(I) .LE. 1.0E-04) W(I)=0.0
145 AX=1./XAR
150 DCT(I)=0.0
160 IF (AX .LT. 2.0) GO TO 170
165 AN1(I)=0.9998
168 GO TO 180
```

```
170 AN1(I)=1.0
180 AN3(I)=1.0
200 H=H+DH
204 A12=(COS(DCT(I))*COS(CT(I))*SIN(W(I))-SIN(DCT(I))*SIN(CT(I))
205C*SIN(W(I)))
208 A13=-(COS(DCT(I))*SIN(CT(I))+SIN(DCT(I))*COS(CT(I)))
210 A21=-SIN(W(I))
220 A22=COS(W(I))
230 A23=0.0
240 A31=COS(DCT(I))*SIN(CT(I))*COS(W(I))+SIN(DCT(I))*COS(W(I))
241C*COS(CT(I))
245 A32=COS(DCT(I))*SIN(CT(I))*SIN(W(I))+SIN(DCT(I))*COS(CT(I))
246C*SIN(W(I))
250 A33=COS(DCT(I))*COS(CT(I))-SIN(DCT(I))*SIN(CT(I))
260 C(I,2,2)=A12**2/AN2**2+A22**2/AN3(I)**2+A32**2/AN1(I)**2
270 C(I,2,3)=A12*A13/AN2**2+A22*A23/AN3(I)**2+A32*A33/AN1(I)**2
280 C(I,3,3)=A13**2/AN2**2+A23**2/AN3(I)**2+A33**2/AN1(I)**2
282 CBC=C(I,2,2)-C(I,3,3)
290 D=2.*C(I,2,3)
292 IF (D .EQ. 0.0) GO TO 305
300 X=0.5*ATAN(D/CBC)
301 GO TO 310
305 X=0.0
310 X1=(C(I,2,2)-COS(X)**2*(C(I,2,2)+C(I,3,3)))/(1.0-2.*COS(X)
311C**2)
320 X2=C(I,2,2)+C(I,3,3)-X1
325 BP=SQRT(1.0/X2)
327 AP=SQRT(1.0/X1)
330 IF (AP .GE. BP) GO TO 365
335 IF (X .LT. 0.0) GO TO 350
338 IF (X .EQ. 0.0) GO TO 347
340 C1=SIN(X)
345 S1=-COS(X)
346 GO TO 355
347 C1=0.0
348 S1=1.0
349 GO TO 355
350 C1=-SIN(X)
352 S1=COS(X)
355 DT=2.*PI*DH*0.0015*(BP-AP)/XLAM
360 GO TO 381
365 C1=COS(X)
370 S1=SIN(X)
380 DT=2.*PI*DH*0.0015*(AP-BP)/XLAM
381 A(I,1,2)=CMPLX(0.0,C1*S1*2.*SIN(DT/2.))
382 A(I,2,1)=CMPLX(0.0,C1*S1*2.*SIN(DT/2.))
383 A(I,1,1)=CMPLX(COS(DT/2.),(2.*C1**2-1.0)*SIN(DT/2.))
386 A(I,2,2)=CMPLX(COS(DT/2.),-(2.*C1**2-1.0)*SIN(DT/2.))
390 CONTINUE
440 DO 550 I=1,60
450 I1=I+1
460 DO 475 J=1,2
465 DO 475 K=1,2
470 B(J,K)=CMPLX(0.0,0.0)
```

```
475 CONTINUE
490 DO 500 J=1,2
492 DO 500 K=1,2
493 DO 500 K1=1,2
495 B(J,K)=B(J,K)+A(I,J,K1)*A(I1,K1,K)
500 CONTINUE
510 DO 540 J=1,2
520 DO 540 K=1,2
530 A(I1,J,K)=B(J,K)
540 CONTINUE
550 CONTINUE
551 BB1=B(1,1)*B(2,2)
552 BB2=B(1,2)*B(2,1)
553 BB=BB1-BB2
554 AX3=B(2,1)-B(1,2)
555 AX4=B(1,1)+B(2,2)
557 IF (ABS(AX4) .LE. 1.0E-07) AX4=0.0
558 IF (ABS(AX3) .LE. 1.0E-07) AX3=0.0
560 AW=ATAN((B(2,1)-B(1,2))/(B(1,1)+B(2,2)))
565 BD=SQRT(BB)
570 DTT=2.*ACOS((B(1,1)+B(2,2))/(2.*BD*COS(AW)))
572 AX1=(B(1,2)+B(2,1))*CMPLX(0.,-1.0)
573 AX2=(B(1,1)-B(2,2))*CMPLX(0.,-1.0)
577 IF (ABS(AX1) .LE. 1.0E-07) AX1=0.0
578 IF (ABS(AX2) .LE. 1.0E-07) AX2=0.0
586 AL2=((AX1/AX2)-(AX3/AX4))
587 AL1=(1.+(AX1*AX3)/(AX2*AX4))
590 AF=.5*ATAN2(AX2,AX1)
591 IF (AF .GT. PI/2.) GO TO 594
592 IF (AF .LE. -PI/2.) GO TO 596
593 GO TO 597
594 AF=AF-3.141592654
595 GO TO 597
596 AF=AF+3.141592654
597 WF=(AW+AF)/3.141592654*180.
598 E=CABS(B(2,1))
600 XIT=1.0E8*E*E
602 ALI=ALOG(XIT)
605 PRINT 610,R,FAI,AW,DTT,AF,WF,ALI
610 FORMAT (2X,F3.1,2X,F6.4,2X,F5.2,3(2X,F7.3),2X,F10.4)
620 FAI=FAI+DFAI
630 IF (FAI-FAIMAX) 70,70,640
640 R=R+DR
645 CONTINUE
650 END
655 ENDPROG
```

Appendix V

Computer Program for Least Square Analysis

```
1  PROGRAM LINE
10* DESCRIPTION: COMPUTES THE SLOPE AND OTHER STATISTICS
15* FOR A SIMPLE LINEAR REGRESSION WITH ONE INDEPENDENT
20* VARIABLE FOR TAYLORS SERIES EXPANSION OF AVRAMI EQUATION
30* PUT DATA IN LINE 600 AND FOLLOWING
35* FIRST DATA IS N, THEN NUMBER OF POINTS, THEN THE DATA
40 READ , N
50 DIMENSION T(50),F(50),X(50),Y(50)
55 DO 65 I = 1,N,1
60 READ , X(I), Y(I)
65 CONTINUE
85 X1 = 0.0
87 Y1 = 0.0
90 Y2 = 0.0
92 X2 = 0.0
95 Z = 0.0
100  DO 140 I =1,N,1
110 X1 = X1 + X(I)
115 Y1 = Y1 + Y(I)
120 X2 = X2 + X(I)*X(I)
125 Y2 = Y2 + Y(I)*Y(I)
130 Z = Z + X(I)*Y(I)
140 CONTINUE
145 C = N
150 S1 = C*X2 - X1*X1
155 S2 = C*Z - X1*Y1
160 B = S2/S1
165 Y3 = Y1/C
170 X3 = X1/C
175 B1 = Y3 - B*X3
180 N1 = N - 1
181 C1 = N1
185 N2 = N1 - 1
186 C2 = N2
190 S3 = (Y2 - Y1*Y3 - B*S2/C)
195 S4 = S3/C2
200 PRINT 210, X(1),Y(1)
210 FORMAT(F10.5,1X,*= FIRST X(I),FIRST Y(I) = *,F11.5,/)
211A
225 PRINT 230,N,B
230 FORMAT(*NUMBER(N) = *,5X,I2,5X,*SLOPE =*,5X,E10.4,/)
235 PRINT 240,B1
240 FORMAT(*Y-INTERCEPT =*,1X,F12.7,/)
245 PRINT 250
```

```
250 FORMAT(*STANDARD DEVIATIONS*)
254 D = SQRT(S1/C/C1)
255 PRINT 260,D
260 FORMAT(10X,*X*,10X,F15.10)
264 E = SQRT((Y2-Y1*Y3)/C1)
265 PRINT 270,E
270 FORMAT(10X,*Y*,10X,F15.10)
274 FOX = SQRT(S4)
275 PRINT 280,FOX
280 FORMAT(10X,*ERROR*,6X,F12.5)
283 G = SQRT(S4/C)
284 PRINT 290,G
290 FORMAT(10X,*Y=EAR*,6X,F12.5)
294 H = SQRT(S4/S1*C)
296 PRINT 300,H
300 FORMAT(10X,*SLOPE*,6X,F12.6)
310 CONTINUE
320 END
360 END PROG
600 12
605 2.69E2,1.06E-04
610  5.35E2,2.2E-04
615 8.09 2,2.77E-04
620 10.75E2,3.34E-04
625 13.1E2,4.02E-04
630 15.5E2,4.72E-04
635 17.95E2,5.21E-04
640 20.E2,5.76E-04
645 22.2E2,6.18E-04
650 24.4E2,6.59E-04
655 26.4E2,7.03E-04
660 28.5E2,7.4E-04
```